Antenna Laboratory Report No. 72-5

ANALYSIS OF MICROSTRIP TRANSMISSION LINES

by

Tatsuo Itoh

and

Raj Mittra

Scientific Report

June 1972

NATIONAL TECHNICAL
INFORMATION SERVICE

Antenna Laboratory
Department of Electrical Engineering
Engineering Experiment Station
University of Illinois
Urbana, Illinois 61801

124

DOCUMENT CONTROL DATA - R&D

(Security classification of title, body of abstract and indexing annotation must be entered when the overall report is classified)

1. ORIGINATING ACTIVITY (Corporate author)	2a. REPORT SECURITY CLASSIFICATION
Department of Electrical Engineering University of Illinois Urbana, Illinois 61801	2b. GROUP

3. REPORT TITLE

ANALYSIS OF MICROSTRIP TRANSMISSION LINES

4. DESCRIPTIVE NOTES *(Type of report and inclusive dates)*

Scientific Report

5. AUTHOR(S) *(Last name, first name, initial)*

Itoh, Tatsuo
Mittra, Raj

6. REPORT DATE	7a. TOTAL NO. OF PAGES	7b. NO. OF REFS
June 1972	124	43

8a. CONTRACT OR GRANT NO. DA-ARO-D-31-124-71-G77, NSF GK-15288	9a. ORIGINATOR'S REPORT NUMBER(S)
b. PROJECT AND TASK NO. NSF GK-25074	Antenna Laboratory Report No. 72-5
c.	9b. OTHER REPORT NO(S) (Any other numbers that may be assigned this report)
d.	UILU-ENG-72-2543

10. AVAILABILITY/LIMITATION NOTICES

Distribution is unlimited.

11. SUPPLEMENTARY NOTES	12. SPONSORING MILITARY ACTIVITY
	U. S. Army Research Office - Durham National Science Foundation

13. ABSTRACT

In this work a number of semirigorous and numerical techniques are presented for analyzing the microstrip transmission line configurations. The methods of quasi-TEM as well as hybrid-mode analyses are presented in some detail. A discussion of the higher-order modes in such transmission lines is also included.

In addition to analyzing the uniform line configurations, the problem of evaluating the effect of losses, end loading, etc., are examined and methods for handling these problems are discussed.

DD FORM 1473
1 JAN 64

i

14. KEY WORDS	LINK A		LINK B		LINK C	
	ROLE	WT	ROLE	WT	ROLE	WT
Microstrip Transmission Line						
Quasi-TEM Modes						
Hybrid-Mode Analysis						
Higher-Order Modes						
End Loading						
Numerical Techniques						
Semirigorous Techniques						

INSTRUCTIONS

1. ORIGINATING ACTIVITY: Enter the name and address of the contractor, subcontractor, grantee, Department of Defense activity or other organization (corporate author) issuing the report.

2a. REPORT SECURITY CLASSIFICATION: Enter the overall security classification of the report. Indicate whether "Restricted Data" is included. Marking is to be in accordance with appropriate security regulations.

2b. GROUP: Automatic downgrading is specified in DoD Directive 5200.10 and Armed Forces Industrial Manual. Enter the group number. Also, when applicable, show that optional markings have been used for Group 3 and Group 4 as authorized.

3. REPORT TITLE: Enter the complete report title in all capital letters. Titles in all cases should be unclassified. If a meaningful title cannot be selected without classification, show title classification in all capitals in parenthesis immediately following the title.

4. DESCRIPTIVE NOTES: If appropriate, enter the type of report, e.g., interim, progress, summary, annual, or final. Give the inclusive dates when a specific reporting period is covered.

5. AUTHOR(S): Enter the name(s) of author(s) as shown on or in the report. Enter last name, first name, middle initial. If military, show rank and branch of service. The name of the principal author is an absolute minimum requirement.

6. REPORT DATE: Enter the date of the report as day, month, year, or month, year. If more than one date appears on the report, use date of publication.

7a. TOTAL NUMBER OF PAGES: The total page count should follow normal pagination procedures, i.e., enter the number of pages containing information.

7b. NUMBER OF REFERENCES: Enter the total number of references cited in the report.

8a. CONTRACT OR GRANT NUMBER: If appropriate, enter the applicable number of the contract or grant under which the report was written.

8b, 8c, & 8d. PROJECT NUMBER: Enter the appropriate military department identification, such as project number, subproject number, system numbers, task number, etc.

9a. ORIGINATOR'S REPORT NUMBER(S): Enter the official report number by which the document will be identified and controlled by the originating activity. This number must be unique to this report.

9b. OTHER REPORT NUMBER(S): If the report has been assigned any other report numbers (either by the originator or by the sponsor), also enter this number(s).

10. AVAILABILITY/LIMITATION NOTICES: Enter any limitations on further dissemination of the report, other than those imposed by security classification, using standard statements such as:

(1) "Qualified requesters may obtain copies of this report from DDC."

(2) "Foreign announcement and dissemination of this report by DDC is not authorized."

(3) "U. S. Government agencies may obtain copies of this report directly from DDC. Other qualified DDC users shall request through
_____."

(4) "U. S. military agencies may obtain copies of this report directly from DDC. Other qualified users shall request through
_____."

(5) "All distribution of this report is controlled. Qualified DDC users shall request through
_____."

If the report has been furnished to the Office of Technical Services, Department of Commerce, for sale to the public, indicate this fact and enter the price, if known.

11. SUPPLEMENTARY NOTES: Use for additional explanatory notes.

12. SPONSORING MILITARY ACTIVITY: Enter the name of the departmental project office or laboratory sponsoring (paying for) the research and development. Include address.

13. ABSTRACT: Enter an abstract giving a brief and factual summary of the document indicative of the report, even though it may also appear elsewhere in the body of the technical report. If additional space is required, a continuation sheet shall be attached.

It is highly desirable that the abstract of classified reports be unclassified. Each paragraph of the abstract shall end with an indication of the military security classification of the information in the paragraph, represented as (TS), (S), (C), or (U).

There is no limitation on the length of the abstract. However, the suggested length is from 150 to 225 words.

14. KEY WORDS: Key words are technically meaningful terms or short phrases that characterize a report and may be used as index entries for cataloging the report. Key words must be selected so that no security classification is required. Identifiers, such as equipment model designation, trade name, military project code name, geographic location, may be used as key words but will be followed by an indication of technical context. The assignment of links, rules, and weights is optional.

II

ANALYSIS OF MICROSTRIP TRANSMISSION LINES

by

Tatsuo Itoh

and

Raj Mittra

Scientific Report

June 1972

Antenna Laboratory
Department of Electrical Engineering
Engineering Experiment Station
University of Illinois
Urbana, Illinois 61801

/

ABSTRACT

In this work a number of semirigorous and numerical techniques
are presented for analyzing the microstrip transmission line corfigurations.
The methods of quasi-TEM as well as hybrid-mode analyses are presented
in some detail. A discussion of the higher-order modes in such
transmission lines is also included.

In addition to analyzing the uniform line configurations, the
problem of evaluating the effect of losses, end loading, etc., are
examined and methods for handling these problems are discussed.

ACKNOWLEDGEMENT

TABLE OF CONTENTS

LIST OF FIGURES

I. INTRODUCTION

The microstrip line as it is found today in microwave integrated circuit designs represents the second generation of printed transmission lines. The original version, called the stripline, was introduced around 1949, more than two decades ago! As early as 1955, a special issue of IRE, published in March 1955 as _Transactions on Microwave Theory and Techniques_, was devoted entirely to the subject of microwave strip circuits. The topics covered in this issue included the analysis of strip transmission lines, computation of mutual impedance of coupled lines, radiation effects, evaluation of discontinuity effects, as well as several other related subjects. Though much interest was expressed in this new form of line for a few years immediately after its introduction, its use in microwave design did not become very popular until quite recently when new, low-loss dielectric and ferrite substrate materials became available. The evolution of the stripline led to several different versions of the microstrip line, viz., open, shielded, and boxed lines, all of which make use of dielectric or ferrite materials as low-loss substrate.

In this work we will be concerned with the analysis of several of the above configurations of the microstrip line. We will describe a number of semianalytical and numerical techniques that have been developed for analyzing these lines. It is interesting to point out that the conformal mapping technique used extensively in the fifties to analyze the stripline is not conveniently applied to the microstrip line, since the latter is an inhomogeneously filled structure. However, as will be shown in Section II, a modified version of the conformal

1

mapping technique can still be used to derive an approximate but accurate solution to the microstrip problem.

Two other important factors have prompted the development of new techniques for analyzing the microstrip line. The first of these is the advent of high-speed digital computers that have made it possible to apply numerically rigorous techniques to the solution of electromagnetic and quasi-static boundary value problems. The second factor is the increasing use of microstrip lines in the giga-hertz frequency range where the effect of dispersion in the line is no longer negligible. This, in turn, requires a full hybrid-mode analysis of the boundary value problem. The method of formulation as well as the solution of such problems differs substantially from the TEM or quasi-TEM approach, which are valid at lower frequencies. We will illustrate this point more fully in Section III, where we will present a hybrid-mode analysis of the microstrip line. Finally, the problems of evaluating the effects of end-loading, discontinuities, and losses in the microstrip line, etc., also require the development of techniques that have to be tailor-made for such problems. A discussion of these problems is also included in the following sections.

The topics covered in this work have been and still appear to remain very popular subjects for publications, as evidenced by the prolific number of papers published in the microwave literature. It is physically impossible even to attempt to describe all of the contributions that have appeared in the literature during the past five years on the analysis of microstrip lines and related problems. We will only present herein a discussion of some of the representative

techniques and outline the basic principles underlying the
procedures. The reader interested in additional details on a
particular method is advised to consult the original publications
which are referenced in this work.

II. QUASI-TEM ANALYSIS FOR MICROSTRIP LINE STRUCTURE

2.1 Preliminary Discussion

Having presented a brief historical review, we will now proceed to discuss a number of quasi-TEM techniques suitable for theoretically determining characteristics of the microstrip line. As will be evident later, these analyses are valid only in the low frequency range where the free-space wavelength is much larger than the strip width and the thickness of the substrate. A more complete analysis, valid for arbitrary operating frequencies, will be presented later.

Figure 1 shows some typical cross sections of microstrip-type transmission lines. Before we proceed with the details, however, it will be useful to explain why the quasi-TEM analysis is restricted to the low-frequency region only. Though the comments are applicable to all of the geometries shown in Figure 1, we will illustrate our argument by reference to the structure shown in Figure 1a. The electric and magnetic field components of the characteristic solution in this structure may be expressed in terms of a scalar potential ϕ which is required to satisfy

$$\nabla_t^2 \phi + (k^2 - \beta^2)\phi = 0 \qquad \text{in the air,} \qquad (1a)$$

$$\nabla_t^2 \phi + (\epsilon_r k^2 - \beta^2)\phi = 0 \qquad \text{in the substrate,} \qquad (1b)$$

where $k = 2\pi/\lambda$ is the free-space wavenumber, and β is the propagation constant. In the limit of $\epsilon_r = 1$, the lowest-order solution for (1) is TEM with $\beta = k$. For this limiting case, the potential ϕ satisfies the Laplace equation in the cross section and does not generate longitudinal

4
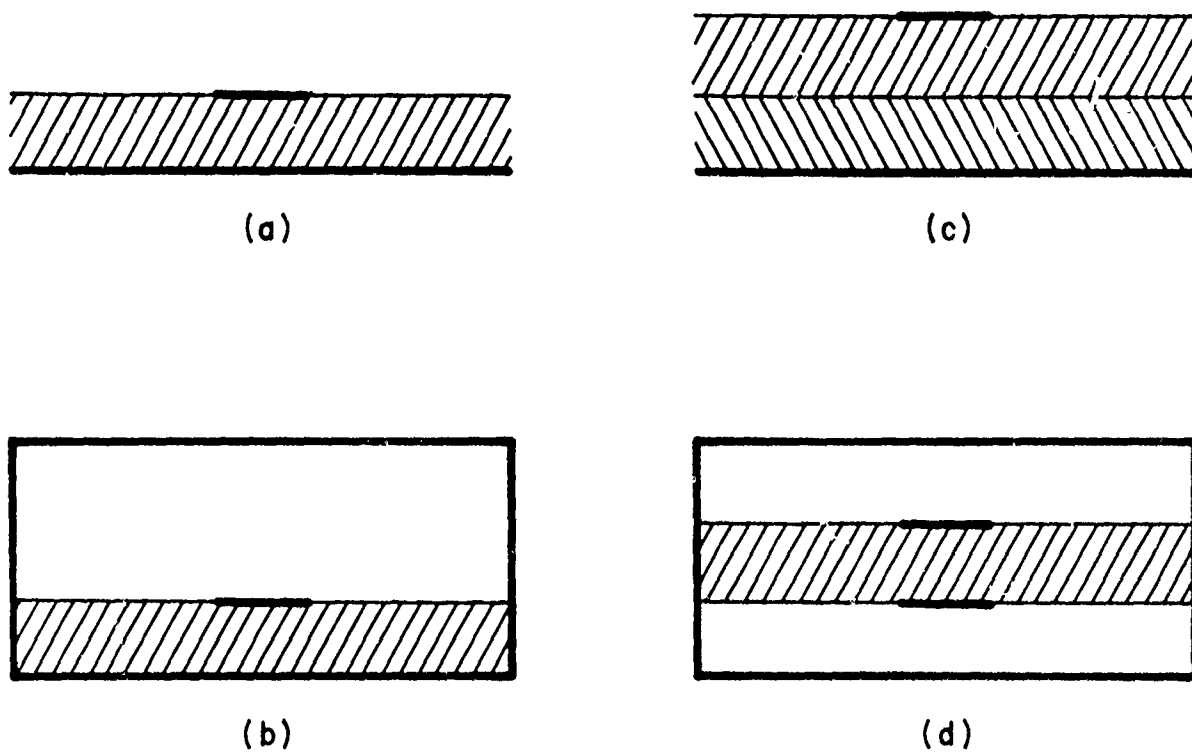
Figure 1. Cross section of some microstrip-type transmission lines.

5

electric or magnetic field components. For the practical case of $\varepsilon_r \neq 1$, Equation (1b) may be regarded as a perturbation of the limiting case $\varepsilon_r = 1$. The effect of this perturbation is small when the operating frequency, i. e., k is small. The quasi-TEM approximation may then be regarded as a zero-order solution to the exact equations shown in (1). Though much simplification in the analysis results with the use of the quasi-TEM approximation, it should be kept in mind that the results obtained via this method are not accurate for larger values of k.

Under the TEM approximation, the microstrip line is adequately described in terms of two basic parameters, viz., the characteristic impedance Z and the propagation constant γ. It is well known that for a low-loss transmission line

$$Z = \sqrt{\frac{L}{C}} \left[1 + \frac{1}{2} \left(\frac{R}{j\omega L} - \frac{G}{j\omega C} \right) \right] \tag{2}$$

$$\gamma = \alpha + j\beta \tag{3a}$$

$$\alpha = \frac{\sqrt{LC}}{2} \left(\frac{R}{L} + \frac{G}{C} \right), \quad \beta = \omega\sqrt{LC} \tag{3b}$$

where R, G, L, C are the resistance, conductance, inductance, and capacitance per unit length, respectively, of the infinitely long transmission line; ω is the angular frequency; and α and β are the attenuation and phase constants, respectively. For a lossless line $R = G = 0$, and hence, $\alpha = 0$, and $Z = \sqrt{L/C}$ is a real quantity. The values of β and Z can also be expressed in terms of the phase velocity $v = 1/\sqrt{LC}$ as

$$\beta = \omega/v, \quad Z = 1/(vC). \tag{4}$$

6

It should be mentioned that dispersion effects are neglected in the TEM approximation; hence, the phase velocity is equal to the group velocity.

Next we will show that for the lossless TEM system the boundary value problem associated with the determination of β (and Z) reduces to that of calculating the capacitance per unit length C. Consider the two configurations of the microstrip line shown in Figure 1a. Note that one of these has a dielectric substrate with relative permittivity ε_r while the companion structure is a homogeneous TEM line obtained by removing the substrate, i. e., by letting $\varepsilon_r = 1$. It is easy to show that for the latter case

$$\beta_o = \omega/c, \ Z_o = 1/(cC_o) \tag{5}$$

where c is the velocity of light in free space. The subscript 0 in (5) serves to distinguish the line from the inhomogeneous microstrip line in which $\varepsilon_r \neq 1$. If the substrate is nonmagnetic, the value of L, the inductance per unit length, is assumed to be identical for both lines. Hence

$$Z = Z_o \sqrt{\frac{C_o}{C}} = \frac{1}{c\sqrt{CC_o}}$$

$$ \tag{6}$$

$$\beta = \beta_o \sqrt{\frac{C}{C_o}} = \frac{\omega}{c} \sqrt{\frac{C}{C_o}}$$

where Z_o and β_o are given by (5). Equation (6) implies that Z and β are obtainable from the capacitance per unit length, C and C_o, of the microstrip and unloaded lines.

Next we will describe a number of quasi-TEM techniques for evaluating the capacitance of microstrip lines of the type shown in

Figure 1. The discussion below will include material from a number
of papers that have appeared in the literature since 1965. As mentioned
earlier, a more rigorous analysis based upon the hybrid-mode approach
will be presented in a later section.

2.2 Modified Conformal Mapping Method

This method was introduced by Wheeler (1965) for computing the
capacitance per unit length of microstrip lines of the type shown
in Figure 1a. The concept of the so-called "filling factor," also
introduced by Wheeler, is considered to be a rather convenient and
useful way of describing the parameters of microstrip structures.

The right half of the cross section of the microstrip line is
shown in Figure 2 where a magnetic wall is placed along the axis of
symmetry, the y-axis. The strip thickness is assumed to be infinitesimally
small.

The first step in Wheeler's technique entails the application of
conformal mapping to the geometry under consideration with the result
that a simpler, parallel-plate geometry is obtained in the new domain.
For the wide strip, the mapping function is chosen to be

$$z = j\pi + d \tanh \frac{1}{2} z' - z' \tag{7}$$

with $d \simeq g'$ for $g'/2 \gg 1$ where g' is the effective width of the
parallel plate in the mapped plane shown in Figure 3a.

Note that the mapping from z to z' transforms the original
microstrip line into a parallel-plate structure bounded by two
vertical magnetic sidewalls ($x' = 0$ and g'). Also, the planar dielectric-
air interface ③ - ⑦ in Figure 2 maps into a curved surface ③ - ⑦ in

8

z - plane

x + jy = z
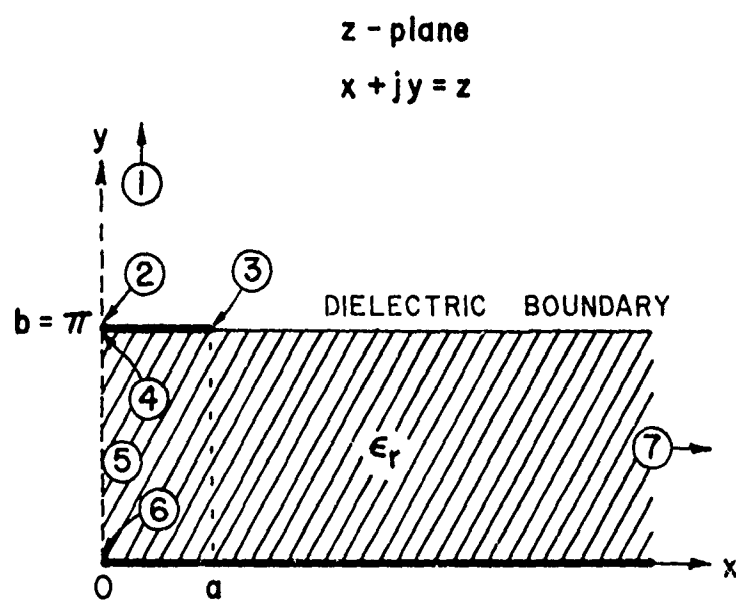
Figure 2.   Cross section of the right-hand half of an open microstrip line.
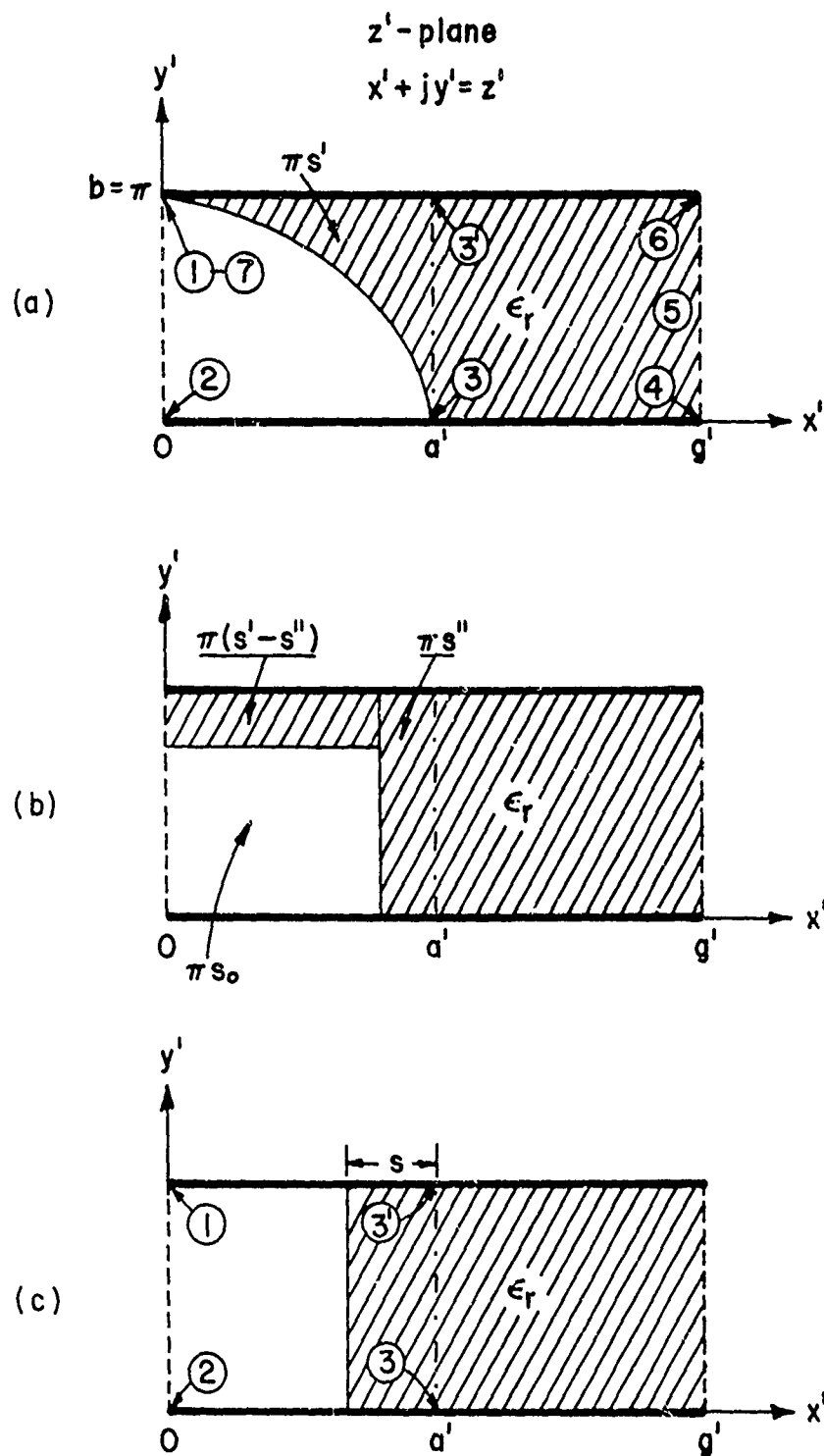
Figure 3. Cross section of the open microstrip line after conformal mapping and its approximations.

10

Figure 3a. Although the geometry in the transformed plane is seemingly simpler to analyze, it should be realized that the space between the parallel plates is now inhomogeneously filled with a dielectric which has a curved boundary. Since an exact solution is difficult to obtain for the partially filled capacitor problem in Figure 3a, it is necessary at this stage to introduce some approximations. In Wheeler's approach, the approximation is introduced in the following manner. Let the area enclosed by the curve ③-⑦, and the lines ③-⑤ and ④-⑦ in Figure 3a be $\pi s'$. Let this area be approximated by two rectangles with areas $\pi s''$ and $\pi(s' - s'')$ as shown in Figure 3b. The area $\pi s''$ effectively adds s'' to the width of the completely filled region on the right $(a' \leq x' \leq g')$ and hence is termed the "parallel" portion. The other area $\pi(s' - s'')$ is effectively in series with the free-space region πs_o. Combining these two effects we can approximately replace the original, partially filled rectangular region bounded by ①②③④ in Figure 3a by an equivalent geometry ①②③④ shown in Figure 3c, in which the dielectric filling has the width s. It is obvious that the capacitance calculation is straightforward in the equivalent geometry due to the planar nature of the dielectric filling.

The effective width s may be expressed as

$$s = s'' + \frac{s' - s''}{\varepsilon_r} . \tag{9}$$

The effective filling factor can be defined by

$$q = \frac{g' - a' + s}{g'} . \tag{9}$$

The effective dielectric constant ε_{eff} may now be expressed in terms of the filling factor q via the relation

$$\varepsilon_{eff} = (1 - q) + q\varepsilon_r. \tag{10}$$

Finally, the capacitance per unit length is given by $C = \varepsilon_{eff}C_o$ where C_o is the capacitance per unit length of the unloaded TEM line. It is evident that the problem is now reduced to that of deriving approximate values of the quantities s', s'', or q.

An approximate expression for wide strips has been provided by Wheeler that reads

$$s' = 0.732 \, [a' - \cosh^{-1}(0.358 \cosh a' + 0.953)] \tag{11a}$$

$$s'' = 0.386 - 1/2(d - 1). \tag{11b}$$

The effective dielectric constant ε_{eff} can be derived by the use of (11) in (8), (9), and (10). Also, he has shown that in the case of narrow strips, the effective dielectric constant is given by

$$\varepsilon_{eff} = \frac{\varepsilon_r + 1}{2} + \frac{g'(\varepsilon_r - 1)}{2\pi^2} \, [\ln \pi/2 + \frac{1}{\varepsilon_r} \ln 4/\pi]. \tag{12}$$

2.3 Finite-Difference Method (Relaxation Method)

This method is strictly a numerical technique for determining the cross-sectional field distribution; this knowledge allows one to compute the desired characteristic parameters of the transmission line. The essential step in this method is to quantize the unknown field distribution at discrete intersections of coordinate grids called the net-points or mesh-points. The relaxation method is a numerical algorithm for solving the unknowns at a large grid of the net-points by applying the method of successive approximations.

Figure 4a shows a portion of the distribution of such net-points. Let the potential at the net-point A be ϕ_A. Now let the potential

12
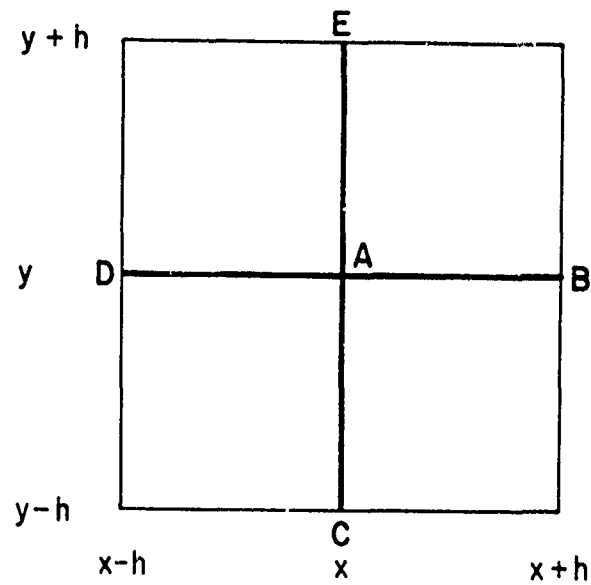
(a)
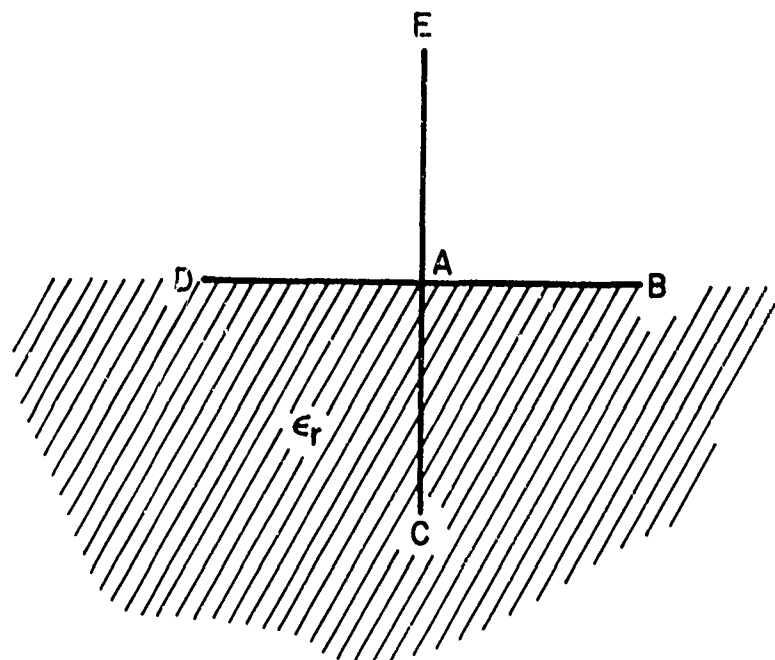
(b)

Figure 4. Net-points for finite difference approximation.

$\phi(x, y)$ be expanded in Taylor's series about the point A to find the potentials at the adjacent net-points B, C, D, and E. The expressions read

$$\phi_B = \phi_A + h \left(\frac{\partial \phi}{\partial x}\right)_A + \frac{1}{2!} h^2 \left(\frac{\partial^2 \phi}{\partial x^2}\right)_A + O(h^4)$$

$$\phi_C = \phi_A - h \left(\frac{\partial \phi}{\partial y}\right)_A + \frac{1}{2!} h^2 \left(\frac{\partial^2 \phi}{\partial y^2}\right)_A + O(h^4)$$

$$\phi_D = \phi_A - h \left(\frac{\partial \phi}{\partial x}\right)_A + \frac{1}{2!} h^2 \left(\frac{\partial^2 \phi}{\partial x^2}\right)_A + O(h^4) \qquad (13)$$

$$\phi_E = \phi_A + h \left(\frac{\partial \phi}{\partial y}\right)_A + \frac{1}{2!} h^2 \left(\frac{\partial^2 \phi}{\partial y^2}\right)_A + O(h^4)$$

where $O(h^4)$ implies the terms in h^4 and higher. Adding the above expressions for the potentials, we obtain the equation

$$\phi_B + \phi_C + \phi_D + \phi_E = 4\phi_A + h^2 \left(\frac{\partial^2 \phi}{\partial x^2} + \frac{\partial^2 \phi}{\partial y^2}\right) + O(h^4). \qquad (14)$$

Utilizing the fact that the potential ϕ satisfies Laplace's equation, we note that the coefficient of h^2 in the right-hand side of (14) is zero Further, if we neglect the terms of $O(h^4)$, Equation (14) reduces to

$$\phi_A = \frac{1}{4} (\phi_B + \phi_C + \phi_D + \phi_E). \qquad (15)$$

The numerical solution to this equation can be obtained by systematically assuming the net-point potential at each of the points where the potential is unknown, numerically testing the residual error in this assumption, and using the residual error in the following way to update the assumed potential. The pertinent equations for applying the relaxation method are

14

$$\Gamma_A^{(n)} = \phi_A^{(n)} - \frac{1}{4} (\phi_B^{(n)} + \phi_C^{(n)} + \phi_D^{(n)} + \phi_E^{(n)}) \quad (16a)$$

$$\phi_A^{(n+1)} = \phi_A^{(n)} - \alpha\Gamma_A^{(n)} \quad (16b)$$

where the quantities with superscript n are to be associated with the values obtained after the nth iteration and $\Gamma_A^{(n)}$ is the so-called residual at the net-point A. Equation (16b) represents the updated estimate of the net-point potential for the $(n+1)^{th}$ iteration and the constant α is called the accelerating factor. The iteration equations in (16) are repeatedly used until the values of the residual $\Gamma_A^{(n)}$ become smaller than some prescribed value for all the net points.

The iteration method is convergent as long as $0 < \alpha < 2$. The range $0 < \alpha < 1$ is referred to as underrelaxation whereas $1 < \alpha < 2$ is called the range of overrelaxation for the acceleration factor. The convergence of the procedure is most rapid for α somewhere between 1 and 2 (Green, 1965) and the iterative procedure with α in this range is referred to in the literature as the method of successive over-relaxation (SOR).

The expression for the potential requires a modification at the interface between air and the dielectric substrate (see Figure 4b). The appropriate equation to use instead of (15) (Green, 1965) is

$$\phi_A = \frac{1}{4} (\phi_B + \phi_D) + \frac{1}{2(\varepsilon_r + 1)} (\varepsilon_r\phi_C + \phi_E). \quad (17)$$

Finite difference equations at the various boundary points have been tabulated by Green (1965) and some general discussion can be found in a paper by Wexler (1969). Interested readers are encouraged to consult these publications for further details.

15

It is worthwhile to mention that the method of solution of Equation (15) is by no means the only one available to us. In fact one can derive a matrix equation of the form

$$\begin{bmatrix} \ddots & & & & 0 \\ & \ddots & & & \\ & & a_{ij} & & \\ & & & \ddots & \\ 0 & & & & \ddots \end{bmatrix} \begin{bmatrix} \\ \\ \phi_j \\ \\ \end{bmatrix} = \begin{bmatrix} \\ \\ b_i \\ \\ \end{bmatrix} \qquad (18)$$

by applying either (15) or its variants [e.g. (14)] to all of the net points in the cross section. The matrix equation (18) can now be inverted to obtain the solution. However, the disadvantage of this approach is that a large coefficient matrix is required to obtain a reasonably accurate solution. Furthermore, since a large number of the elements of the coefficient matrix are zero, the matrix is very sparse; the direct inversion of Equation (18) is numerically inferior to the SOR technique.

Once the potential at each net-point is calculated, it is relatively straightforward to calculate the capacitance of the line.

One uses the formula

$$Q = \oint_L \rho \, d\ell = \oint_L \varepsilon_r \frac{\partial \phi}{\partial n} \, d\ell \qquad (19)$$

for calculating the charge per unit length where L is the contour surrounding the center strip, n is the outward normal, and ε_r is unity if the net-point is in the air and equal to the relative permittivity of the dielectric otherwise . Equation (19) may be written in a discretized form as

$$Q = \varepsilon_r h \sum_s \sideset{}{'}\sum_{i=1}^{N'} \left(\frac{\partial \phi}{\partial n}\right) P_i \qquad \text{(20a)}$$

$$\left(\frac{\partial \phi}{\partial n}\right)_{P_i} = \frac{\phi_B - \phi_A}{2h} \; . \qquad \text{(20b)}$$

In this case, the prime on the summation in (20a) indicates that the first and the last terms in the summation are to be halved in order to approximate the line integral by the trapezoidal rule. The summation over s implies that the contour is subdivided into s straight sections. The point P_i is taken along the dotted line (contour) shown in Figure 5 (Green, 1965). The capacitance per unit length is readily obtained from the value of Q by using

$$C = \frac{Q}{V_t} \qquad \text{(21)}$$

where V_t is the potential difference between the strip and the ground plane. To evaluate the characteristic parameters, say the characteristic impedance Z and the phase constant β, we need to calculate C_o for the case where the substrate is removed. Equation (6) may then be used to obtain Z and β.

Figure 6 shows a few examples of calculated curves (Stinehelfer, 1968) of Z for the microstrip line enclosed in a shield (see Figure 1b). For comparison purposes, Wheeler's results for a flat (open) microstrip line are also shown in Figure 6.

2.4 Variational Method in the Fourier Transform Domain

This method, which uses a combination of variational technique and the Fourier transform approach, was first introduced by Yamashita and Mittra in 1968 for calculating the characteristic parameters of

17
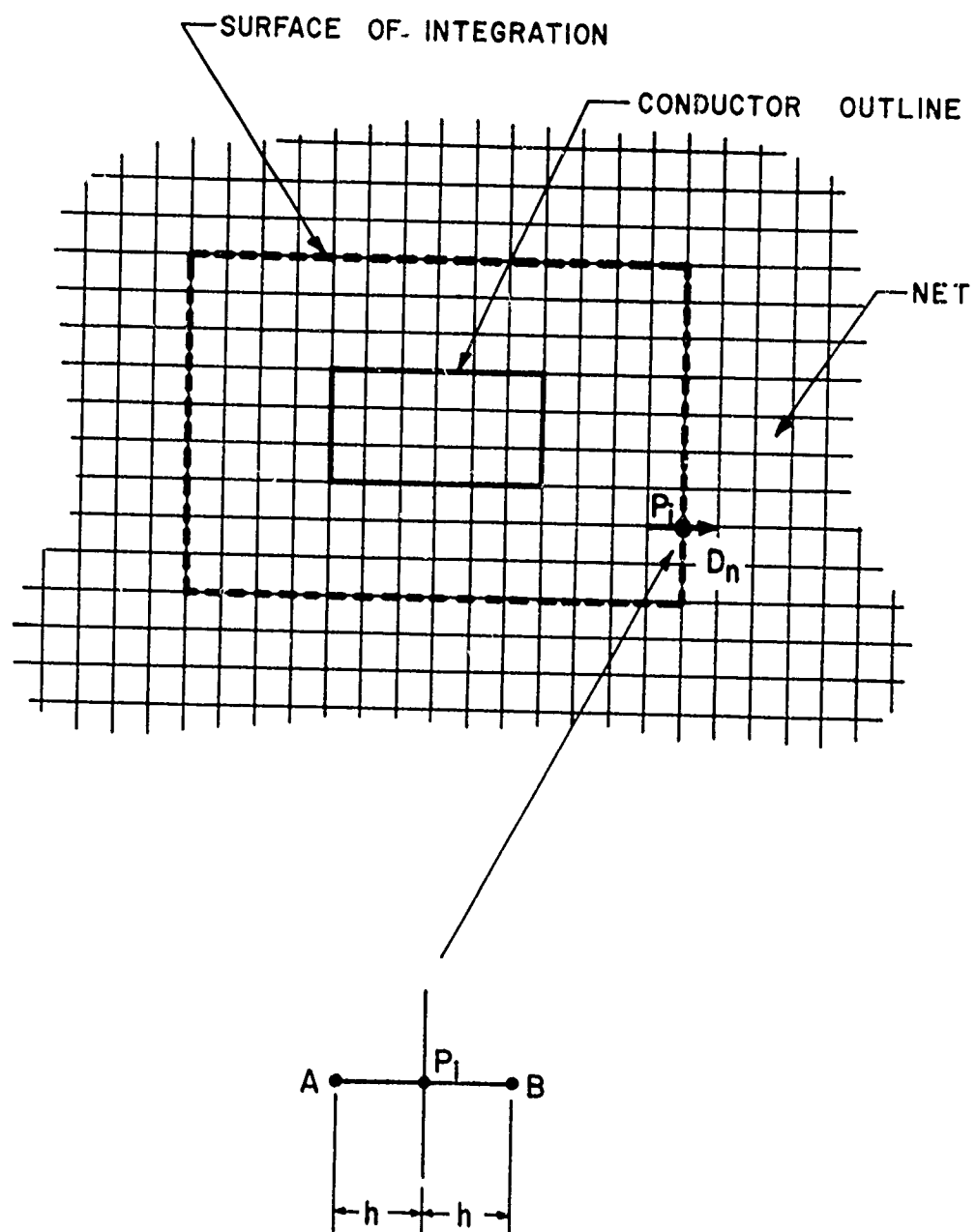
Figure 5. Surface of integration for calculating the total charge on the strip conductor.
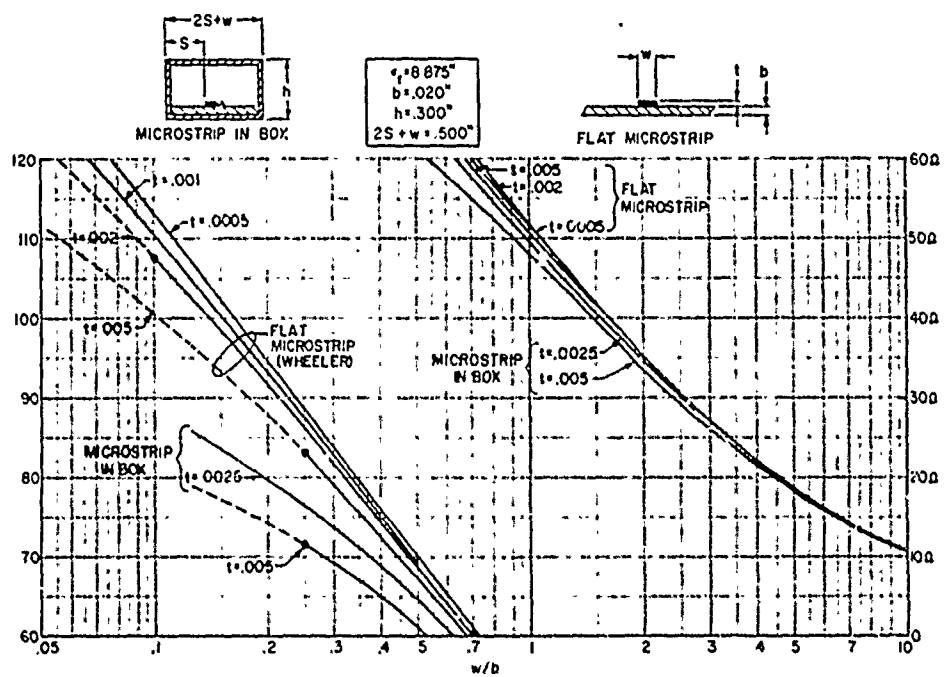
Figure 6. Characteristic impedance of the microstrip line calculated by Stinehelfer (1968).

microstrip lines and other related structures (Yamashita and Mittra, 1968; Yamashita, 1968). It has been shown by the above authors that the method is numerically very efficient.

For the sake of illustration we consider the shielded double-layer microstrip line shown in Figure 7. The conventional microstrip line may be obtained from this structure by letting $\varepsilon_1^* = \varepsilon_2^*$, $\varepsilon_3^* = 1$, and $d \to \infty$, where ε_1^*, ε_2^* and ε_3^* are the relative dielectric constants.

Once again we will compute the capacitance per unit length along the uniform microstrip line. To this end, we first write Poisson's equation for the potential distribution $\phi(x, y)$ in the cross-sectional area of the line. For an infinitely thin strip,

$$\nabla_t^2 \phi(x, y) = -\frac{1}{\varepsilon} \rho(x) \, \delta(y - h - s - p)$$

$$\rho(x) = 0 \quad |x| > w/2 \tag{21}$$

where $\rho(x)$ is the charge distribution on the strip, ε is the permittivity, and δ is the Dirac delta function. Initially it is assumed that the spacing between the center strip and the dielectric sheet is p. The original structure is recovered by letting $p \to 0$ after applying the interface and boundary conditions. This artifice is convenient for separating the boundary condition at the dielectric interface and the continuity condition at $y = h + s$.

Next, we introduce the Fourier transform via the equation

$$\tilde{f}(\beta) = \int_{-\infty}^{\infty} f(x) \, e^{j\beta x} \, dx \tag{22}$$

and transform Equation (21) into the form

$$\left(\frac{d^2}{dy^2} - \beta^2 \right) \tilde{\phi}(\beta, y) = -\frac{1}{\varepsilon} \tilde{\rho}(\beta) \, \delta(y - h - s - p) \tag{23}$$
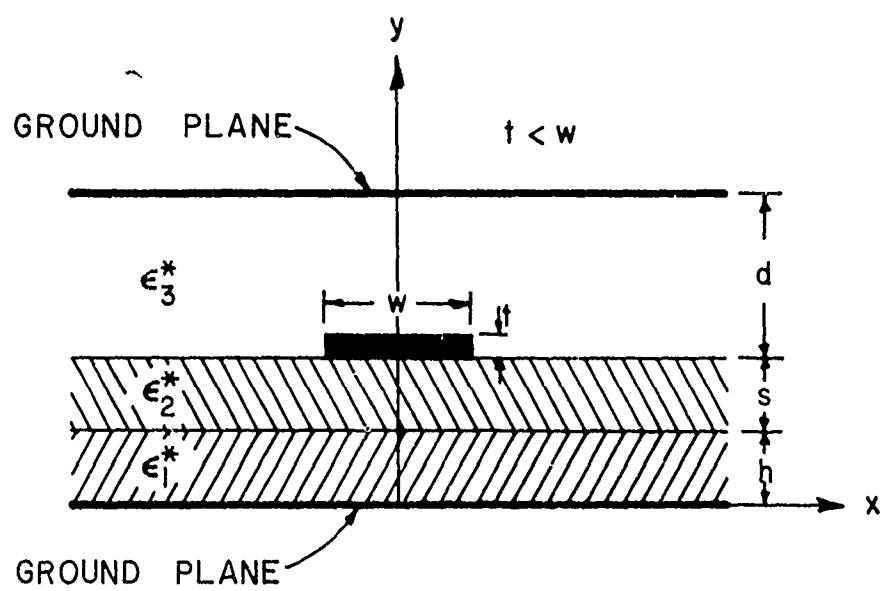
Figure 7. Shielded double-layer microstrip line.

where $\tilde{\phi}(\beta, y)$ is the Fourier transform of $\phi(x, y)$ and $\tilde{\rho}(\beta)$ is the transform of $\rho(x)$.

The general solution for $y \neq h + s + p$ is a combination of $\exp(\beta y)$ and $\exp(-\beta y)$. For the limiting case of $d \to \infty$, only the $\exp(-\beta y)$ type of solution is retained in the unbounded region. Returning to the case of finite d, the boundary and interface conditions for the transformed potential are given by

$$\tilde{\phi}(\beta, 0) = 0 \tag{24a}$$

$$\tilde{\phi}(\beta, h+0) = \tilde{\phi}(\beta, h-0) \tag{24b}$$

$$\varepsilon_2^* \frac{d}{dy} \tilde{\phi}(\beta, h+0) = \varepsilon_1^* \frac{d}{dy} \tilde{\phi}(\beta, h-0) \tag{24c}$$

$$\tilde{\phi}(\beta, h+s+0) = \tilde{\phi}(\beta, h+s-0) \tag{24d}$$

$$\varepsilon_3^* \frac{d}{dy} \tilde{\phi}(\beta, h+s+0) = \varepsilon_2^* \frac{d}{dy} \tilde{\phi}(\beta, h+s-0) \tag{24e}$$

$$\tilde{\phi}(\beta, h+s+p+0) = \tilde{\phi}(\beta, h+s+p-0) \tag{24f}$$

$$\varepsilon_3^* \frac{d}{dy} \tilde{\phi}(\beta, h+s+p+0) = \varepsilon_3^* \frac{d}{dy} \tilde{\phi}(\beta, h+s+p-0) - \frac{1}{\varepsilon_o} \tilde{\rho}(\beta) \tag{24g}$$

$$\tilde{\phi}(\beta, h+s+d) = 0 . \tag{24h}$$

After incorporating these boundary conditions into the general representation of the solutions, we obtain a set of linear inhomogeneous equations for the unknown coefficients of potential functions. Letting $p \to 0$ the solution for the potential on the strip is found to be

$$\tilde{\phi}(\beta, h+s) = \frac{1}{\varepsilon_o} \tilde{\rho}(\beta) \tilde{g}(\beta) \tag{25}$$

where ε_o is the free-space permittivity and

22

$$\tilde{g}(\beta) = \frac{\epsilon_1^* \coth(|\beta|h) + \epsilon_2^* \coth(|\beta|s)}{|\beta|\{\epsilon_1^* \coth(|\beta|h)[\epsilon_3^* \coth(|\beta|d)+\epsilon_2^* \coth(|\beta|s)]+\epsilon_2^*[\epsilon_2^*+\epsilon_3^* \coth(|\beta|d)\coth(|\beta|s)]\}} .$$

(26)

The quantity given by (26) is actually the transform of the Green's function evaluated at $y = h + s$. Also, the product appearing on the right-hand side in (25) corresponds to the convolution integral in the space domain. To compare Equation (25) with the corresponding equation in the space domain, the companion equation is included

$$\phi(x, \ h+s) = \frac{1}{\epsilon_o} \int_{-w/2}^{w/2} \rho(x')g(x, \ x'; \ h+s, \ h+s)dx'.$$

(27)

The value of the line capacitance, which is the desired quantity, can be obtained in the following manner from the variational expression. In the space domain we have

$$\frac{1}{C} = \frac{1}{Q^2} \int_{-w/2}^{w/2} \rho(x) \ \phi(x, \ h+s)dx$$

(28)

where

$$Q = \int_{-w/2}^{w/2} \rho(x)dx$$

(29)

is the total charge on the strip per unit length. Using Parseval's formula, Equation (28) can be converted into the transform domain

$$\frac{1}{C} = \frac{1}{2\pi Q^2} \int_{-\infty}^{\infty} \tilde{\rho}(\beta) \ \tilde{\phi}(\beta, \ h+s)d\beta.$$

(30)

The above formula is numerically more efficient to handle than the corresponding space domain version (28), because $\tilde{\phi}$ in (30) is just a product of two functions while ϕ in (28) is a convolution integral

23

represented by (27). This is, in fact, the major advantage to be gained by the use of the transform technique.

So far, we have considered only an infinitely thin strip. However, it is possible to approximately extend the method to the case of finite t providing t is not too large. This is done by replacing $\overset{\sim}{\phi}(\beta, h+s)$ in (30) by the average of $\overset{\sim}{\phi}(\beta, h+s)$ and $\overset{\sim}{\phi}(\beta, h+s+t)$ where $\overset{\sim}{\phi}(\beta, h+s+t)$ is the potential distribution at $y = h + s + t$. The expression for the transform of this potential is

$$\overset{\sim}{\phi}(\beta, h+s+t) = \frac{\sinh[|\beta|(d - t)]}{\sinh(|\beta|d)} \overset{\sim}{\phi}(\beta, h+s). \tag{31}$$

The line capacitance may now be expressed as

$$\frac{1}{C} = \frac{1}{2\pi Q^2} \int_{-\infty}^{\infty} \overset{\sim}{\rho}(\beta) \overset{\sim}{\phi}(\beta, h+s) \tilde{h}(\beta) \, d\beta \tag{32}$$

where

$$\tilde{h}(\beta) = \frac{1}{2} \left\{ 1 + \frac{\sinh[|\beta|(d - t)]}{\sinh(|\beta|d)} \right\}. \tag{33}$$

The final form of the line capacitance including the strip thickness is

$$\frac{1}{C} = \frac{1}{\pi Q^2 \varepsilon_0} \int_{0}^{\infty} [\overset{\sim}{\rho}(\beta)]^2 \tilde{g}(\beta) \tilde{h}(\beta) \, d\beta. \tag{34}$$

The unloaded line capacitance C_0 is obtained by letting $\varepsilon_1^* = \varepsilon_2^* = \varepsilon_3^* = 1$ in (34).

Although $\overset{\sim}{\rho}(\beta)$ is still unknown, the variational nature of (34) introduces only a second-order error when an approximate form of $\overset{\sim}{\rho}(\beta)$ is substituted into it. Since the stationary expression (34) gives an upper bound of 1/C, the calculated value of C is always

24

smaller than the correct value. Hence the choice of $\tilde{\rho}(\beta)$ that

maximizes the value of C clearly yields the result that is closest

to the exact value for the capacitance. Several trial functions for

this problem have been tested by Yamashita and Mittra (1968) and

Yamashita (1968),and numerical results have been reported for two

different trial functions. These are

$$(1) \quad \rho(x) = \begin{cases} |x|, & -\dfrac{w}{2} \le x \le \dfrac{w}{2} \\ 0 & \text{otherwise} \end{cases} \tag{35a}$$

$$\frac{\tilde{\rho}(\beta)}{Q} = \frac{2\,\sin(\beta\,w/2)}{\beta\,w/2} - \left[\frac{\sin(\beta\,w/4)}{\beta\,w/4}\right]^2 \tag{35b}$$

$$(2) \quad \rho(x) = \begin{cases} 1 + |2x/w|^3, & -\dfrac{w}{2} \le x \le \dfrac{w}{2} \\ 0 & \text{otherwise} \end{cases} \tag{36a}$$

$$\frac{\tilde{\rho}(\beta)}{Q} = \frac{8}{5}\left\{\frac{\sin(\beta\,w/2)}{\beta\,w/2}\right\} + \frac{12}{5(\beta\,w/2)^2}\left\{\cos(\beta\,w/2)\right.$$

$$\left. - \frac{2\,\sin(\beta\,w/2)}{\beta\,w/2} + \frac{\sin^2(\beta\,w/4)}{(\beta\,w/4)^2}\right\}. \tag{36b}$$

Figures 8-12 present the numerical results for the microstrip

lines where $\varepsilon_1^* = \varepsilon_2^* = \varepsilon^*$, $\varepsilon_3^* = 1$ and $d \to \infty$. The trial function in

(35b) has been used for computing these data. Figure 9 presents a

comparison of the results obtained by this process with those of

Wheeler. In addition, a comparison with the experimental results

obtained by Arditi (1955), Dukes (1956), and Hyltin (1965) is

exhibited in Figures 10 and 12. Numerical results for the shielded

microstrip line were calculated using the expression in Equation (36b)

for the trial charge distribution. These data are presented in

Figures 13-16. Typical computation time was less than 10 seconds

on an IBM 7094 computer.

25
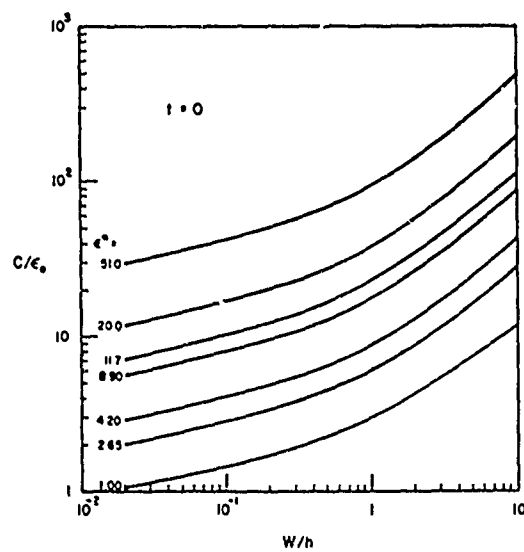
Figure 8. Line capacitance versus strip width and strip height.
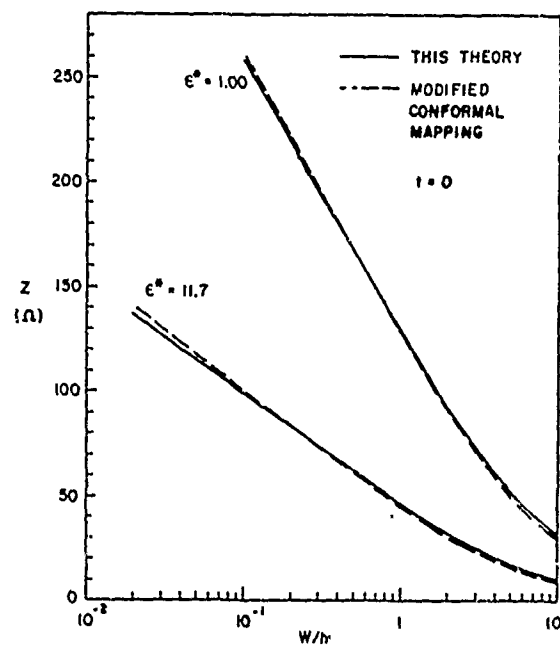
Figure 9. Calculated result for characteristic impedance and comparison
with the results by Wheeler (1965).
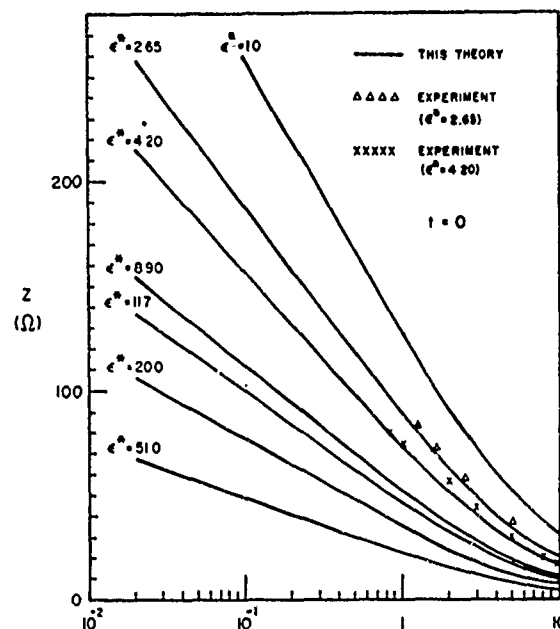
Figure 10. Theoretical and experimental characteristic impedance for various dielectric constants. Experimental results are those of Dukes (1956) [ΔΔΔΔ] and Arditi (1955) [xxxxx].
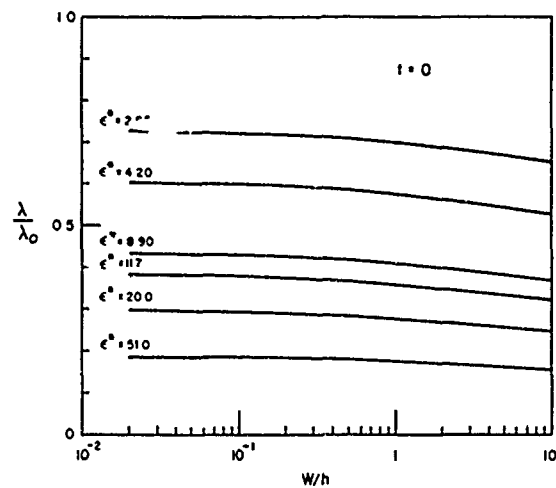
Figure 11.   Guide wavelength versus strip width and strip height.
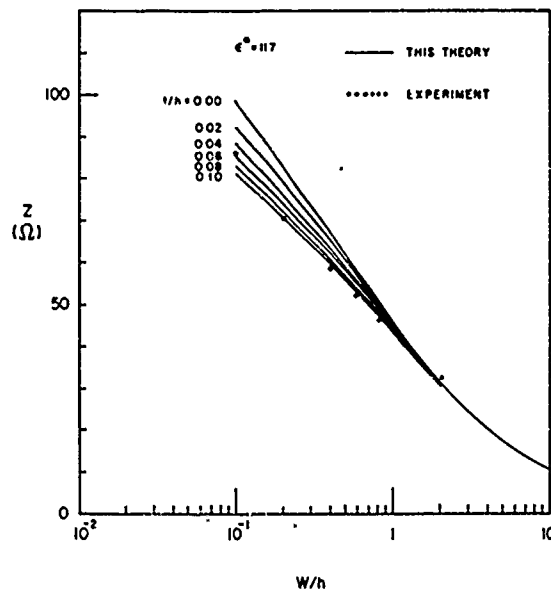
Figure 12. Theoretical and experimental results for the effect of strip thickness on characteristic impedance with ε* = 11.7. The experimental results are those of Hyltin (1965).

30
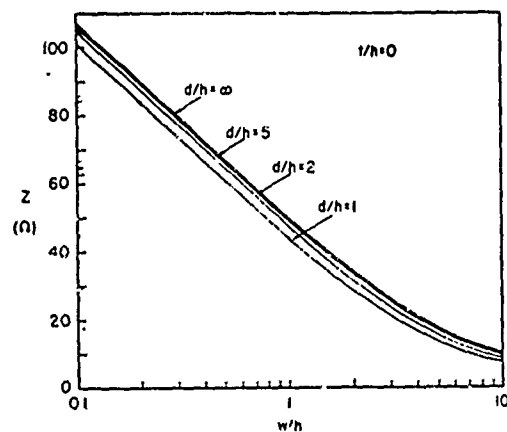
Figure 13. The calculated characteristic impedance. $\varepsilon_1^* = 9.9$ (Sapphire); $\varepsilon_3^* = 1$; $s = 0$; $t = 0$.
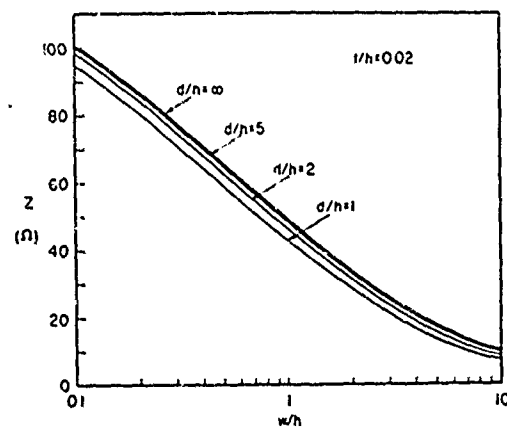
Figure 14. The calculated characteristic impedance. $\varepsilon_1^* = 9.9$ (Sapphire); $\varepsilon_3^* = 1$; $s = 0$; $t = 0.02h$.
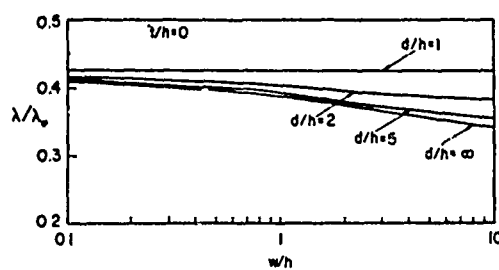
Figure 15. The calculated guide wavelength. $\varepsilon_1^* = 9.9$ (Sapphire); $\varepsilon_3^* = 1$; $s = 0$; $t = 0$.
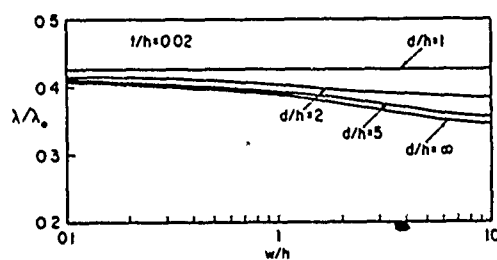
Figure 16. The calculated guide wavelength. $\varepsilon_1^* = 9.9$ (Sapphire); $\varepsilon_3^* = 1$; $s = 0$; $t = 0.02h$.

32

Before terminating this discussion, it will be useful to present a systematic procedure for improving the approximate solution for the charge distribution. This is accomplished via the application of Galerkin's method or Rayleigh-Ritz procedure in the transform domain (Ward, Mittra, and Itoh, 1971). The procedure is outlined in the following.

Let us first rewrite Equation (25) as follows

$$\tilde{\phi}_i(\beta, h+s) \div \tilde{\phi}_o(\beta, h+s) = \frac{1}{\varepsilon_o} \tilde{\rho}(\beta) \tilde{g}(\beta) \qquad (37)$$

where

$$\tilde{\phi}_i(\beta, h+s) = \int_{-w/2}^{w/2} \phi(x, h+s) e^{j\beta x} dx \qquad (38a)$$

$$\tilde{\phi}_o(\beta, h+s) = \int_{-\infty}^{-w/2} \phi(x, h+s) e^{j\beta x} dx + \int_{w/2}^{\infty} \phi(x, h+s) e^{j\beta x} dx.$$

$$(38b)$$

It should be noted that $\tilde{\phi}_i$ is known since $\phi(x, h+s)$ is given for $|x| < w/2$ on the strip. However $\tilde{\phi}_o$, the transform of $|x| > w/2$, is not known since $\phi(x, h+s)$ is as yet unknown for $|x| > w/2$ (outside the strip).

The next step is to apply Galerkin's method to Equation (37). To this end $\tilde{\rho}(\beta)$ is expanded in terms of known basis functions $\tilde{\rho}_n(\beta)$ with the following unknown weight coefficients

$$\tilde{\rho}(\beta) = \sum_{n=1}^{N} c_n \tilde{\rho}_n(\beta). \qquad (39)$$

We choose the basis functions $\tilde{\rho}_n(\beta)$ such that their inverse transforms have finite support in the space domain, i. e.,

$$\rho_n(x) = \frac{1}{2\pi} \int_{-\infty}^{\infty} \tilde{\rho}_n(\beta) e^{-j\beta x} d\beta = 0, \quad |x| > w/2.$$

$$(40)$$

33

Next Equation (39) is substituted into (37) and the inner product is taken of both sides of the resultant equation with $\overset{\sim}{\rho}_n(\beta)$, $n = 1, 2, \cdots$.

This leads to the following matrix equation

$$b_m = \sum_{n=1}^{N} K_{mn} \, c_n \qquad\qquad m = 1, 2, \cdots N \qquad (41)$$

where

$$b_m = \int_{-\infty}^{\infty} \overset{\sim}{\rho}_m(\beta) \, \overset{\sim}{\phi}_i(\beta, \, h+s)d\beta = \frac{1}{2\pi} \int_{-w/2}^{w/2} \rho_m(x)\phi_i(x, \, h+s)dx$$
$$(42a)$$

$$K_{mn} = \frac{1}{\varepsilon_0} \int_{-\infty}^{\infty} \overset{\sim}{\rho}_m(\beta) \, \tilde{g}(\beta) \, \overset{\sim}{\rho}_n(\beta)d\beta. \qquad (42b)$$

It should be mentioned that (42a) has been derived via the use of Parseval's formula. An application of this formula helps to eliminate unknown $\overset{\sim}{\phi}_0$ which is no longer present in (42a). The integral of the product $\overset{\sim}{\phi}_0$ and $\overset{\sim}{\rho}_m$ does not contribute to (42a) because the inverse transforms of these functions are nonzero in complementing regions only, and hence their product is identically zero.

The next step in the solution is to invert the matrix Equation (41) and solve for the coefficients c_n. The line capacitance can then be obtained in terms of the c_n by using the formula

$$C = \frac{1}{V_t} \sum_{n=1}^{N} c_n \int_{-w/2}^{w/2} \rho_n(x)dx \qquad (43)$$

where V_t is the potential difference between the strip and the ground plane.

It is well known that the expression in (43) gives a stationary value of C and that the accuracy of the result may be improved by

34

increasing N. Experience has shown that the increase in the accuracy is usually rather slow after initial improvement when N is increased from a very small value.

2.5 Integral Equation Method

So far we have discussed three different techniques for determining the characteristics of the microstrip line. Two of these, viz., the modified conformal mapping and the variational methods find their principal use in the cases where the center strip is thin. However, for some practical microwave integrated circuit structures, the effect of finite thickness of the center strip cannot be neglected.

Since the relaxation method is principally a numerical technique, it can be applied to the case of the arbitrarily thick center strip. However, as mentioned earlier, the drawback of this method is that its numerical convergence is rather slow.

In this section, an integral equation approach will be presented that can be used to solve the thick-strip problem in a numerically efficient manner (Yamashita and Atsuki, 1970). Consider the cross section of the transmission line shown in Figure 17. The potential satisfies the Poisson's equation.

$$\nabla^2_t \phi(x, \ y) = - \frac{1}{\varepsilon} \rho(x, \ y). \qquad (44)$$

Define a Green's function $G(x, \ y,; \ x_o, \ y_o)$ via

$$\nabla^2_t G(x, \ y; \ x_o, \ y_o) = - \frac{1}{\varepsilon} \ \delta(x - x_o) \ \delta(y - y_o) \qquad (45)$$

where G satisfies the same boundary and continuity conditions except for the source condition. The Green's function is the potential at

35
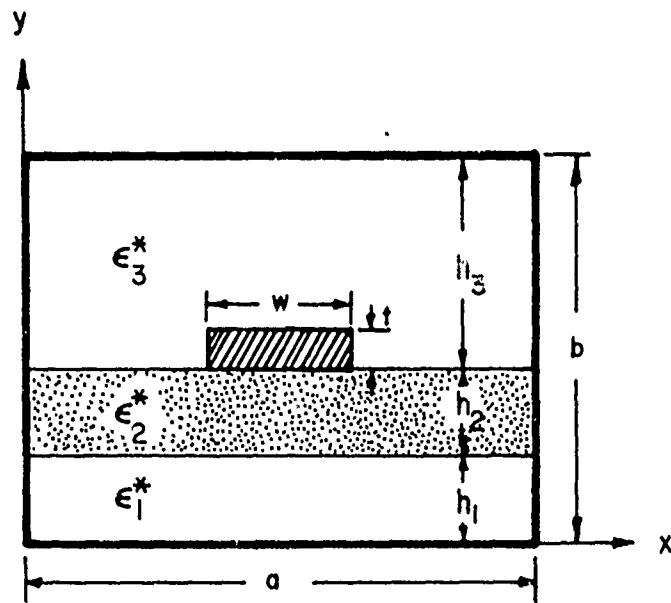
Figure 17. Cross-sectional view of thick-strip transmission line with
multi-dielectric layers and shielding structure.

the point (x, y) due to a unit charge located at (x_o, y_o). Applying the superposition principle, the potential function $\phi(x, y)$ in (44) may be expressed as

$$\phi(x, y) = \int G(x, y; x_o, y_o)\rho(x_o, y_o)d\ell_o \quad (46)$$

where the integral is defined over the conductor surface.

To find the Green's function we proceed as follows: First, we expand the Green's function in a Fourier series in the x-coordinate. Next, the partial differential equation (45) is reduced to a set of ordinary differential equations of the variable y. The solution of each ordinary differential equation in each region of dielectric materials is a linear combination of hyperbolic functions. When the boundary and interface conditions are applied to each of these solutions, the amplitude coefficients of these functions generate a set of linear inhomogeneous equations which are subsequently solved for the unknown amplitude coefficients. Substituting these coefficients in the equation for the Green's function completes the derivation of the desired expression for the Green's function. When the source located in the range $h_1 + h_2 \leq y_o \leq b$ and the boundary condition at the outer conductor is $G = 0$, the expression for the Green's function is given by (Yamashita and Atsuki, 1970, 1971)

$$G(x, y; x_o, y_o) = \sum_{n=1}^{\infty} \frac{2}{n\pi\epsilon_3^*} \frac{\Delta_n(y_o - h_1 - h_2)}{\Delta_n(h_3)} \sinh\left[\frac{n\pi(b - y)}{a}\right]$$

$$\cdot \sin\left(\frac{n\pi x_o}{a}\right) \sin\left(\frac{n\pi x}{a}\right), \qquad h_1 + h_2 \leq y_o \leq y \leq b$$

$$= \sum_{n=1}^{\infty} \frac{2}{n\pi\epsilon_3^*} \frac{\Delta_n(y - h_1 - h_2)}{\Delta_n(h_3)} \sinh\left[\frac{n\pi(b - y_o)}{a}\right]$$

$$\cdot \sin\left(\frac{n\pi x_o}{a}\right) \sin\left(\frac{n\pi x}{a}\right), \qquad h_1 + h_2 \leq y \leq y_o \leq b$$

$$(47)$$

37

where

$$\Delta_n(y) = \varepsilon_1^* \varepsilon_2^* \cosh\left(\frac{n\pi h_1}{a}\right) \cosh\left(\frac{n\pi h_2}{a}\right) \sinh\left(\frac{n\pi y}{a}\right)$$

$$+ \varepsilon_2^* \varepsilon_3^* \sinh\left(\frac{n\pi h_1}{a}\right) \cosh\left(\frac{n\pi h_2}{a}\right) \cosh\left(\frac{n\pi y}{a}\right)$$

$$+ \varepsilon_3^* \varepsilon_1^* \cosh\left(\frac{n\pi h_1}{a}\right) \sinh\left(\frac{n\pi h_2}{a}\right) \cosh\left(\frac{n\pi y}{a}\right)$$

$$+ \varepsilon_2^{*2} \sinh\left(\frac{n\pi h_1}{a}\right) \sinh\left(\frac{n\pi h_2}{a}\right) \sinh\left(\frac{n\pi y}{a}\right).$$

(48)

The representations of the Green's functions for the first- and second-dielectric regions have been omitted[*] here as they are not needed for subsequent derivation.

By following the conventional methods for deriving the integral equation for the charge distribution, one arrives at the desired equation

$$\phi(x, y) = V = \int G(x, y; x_o, y_o)\rho(x_o, y_o)d\ell_o.$$

(49)

The equation can now be transformed into a matrix form by the conventional discretization procedure. The results obtained by solving this matrix equation are presented in Figure 18.

Typical computation time of the characteristic impedance per one structure is about 30 seconds when the strip conductor was divided into 30 sections (Yamashita and Atsuki, 1971).

2.6 Generalized Wiener-Hopf Techniques

In contrast to some other approaches, the method to be described

---

[*] However the interested reader may find the pertinent expressions in Yamashita and Atsuki (1970).
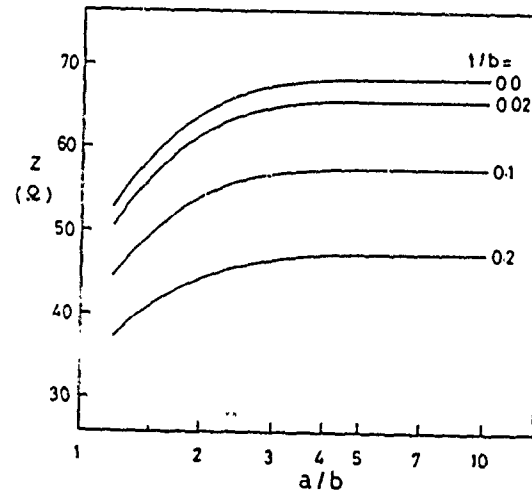
Figure 18. Characteristic impedance of thick-strip line of Figure 17; $\varepsilon_1^* = \varepsilon_3^* = 1$; $\varepsilon_2^* = 9.35$; $h_1 = h_3 = 0.4b$; $h_2 = 0.2b$; $w = 0.5b$.

below is useful for deriving accurate numerical results for both the

charge and the potential distributions for the microstrip line shown

in Figure 7. The technique was presented in a recent paper by Mittra

and Itoh (1970). The starting point is the equation for the charge

distribution ρ in the transformed domain. This equation, which was

derived earlier in Section 2.6, is reproduced here for reference

purposes. The transformed equation reads

$$\frac{1}{\varepsilon_o} \; \overset{\sim}{\rho}(\beta)\tilde{g}(\beta) \; = \; \overset{\sim}{\phi}(\beta, \; h+s). \tag{25}$$

A semirigorous rather than variational method for solving this

equation will now be discussed. Note first of all that the potential

of the center strip is one volt. Thus, we can write the potential

function at $y = h + s$, i. e., in the plane of the strip, in the form

$$\phi(x, \; h+s) \; = \; h(x - \frac{w}{2}) \; U(x - \frac{w}{2}) \; + \; [U(x + \frac{w}{2}) \; - \; U(x - \frac{w}{2})] \; + \; h(-x - \frac{w}{2}) \; U(-x - \frac{w}{2})$$

$$\tag{50}$$

where $h(x)$ is an unknown function representing the potential distribution

at $y = h + s$ for $|x| > w/2$. Also, $U(x)$ is the unit step function with

the usual definition $U(x) = 1$, $x > 1$ and zero, otherwise. The Fourier

transform of $\phi(x, \; h+s)$ can now be written as

$$\overset{\sim}{\phi}(\beta, \; h+s) \; = \; 2 \; \frac{\sin(\beta \; w/2)}{\beta} \; + \; e^{j\beta w/2} \; H_+(\beta) \; + \; e^{-j\beta w/2} H_+(-\beta)$$

$$\tag{51}$$

where $H_+(\beta)$ is the Fourier transform of $h(x)U(x)$. The subscript +

has been introduced to indicate that $H_+(\beta)$ is regular in the upper half

of the complex β-plane. We also note that in view of the symmetry

in the space domain $\overset{\sim}{\phi}$ is symmetric in β in the transform domain.

Substituting (51) in (25) we get

40

$$\frac{\tilde{g}(\beta)\overset{\sim}{\rho}(\beta)}{\varepsilon_o} = 2\,\frac{\sin(\beta\ w/2)}{\beta} + e^{j\beta w/2}\,H_+(\beta) + e^{-j\beta w/2}\,H_+(-\beta) \qquad (52)$$

which is the desired equation to be solved for the two unknowns $\rho(\beta)$

and $H_+(\beta)$. This can be done by an extension of the Wiener-Hopf

technique introduced by Mittra and Lee (1971). In order to extract

the solution for the two unknowns from a single equation, we must make

use of certain additional information available to us. First, $\overset{'}{\rho}(\beta)$,

which is the Fourier transform of a function with a finite support

in the x domain, must be regular in the entire finite region of the

complex β-plane. Second, the other unknown $H_+(\beta)$ must have all of its

singularities only in the lower half of the β-plane. We will now

show how these analyticity properties of the functions involved may

be put to advantageous use for constructing a matrix equation that

is capable of yielding accurate solutions in an efficient manner.

As a first step, $\overset{\cdot}{g}(\beta)$ is rewritten as follows

$$\overset{\backslash}{g}(\beta) = K_o \prod_{n=1}^{\infty} \frac{\left(1 - \dfrac{\beta^2}{\beta_n^2}\right)\left(1 - \dfrac{\beta^2}{\gamma_n^2}\right)}{\left(1 - \dfrac{\beta^2}{\alpha_n^2}\right)} \qquad (53)$$

where K_o is a known constant; $I_m(\alpha_n) > 0$, $I_m(\beta_n) > 0$, $I_n(\gamma_n) > 0$, $: \alpha_n$

are the poles; and $\pm\beta_n$, $:\gamma_n$ are zeros of $\tilde{g}(\beta)$. Since both $\overset{\sim}{\rho}(\beta)$ and

the first term of the right-hand side of (52) are regular in the finite part

of the β-plane, the lower half-plane singularities at $\beta = -\alpha_n$ of the

left-hand side of (52) must coincide with the poles of $H_+(\beta)$ Likewise,

the singularities at $\beta = +\alpha_n$ must be coincident with the poles of $H_+(-\beta)$.

Furthermore, $H_+(\beta)$ and $H_+(-\beta)$ can have no other singularities.

41

Substituting (53) in (52) and evaluating both sides of the resultant equation at $\beta = \beta_m$, $\beta = \gamma_m$, $m = 1, 2, \cdots \infty$ we obtain

$$\sum_{n=1}^{\infty} \frac{c_n}{\alpha_n - \beta_m} + \lambda_m \sum_{n=1}^{\infty} \frac{c_n}{\alpha_n + \beta_m} = \frac{1 - \lambda_m}{j\beta_m} \qquad (54a)$$

$$m = 1, 2, \cdots \infty$$

$$\sum_{n=1}^{\infty} \frac{c_n}{\alpha_n - \gamma_m} + \xi_m \sum_{n=1}^{\infty} \frac{c_n}{\alpha_n + \gamma_m} = \frac{1 - \xi_m}{j\gamma_m} \qquad (54b)$$

where

$$\lambda_m = e^{j\beta_m w} \quad , \quad \xi_m = e^{j\gamma_m w} . \qquad (55)$$

The solutions of the simultaneous equation of the type (54) have been discussed in a number of recent publications (Mittra and Itoh, 1970, 1972; Mittra and Lee, 1971) and will not be elaborated on. The essential step in deriving the solution entails the construction of a complex function $f(\omega)$ with the following properties:

(a) $f(\omega)$ has simple poles at $\omega = \alpha_n$, $n = 1, 2, \cdots \infty$ and at $\omega = 0$;

(b) $f(\beta_m) + \lambda_m \bar{f}(-\beta_m) = 0$

$$m = 1, 2, \cdots \infty$$

$f(\gamma_m) + \xi_m f(-\gamma_m) = 0;$

(c) $f(\omega) \sim |\omega|^{-3/2}$ for $|\omega| \to \infty$;

(d) the residue of $f(\omega)$ at $\omega = 0$, say $R_f(0)$, is $-j$. If such a function is available, then

$$c_n = R_f(\alpha_n). \qquad (56)$$

42

The function $f(w)$ may be expressed as (Mittra and Itoh, 1970)

$$f(w) = Kf_o(w)P(w) \qquad (57a)$$

$$f_o(w) = e^{Lw} \prod_{n=1}^{\infty} \frac{\left(1 - \dfrac{w}{\beta_n}\right)\left(1 - \dfrac{w}{\gamma_n}\right)}{\left(1 - \dfrac{w}{\alpha_n}\right)} \qquad (57b)$$

where K is a constant determinable by the application of condition (d) above, and $P(w)$ is

$$P(w) = 1 + \sum_{n=1}^{\infty} \frac{F_n}{1 - \dfrac{w}{\beta_n}} + \sum_{n=1}^{\infty} \frac{G_n}{1 - \dfrac{w}{\gamma_n}} . \qquad (58)$$

F_n and G_n are as yet undetermined. The factor e^{Lw} in (57b), in which L is a known constant, ensures the algebraic nature of $f_o(w)$, viz., $f_o(w) \sim |w|^{-(3/2)}$ as $|w| \to \infty$.

There still remains the task of determining the infinitely many unknown constants F_n and G_n. However, the summation in (58) can be effectively truncated at a finite number, say $n = N$, with N small, because λ_m and ξ_m decrease exponentially with m as β_m and ξ_m have positive imaginary parts. Hence, for $n > N$, the condition (b) can be satisfied by $f(\beta_m) = f(\gamma_m) = 0$. There are now 2N unknowns F_n and G_n. These may be obtained by substituting $f(w)$ in the condition (b) followed by the inversion of the resultant matrix equation for F_n and G_n. Typically, highly accurate solutions are obtained with a matrix size 2N equal to 10 or less. This is due mainly to the fact that the asymptotic nature of the function $f(w)$ is incorporated in the solution process making the series representation a highly convergent one

Once the function $f(w)$ has been generated, c_n can be obtained by taking the residues of $f(w)$ at $w = \alpha_n$. $H_+(\beta)$ and $\rho(\beta)$ may be readily

43

obtained once the coefficients c_n are known. The potential distribution,

e. g. at $y = h$, and the charge distribution on the strip are obtained

by taking the inverse transforms, specifically

$$h(x) = -j \sum_{n=1}^{\infty} c_n e^{j\alpha_n x} \tag{59}$$

$$\frac{\rho(x)}{\varepsilon_o} = \frac{1}{K_o} + j \sum_{n=1}^{\infty} \left\{ \frac{\beta_n - \beta}{\tilde{g}(\beta)} \right|_{\beta \to \beta_n} f(-\beta_n) \left[e^{i\beta_n[(w/2)+x]} + e^{j\beta_n[(w/2)-x)]} \right] $$

$$+ \frac{\gamma_n - \beta}{\tilde{g}(\beta)} \right|_{\beta \to \gamma_n} \cdot f(-\gamma_n) \left[e^{j\gamma_n[(w/2)+x]} + e^{j\gamma_n[(w/2)-x]} \right] \right\}. \tag{60}$$

Figure 19 shows the potential and charge distribution in the shielded

microstrip line (Mittra and Itoh, 1970).For a shielded line (60)

becomes

$$\frac{\rho(z)}{\varepsilon_o} = \frac{\varepsilon_1^*}{h} + \frac{\varepsilon_3^*}{d} + \sum_{n=1}^{\infty} \left\{ \frac{\varepsilon_1^* \beta_m}{jh} f(-\beta_m) \left[e^{j\beta_m[(w/2)+x]} + e^{j\beta_m[(w/2)-x]} \right] \right. $$

$$\left. + \frac{\varepsilon_3^* \gamma_m}{jd} f(-\gamma_m) \left[e^{j\gamma_m[(w/2)+x]} + e^{j\gamma_m[(w/2)-x]} \right] \right\}. \tag{61}$$

The infinite series in (59), (60), or (61) converges very efficiently

because of the decaying exponential multicative factors appearing

in the summation terms. It is interesting to note that the first

two terms in (61) correspond to the parallel plate capacitance while

the infinite summation represents the edge capacitance. Thus, the

fringing effect is accurately estimated by the application of this

method.

44
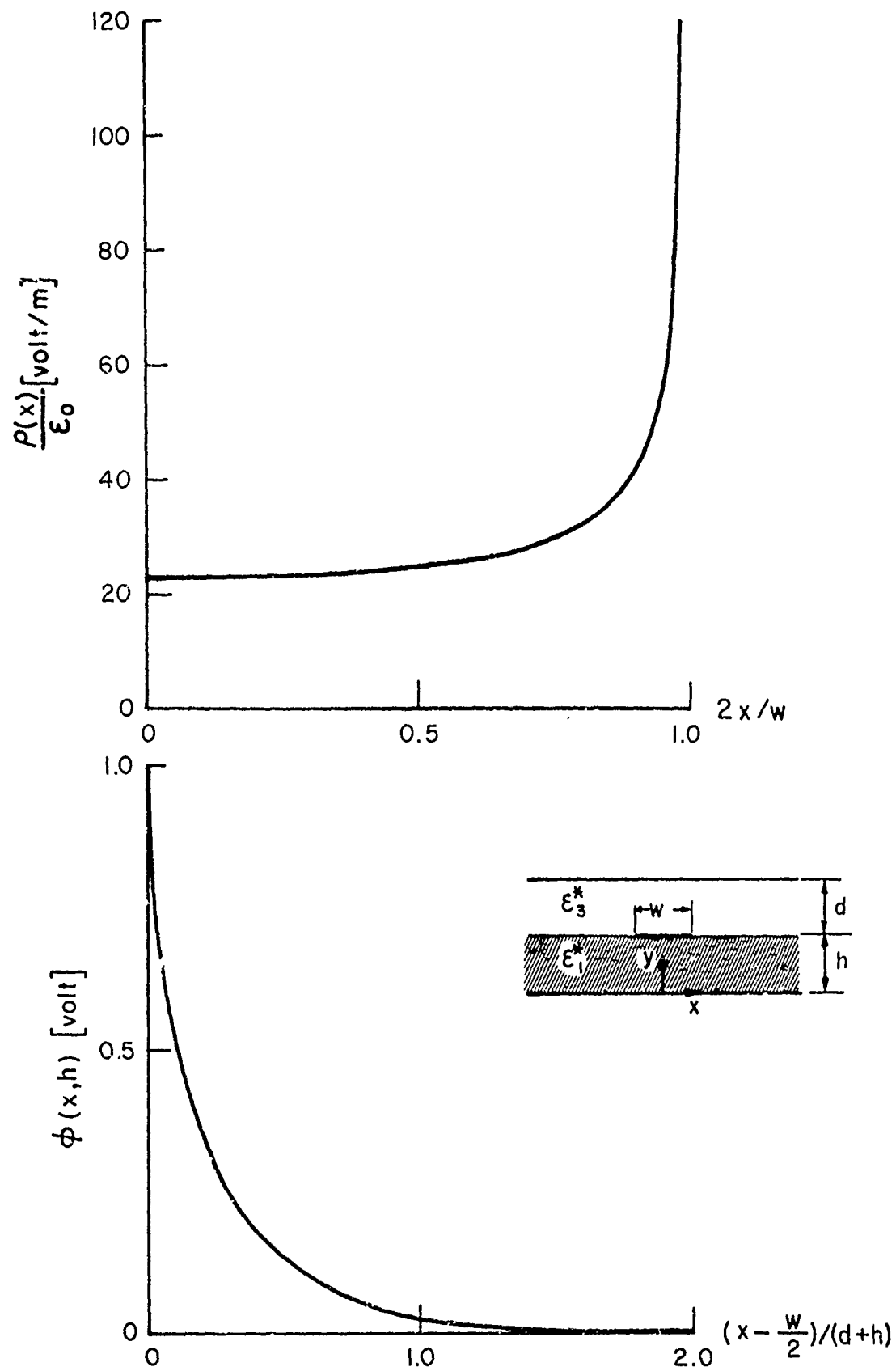
Figure 19. The charge distribution on the strip and the potential distribution at $y = h$. $\varepsilon_1^* = 9.9$ (Sapphire); $\varepsilon_3^* = 1$; $s = 0$; $h = d$; $w = d$.

Furthermore, a knowledge of the rate of fall-off of the potential away from the center strip is useful in estimating the coupling between two adjacent lines on the same substrate.

III. WAVE THEORY ANALYSIS OF MICROSTRIP LINES

3.1 Preliminary Discussion

In the last section a number of quasi-TEM techniques were presented
for calculating the characteristic parameters of microstrip lines.
However, strictly speaking, since the wave velocity in the dielectric
is different from that in free space, it is not possible to support
a TEM mode in the structure. In fact, one can show that not even
pure TE or TM modes can exist in the structure but that it can
only support a hybrid mode (i. e., one in which both the longitudinal
electric and magnetic components are nonzero) This can be seen
rather easily from the following consideration   Consider the cross
section of a shielded microstrip line shown in Figure 20. If the
center strip is removed from the waveguide, it reduces to a partially
filled guide that can support longitudinal section electric (LSE) or
longitudinal section magnetic (LSM) types of mode (see for instance
Collin, 1960), but not a pure TE or TM mode. The insertion of the
center strip in the waveguide causes currents to flow in both the x-
and z- directions on this strip. These, in turn, serve to couple the
LSE and LSM modes so that the final mode configuration in the shielded
microstrip line is hybrid in nature.

Although this fact has been recognized for quite some time
(Deschamps, 1954; Wu, 1957), a rigorous full-wave analysis of the
dispersion characteristics of the microstrip line was not carried out
until quite recently. The following paragraphs will describe a
number of these full-wave techniques suitable for calculating the
dispersion characteristics of microstrip lines at arbitrary frequencies.

47
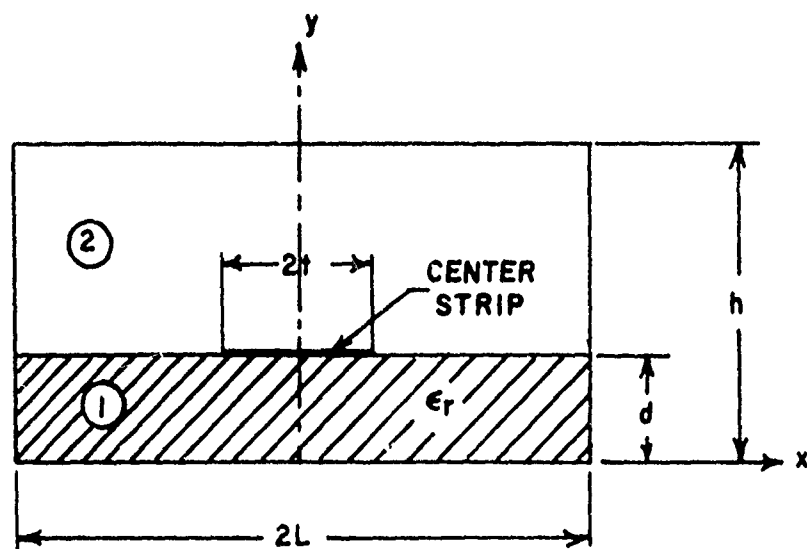
Figure 20. Cross section of the microstrip line in a shielding case.

We will begin with the hybrid-mode analysis of the shielded version of the microstrip line and follow this with a discussion of the open microstrip line. The important steps in this analysis are

(i) Representation of the field components in terms of E- and H- type of scalar potentials;

(ii) Application of boundary and interface conditions to the field components;

(iii) Derivation of a characteristic equation for the propagation constant in the guide; and finally,

(iv) Solution of the characteristic equation and computation of the dispersion $(k - \beta)$ diagram.

3.2 Shielded Microstrip Lines

Figure 20 shows the cross section of the shielded microstrip line. The center strip is assumed to be infinitely thin and perfectly conducting. In addition, the dielectric material and the metal shielding are assumed to be lossless. It is well known that the hybrid field components can be expressed in terms of a super-position of the TE and TM fields, which are, in turn, derivable from scalar potentials $\psi^{(e)}$ and $\psi^{(m)}$ (Harrington, 1961). The total field can be written as follows:

$$E_{zi} = j \; \frac{k_i^2 - \beta^2}{\beta} \; \psi_i^{(e)}(x, y) \; e^{-j\beta z} \tag{62a}$$

$$H_{zi} = j \; \frac{k_i^2 - \beta^2}{\beta} \; \psi_i^{(h)}(x, y) \; e^{-j\beta z} \tag{62b}$$

$$\overline{E}_{ti} = \nabla_t \psi_i^{(e)}(x, y) \; e^{-j\beta z} - \frac{\omega\mu}{\beta} \; \hat{z} \times \nabla_t \psi_i^{(h)}(x, y) e^{-j\beta z} \tag{62c}$$

49

$$\overline{H}_{ti} = \frac{\omega \varepsilon_i}{\beta} \hat{z} \times \nabla_t \Psi_i^{(e)}(x, y) \ e^{-j\beta z} + \nabla_t \Psi_i^{(h)}(x, y) \ e^{-j\beta z}. \quad (62d)$$

The parameter β in the above equation is the unknown propagation constant, $\hat{z}$ is the z-directed unit vector, ω is the operating frequency

$$k_1 = \omega \sqrt{\varepsilon_r \varepsilon_o \mu_o}, \quad k_2 = \omega \sqrt{\varepsilon_o \mu_o}, \quad (63)$$

ε_r is the relative dielectric constant of the substrate, and ε_o and μ_o are the permittivity and permeability of free space, respectively. The subscript t in Equation (62) denotes the transverse coordinate variables x and y and the superscripts (e) and (h) are to be associated with the TM and TE types of fields, respectively. The subscripts i = 1, 2 serve to designate the regions 1 (substrate) or 2 (air).

From the symmetry of the structure, it is clear that two orthogonal sets of modes exist, one of which has a symmetric E_z and an antisymmetric H_z component (E_z even – H_z odd) while the other is characterized by E_z odd – H_z even. The dominant mode is the lowest order E_z even – H_z odd mode which approaches the quasi-TEM solution for low frequencies. In what follows we consider only the E_z even – H_z odd modes, although the methods presented here are equally applicable to the other types of modes as well.

3.2.1 Various methods for solving the shielded microstrip lines

(a) Integral Equation Method

The scalar potentials $\Psi_i^{(e)}$ and $\Psi_i^{(h)}$ satisfy the two-dimensional wave equation in region 1 and 2 as well as the requirement that the total tangential electric field derived from them vanish on the metallic periphery of the box. An additional boundary condition is that the total tangential magnetic fields vanish at the plane of

symmetry $x = 0$. In view of the boundary conditions on the side walls, it is appropriate to write

$$\Psi_1^{(e)} = \sum_{n=1}^{\infty} A_n^{(e)} \sinh \alpha_n^{(1)} y \cos \hat{k}_n x \qquad (64a)$$

$$\Psi_2^{(e)} = \sum_{n=1}^{\infty} B_n^{(e)} \sinh \alpha_n^{(2)} (h - y) \cos \hat{k}_n x \qquad (64b)$$

$$\Psi_1^{(h)} = \sum_{n=1}^{\infty} A_n^{(h)} \cosh \alpha_n^{(1)} y \sin \hat{k}_n x \qquad (64c)$$

$$\Psi_2^{(h)} = \sum_{n=1}^{\infty} B_n^{(h)} \cosh \alpha_n^{(1)} (h - y) \sin \hat{k}_n x \qquad (64d)$$

where $\hat{k}_n = [n - (1/2)] \, \pi/L$,

$$\alpha_n^{(1)} = \sqrt{\hat{k}_n^2 + \beta^2 - \varepsilon_r k_o^2} \, ,$$

$$\alpha_n^{(2)} = \sqrt{\hat{k}_n^2 + \beta^2 - k_o^2} \, ,$$

with $k_o = \omega \sqrt{\varepsilon_o \mu_o}$, the free-space wavenumber. The coefficients $A_n^{(e)}$, $A_n^{(h)}$, $B_n^{(e)}$, and $B_n^{(h)}$ are as yet unknown.

The total fields derived from $\Psi_i^{(e)}$ and $\Psi_i^{(h)}$ must satisfy the interface conditions at $y = d$. Imposing these on the symmetry conditions with respect to the y axis, one arrives at the following four conditions which are mutually independent.

(1) $E_{z1} = E_{z2}$ $\qquad$ $0 < x < L$

(2) $E_{x1} = E_{x2}$ $\qquad$ $0 < x < L$

(3) (a) $E_{z1} = 0$ $\qquad$ $0 < x < t$

$\qquad$ (b) $H_{x1} = H_{x2}$ $\qquad$ $t < x < L$

51

(4)   (a) $E_{x1} = 0$ $0 < x < t$

      (b) $H_{z1} = H_{z2}$ $0 < x < L$.

These conditions are now imposed on the field components derived

from (62) and (64). By using continuity requirements at $y = d$ and

applying the conditions that E_z and E_x vanish on the center strip,

one obtains a pair of coupled homogeneous Fredholm integral equations

of the first kind (Zysman and Varon, 1969). These are given by

$$\sum_{n=1}^{\infty} [G_n^{(1)}(\beta) \int_0^t h_1(\xi) \cos \hat{k}_n \xi d\xi + G_n^{(2)}(\beta) \int_t^L h_2(\xi) \sin \hat{k}_n \xi d\xi] \sin \hat{k}_n x = 0$$

(65a)

$$\sum_{n=1}^{\infty} [G_n^{(3)}(\beta) \int_0^t h_1(\xi) \cos \hat{k}_n \xi d\xi + G_n^{(4)}(\beta) \int_t^L h_2(\xi) \sin \hat{k}_n \xi d\xi] \cos \hat{k}_n x = 0.$$

(65b)

Here $G_n^{(i)}(\beta), i = 1, 2, 3, 4$ are known functions of β, and the

functions $h_1(\xi)$ and $h_2(\xi)$ are unknown functions of ξ. These

equations may be transformed into a matrix equation algorithm. The roots

of the determinantal equation of the resulting matrix may be

sought with the aid of a digital computer to yield the desired values

of β.

(b) Singular Integral Equation Method

      The singular integral equation method is known to provide

efficient solutions to a number of diffraction grating and waveguide

discontinuity problems, e. g., an iris diaphragm in a waveguide.

Recently, it has been shown that this technique can be advantageously

employed to solve the problem of dispersion in a shielded microstrip

line (Mittra and Itoh, 1971). The beginning stages of formulation

in this method are identical to the one presented in the previous

section; in fact, the starting point of this method is Equation (64)

52

of the last section. However, from that point on, the singular

integral equation method deviates fundamentally from the conventional

integral equation approach. A matrix equation is also derived in

this method but it is totally different in character and much more

efficient for extracting numerical solutions than the one obtained

from (65).

The first step in the singular integral equation approach is

to employ the conditions (1) and (2) to express $B_n^{(e)}$ and $B_n^{(h)}$ in terms

of $A_n^{(e)}$ and $A_n^{(h)}$. The imposition of conditions (3) and (4) then

leads to the following coupled equations for the coefficients $\overline{A}_n^{(e)}$

and $\overline{A}_n^{(n)}$

$$\sum_{n=1}^{\infty} \overline{A}_n^{(e)} \cos \hat{k}_n x = 0 \qquad\qquad 0 < x < t \qquad\qquad (66a)$$

$$\sum_{n=1}^{\infty} \overline{A}_n^{(e)} \hat{k}_n P_n(\beta) \cos \hat{k}_n x - \sum_{n=1}^{\infty} \overline{A}_n^{(h)} \hat{k}_n T_n(\beta) \cos \hat{k}_n x = 0$$
$$(66b)$$
$$t < x < L$$

$$\sum_{n=1}^{\infty} \overline{A}_n^{(e)} \hat{k}_n \sin \hat{k}_n x - \sum_{n=1}^{\infty} \overline{A}_n^{(h)} \hat{k}_n \sin \hat{k}_n x = 0 \quad 0 < x < t \quad (66c)$$

$$\sum_{n=1}^{\infty} \overline{A}_n^{(e)} Q_n(\beta) \sin \hat{k}_n x - \sum_{n=1}^{\infty} \overline{A}_n^{(h)} W_n(\beta) \sin \hat{k}_n x = 0$$
$$(66d)$$
$$t < x < L$$

where

$$\overline{A}_n^{(e)} = A_n^{(e)} \sinh \alpha_n^{(1)} d \qquad\qquad (67a)$$

$$\overline{A}_n^{(h)} = \frac{\omega\mu}{\beta} \frac{\alpha_n^{(1)}}{\hat{k}_n} A_n^{(h)} \sinh \alpha_n^{(1)} d \qquad (67b)$$

and $P_n(\beta)$, $T_n(\beta)$, $Q_n(\beta)$, and $W_n(\beta)$ are expressed as follows:

$$P_n(\beta) = \varepsilon_r \frac{\alpha_n^{(1)}}{\hat{k}_n} \coth \alpha_n^{(1)} d + \frac{\varepsilon_r - \overline{\beta}^2}{1 - \overline{\beta}^2} \frac{\alpha_n^{(2)}}{\hat{k}_n} \coth \alpha_n^{(2)} (h - d)$$

$$+ \overline{\beta}^2 \frac{\hat{k}_n}{\alpha_n^{(2)}} \frac{1 - \varepsilon_r}{1 - \overline{\beta}^2} \coth \alpha_n^{(2)} (h - d) \qquad (68a)$$

$$T_n(\beta) = \overline{\beta}^2 \left[\frac{\hat{k}_n}{\alpha_n^{(2)}} \coth \alpha_n^{(1)} d + \frac{\hat{k}_n}{\alpha_n^{(2)}} \coth \alpha_n^{(2)} (h - d) \right] \qquad (68b)$$

$$Q_n(\beta) = \frac{\hat{k}_n}{\alpha_n^{(2)}} \frac{1 - \varepsilon_r}{1 - \overline{\beta}^2} \coth \alpha_n^{(2)} (h - d) \qquad (68c)$$

$$W_n(\beta) = \frac{\varepsilon_r - \overline{\beta}^2}{1 - \overline{\beta}^2} \frac{\hat{k}_n}{\alpha_n^{(1)}} \coth \alpha_n^{(1)} d + \frac{\hat{k}_n}{\alpha_n^{(2)}} \coth \alpha_n^{(2)} (h - d) \qquad (68d)$$

where $\overline{\beta} = \beta/k_o$ is the normalized propagation constant.

At this point Equation (66) may be transformed into an infinite set of homogeneous simultaneous equations for $\overline{A}_n^{(e)}$ and $\overline{A}_n^{(h)}$ via the conventional technique of taking a scalar product with a complete set of functions appropriate for the various ranges in x. The solution for β may then be determined by seeking the zeros of the determinant associated with the above matrix equation.

We will, however, depart from this conventional procedure and instead transform (66) into an auxiliary set of equations with rapid convergence properties. To this end, (66a) is first differentiated with respect to x and the resultant equation is substituted into (66c).

54

This yields

$$\sum_{n=1}^{\infty} \overline{A}_n^{(e)} \hat{k}_n \sin \hat{k}_n x = 0 \qquad 0 < x < t \tag{69a}$$

$$\sum_{n=1}^{\infty} \overline{A}_n^{(h)} \hat{k}_n \sin \hat{k}_n x = 0 \qquad 0 < x < t \ . \tag{69b}$$

Similarly, differentiating (66d) with respect to x, we have, after some rearrangement

$$\sum_{n=1}^{\infty} \overline{A}_n^{(e)} \hat{k}_n \cos \hat{k}_n x = f(x) \qquad t < x < L \tag{70a}$$

$$\sum_{n=1}^{\infty} \overline{A}_n^{(h)} \hat{k}_n \cos \hat{k}_n x = g(x) \qquad t < x < L \tag{70b}$$

where

$$f(x) = \sum_{m=1}^{\infty} (a_m \overline{A}_m^{(e)} + b_m \overline{A}_m^{(h)}) \cos \hat{k}_m x$$

$$g(x) = \sum_{m=1}^{\infty} (c_m \overline{A}_m^{(e)} + d_m \overline{A}_m^{(h)}) \cos \hat{k}_m x$$

and

$$a_m = \hat{k}_m \left[1 - \frac{P_m(\beta)W(\beta) - T(\beta)Q_m(\beta)}{P(\beta)W(\beta) - T(\beta)Q(\beta)} \right] \tag{71a}$$

$$b_m = \hat{k}_m \frac{T_m(\beta)W(\beta) - T(\beta)W_m(\beta)}{P(\beta)W(\beta) - T(\beta)Q(\beta)} \tag{71b}$$

$$c_m = \hat{k}_m \frac{P(\beta)Q_m(\beta) - P_m(\beta)Q(\beta)}{P(\beta)W(\beta) - T(\beta)Q(\beta)} \tag{71c}$$

$$d_m = \hat{k}_m \left[1 - \frac{P(\beta) W_m(\beta) - T_m(\beta)Q(\beta)}{P(\beta)W(\beta) - T(\beta)Q(\beta)} \right] . \tag{71d}$$

55

The functions $P(\beta)$, $T(\beta)$, $Q(\beta)$, and $W(\beta)$ are the asymptotic limits of $P_m(\beta)$, $T_m(\beta)$, $Q_m(\beta)$, and $W_m(\beta)$ as $m \to \infty$. Explicitly,

$$P(\beta) = \epsilon_r + \frac{\epsilon_r - \overline{\beta}^2}{1 - \overline{\beta}^2} + \overline{\beta}^2 \frac{1 - \epsilon_r}{1 - \overline{\beta}^2} \tag{72a}$$

$$T(\beta) = 2\overline{\beta}^2 \tag{72b}$$

$$Q(\beta) = \frac{1 - \epsilon_r}{1 - \overline{\beta}^2} \tag{72c}$$

$$W(\beta) = \frac{\epsilon_r - \overline{\beta}^2}{1 - \overline{\beta}^2} + 1. \tag{72d}$$

It should be pointed out that Equations (69) and (70) are similar to those obtained in connection with the quasi-static formulation of the iris discontinuity problems in a waveguide (Lewin, 1966). Their most important characteristic is that the pairs (69a), (70a) and (69b), (70b) are exactly invertible via a singular integral equation approach. That is, it is possible to express the coefficients $\overline{A}_n^{(e)}$ and $\overline{A}_n^{(h)}$ in terms of integrals involving functions in the right-hand side, viz. $f(x)$, $g(x)$. In the capacitive discontinuity problem, the right-hand side is known and the unknown coefficients are determined in this manner. In the present case the functions $f(x)$ and $g(x)$ themselves contain the unknowns $\overline{A}_n^{(e)}$ and $\overline{A}_n^{(h)}$ and the result of the inversion of (69) and (70) is a homogeneous set of equations, leading in turn to an eigenvalue equation.

Following the standard technique of solving the singular integral equations with the requirement that the tangential E fields are zero on the strip, we obtain the following equations:

$$\sum_{m=1}^{\infty} (\hat{k}_p \delta_{pm} - a_m D_{pm} - M_m K_p) \overline{A}_m^{(e)} - \sum_{n=1}^{\infty} (b_n D_{pn} + N_n K_p) \overline{A}_n^{(h)} = 0 \tag{73a}$$
$$p = 1, 2, \cdots$$

$$\sum_{m=1}^{\infty} (-c_m D_{qm} - X_m K_q) \overline{A}_m^{(e)} + \sum_{n=1}^{\infty} (\hat{k}_q \delta_{qn} - d_n D_{qn} - Y_n K_q) \overline{A}_n^{(h)} = 0 \tag{73b}$$
$$q = 1, 2, \cdots$$

where δ_{pm} is the Kronecker delta, and all other quantities are as follows:

$$D_{nm} = \int_t^L f_m(x) \sin \hat{k}_n x \, dx$$

56

$$K_n = \frac{2}{L} \int_t^L \frac{\cos \frac{\pi x}{2L}}{\sin \theta} \sin \hat{k}_n x \, dx$$

$$f_m(x) = \frac{2}{L} \cos \frac{\pi x}{2L} \left[\sum_{q=1}^{m-1} P_{mq} \sin q\theta - P_{mo} \frac{\cos \theta}{\sin \theta} \right] .$$

The relation between x and θ is given by

$$\cos \frac{\pi x}{L} = \frac{1}{2} (\cos \frac{\pi t}{L} - 1) + \frac{1}{2} (\cos \frac{\pi t}{L} + 1) \cos \theta;$$

the coefficients P_{mq} are

$$\sum_{q=0}^{m-1} P_{mq} \cos q\theta = \frac{\cos \hat{k}_m x}{\cos \hat{k}_1 x} .$$

All other quantities M_m, N_m, X_m, and Y_m are constants proportional to a_m, b_m, c_m, and d_m. The detailed derivations of these quantities may be found in Mittra and Itoh (1971).

The solutions of the determinantal equation corresponding to (73) are the desired values of β — the propagation constant. Although (73) comprises a doubly infinite set of equations, we can truncate the associated matrix to a small size since a_m, b_m, c_m, d_m as well as M_m, N_m, X_m, and Y_m decrease extremely rapidly with m. This can be seen by observing that the asymptotic behavior of these coefficients predicts an exponential decay. For instance, a_m contains difference terms of the type $P(\beta) - P_m(\beta)$ and $Q(\beta) - Q_m(\beta)$ in the numerator. For large m,

$$P(\beta) - P_m(\beta) = \varepsilon_r \left\{ 1 - \frac{\alpha_m^{(1)}}{\hat{k}_m} \coth \alpha_m^{(1)} d \right\} + \varepsilon_r \left\{ 1 - \frac{\alpha_m^{(2)}}{\hat{k}_m} \coth \alpha_m^{(2)}(h - d) \right\}$$

$$\sim \left\{ \exp \left[- \frac{(2m - 1)\pi}{L} d \right] + \exp \left[- \frac{(2m - 1)\pi}{L} (h - d) \right] \right\} \cdot \{ -2\varepsilon_r + 0(m^{-2}) \} .$$

The behavior of $Q(\beta) - Q_m(\beta)$ is similar and it follows that a_m decays exponentially for large m. Similar comments apply to the other

57

coefficients as well.

As will be demonstrated shortly, retaining only a single equation from each set is sufficient for accurate computation of numerical results. Using the fact that $D_{11} = 0$ (Mittra and Itoh, 1971), the determinantal equation of the truncated set may be explicitly written as

$$D(\bar{\beta}) = [\hat{k}_1 - M_1(\bar{\beta}) \ K_1][\hat{k}_1 - Y_1(\bar{\beta}) \ K_1] - N_1(\bar{\beta}) \ X_1(\bar{\beta}) \ K_1^2 = 0. \quad (74)$$

Clearly, this equation is much easier to handle than the determinantal equation of a large-order matrix that results from conventional processing of (65). Though the derivation of (74) requires advance analytical processing, this effort is more than compensated for by the numerical efficiency that results due to the simplicity of the characteristic equation.

(c) Fourier Analysis Method

In this method, the imposition of the interface conditions to Equation (64) is carried out as follows (Hornsby and Gopinath, 1969a): The continuity condition on E_z for $0 < x < L$ is satisfied by choosing

$$(k_1^2 - \beta^2) \ A_n^{(e)} \sinh \alpha_n^{(1)} d = (k_2^2 - \beta^2) \ B_n^{(e)} \sinh \alpha_n^{(2)}(h - d). \quad (75)$$

The remaining interface conditions (2) - (4) [see paragraph following Equation (64)] can be satisfied by equating the functions F_1, F_2, and F_3 to zero. These functions are given by

$$F_1(x) = \left\{ (H_{z1} - H_{z2}) \ D(x) + \frac{\partial H_{z1}}{\partial y} \ [1 - D(x)] \right\}_{y=d} \quad (76a)$$

$$F_2(x) = \left\{ (H_{y1} - H_{y2}) \ D(x) + \frac{\partial H_{z1}}{\partial y} \ [1 - D(x)] \right\}_{y=d} \quad (76b)$$

58

$$F_3(x) = \{(H_{x1} - H_{x2}) D(x) + E_z [1 - D(x)]\}_{y=d} \qquad (76c)$$

where $D(x)$ is a function which is zero on the strip and unity outside of
the strip. The required conditions are met by constructing a complete
set of functions and requiring each $F_i(x)$, $i = 1, 2, 3$ to be orthogonal
to every member of the set. A suitable complete set of functions
may be chosen as

$$\sin \frac{m\pi x}{L} \quad , \quad \cos \frac{m\pi x}{L} \qquad m = 0, 1, 2, \cdots$$

and the orthogonality condition is

$$\int_{-L}^{L} F_i(x) \frac{\sin}{\cos} \left(\frac{m\pi x}{L} \right) dx = 0 \qquad i = 1, 2, 3. \qquad (77)$$

In the actual computation the infinite series in $\Psi_i^{(e)}$ and $\Psi_i^{(h)}$, given
by (64), are truncated at some finite value of n, say N. Substituting
the expressions for $F_i(x)$ into Equation (77) and performing the
necessary differentiations and integrations, there results a homogeneous
set of $3(N + 1)/2$ linear equations for the unknowns $A_n^{(e)}$, $A_n^{(h)}$, and
$B_n^{(h)}$. In order for a nontrivial solution to exist, the determinant
of the coefficient matrix must vanish. Since this matrix is a known
function of β, the dispersion relation can be derived by seeking the
value of β that makes the determinant vanish. In actual calculation
by Hornsby and Gopinath (1969a), N was chosen to be 10 and 20. The
deviation between these two choices of N was found to be less than
2 per cent.

(d) Finite Difference Method

The finite-difference method, which was discussed in connection with
the quasi-TEM solution of the microstrip line problem, can be easily

extended to apply to the shielded microstrip line being investigated

in this section (Hornsby and Gopinath, 1969b). As a first step toward

applying the finite difference method to this problem, the cross

section of the microstrip line shown in Figure 20 is discretized into

a lattice form with the separation between the adjacent net-points

equalling Δx and Δy in the x- and y-directions, respectively. Next,

one defines the discretized potentials as

$$\psi^{(e)}_{mn} = \psi^{(e)}(m\Delta x, \ n\Delta y), \qquad \psi^{(h)}_{mn} = \psi^{(h)}(m\Delta x, \ n\Delta y)$$

and uses these definitions in the wave equations

$$\nabla_t^2 \psi^{(e)} + (k_i^2 - \beta^2) \ \psi^{(e)} = 0 \qquad\qquad (78a)$$
$$i = 1, \ 2$$
$$\nabla_t^2 \psi^{(h)} + (k_i^2 - \beta^2) \ \psi^{(h)} = 0. \qquad\qquad (78b)$$

This leads to the discretized equations of the form

$$\lambda_i \psi^{(e)}_{mn} = 2(1 + R^2) \ \psi^{(e)}_{mn} - \psi^{(e)}_{m+1,n} - \psi^{(e)}_{m-1,n} - R^2 \psi^{(e)}_{m,n+1} - R^2 \psi^{(e)}_{m,n-1}$$

$$(79a)$$

$$\lambda_i \psi^{(h)}_{mn} = 2(1 + R^2) \ \psi^{(h)}_{mn} - \psi^{(h)}_{m+1,n} - \psi^{(h)}_{m-1,n} - R^2 \psi^{(h)}_{m,n+1} - R^2 \psi^{(h)}_{m,n-1}$$

$$(79b)$$

where

$$\lambda_i = (k_i^2 - \beta^2) \ \Delta x^2 \ , \quad R = \Delta x/\Delta y.$$

The expressions in (79) are appropriate for the interior net-points.

The boundary conditions and the resulting equations must be modified

when applied to the net-points that are located on the boundary or

at the interface.

After properly applying the discretized version of the wave equation

60

and the boundary or interface conditions at all of the net-points, one

obtains a matrix equation of the form

$$A\phi = \lambda\phi \tag{80}$$

where ϕ is a vector whose elements are $\psi_{mn}^{(e)}$ or $\psi_{mn}^{(h)}$, and λ is λ_i with

$i = 1$ or 2. The coefficient matrix A is sparse and has the size

$2(MN - 1) \times 2(MN - 1)$ where $M\Delta x = L$, $N\Delta y = h$. The matrix eigenvalue

equation (80) can be solved by one of several standard algorithms,

e. g., the relaxation method.

As pointed out earlier, there are two main advantages of this

method: (i) the algorithm is straightforward; (ii) it requires

a negligible amount of analytical preprocessing. However, the

disadvantage is that the size of the matrix which has to be inverted

is rather large. In fact, in using this method, Hornsby and Gopinath

(1969b) worked with a matrix size of 100 x 100 or larger, but the

results they obtained were not comparable in accuracy to those derived

by using a much smaller size matrix equation formulated by one of the

other methods described earlier.

(e) Mode-Matching Method

The method, to be presented below, has been developed by Kowalski

and Pregla (1971) and is capable of handling the case of the finitely

thick center strip.

The cross section of the right-hand half of the microstrip line is

subdivided into five subdivisions, as shown in Figure 21.

The E- and H-type scalar potentials $\psi_i^{(e)}$ and $\psi_i^{(h)}$ in the ith

region can be written as follows:

61
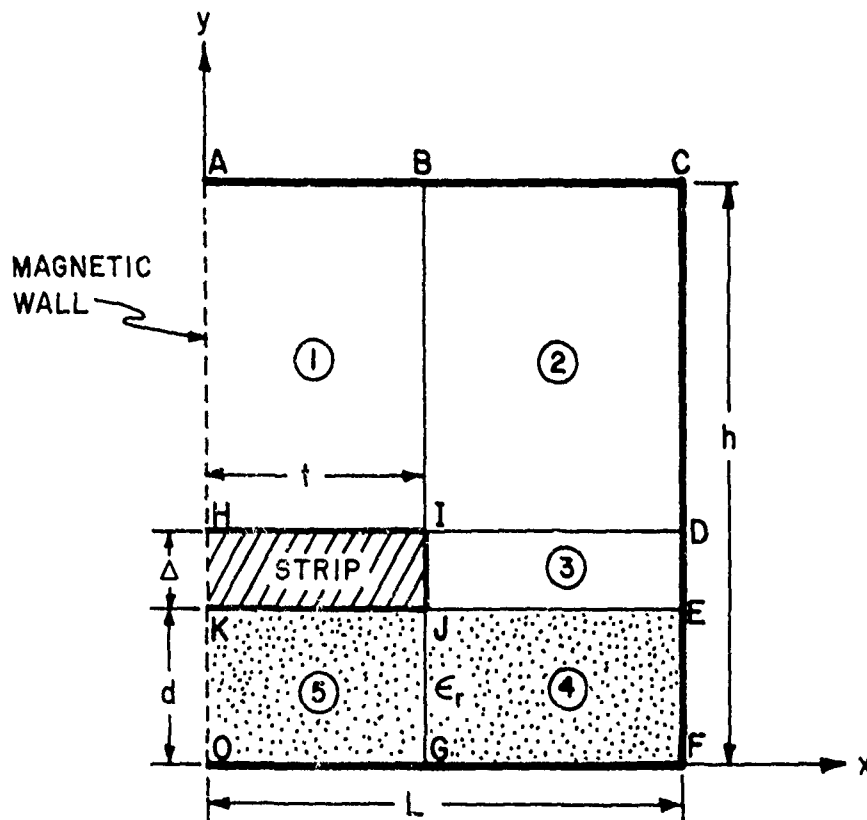
Figure 21. Cross section of the right-hand half of the microstrip line with a finitely thick strip conductor.

$$\psi_1^{(h)} = \sum_{n=1}^{N+1} A_n \sin \xi_n^{(1)} x \cos \eta_n^{(1)}(y - h) \tag{81a}$$

$$\psi_1^{(e)} = \sum_{n=1}^{N} B_n \cos \xi_{n+1}^{(1)} x \sin \eta_{n+1}^{(1)}(y - h) \tag{81b}$$

$$\psi_2^{(h)} = \sum_{n=1}^{N+1} \{C_n \cos \xi_n^{(1)}(x - L) \cos \eta_n^{(1)}(y - h) + \tilde{C}_n \cos \xi_n^{(2)}(x - L)$$
$$\cdot \cos \eta_n^{(2)}(y - h)\} \tag{81c}$$

$$\psi_2^{(e)} = \sum_{n=1}^{N} \{D_n \sin \xi_{n+1}^{(1)}(x - L) \sin \eta_{n+1}^{(1)}(y - h) + \tilde{D}_n \sin \xi_{n+1}^{(2)}(x - L)$$
$$\cdot \sin \eta_{n+1}^{(2)}(y - h)\} \tag{81d}$$

$$\psi_3^{(h)} = \sum_{n=1}^{N+1} \{E_n \cos \xi_n^{(2)}(x - L) \cos \eta_n^{(2)}(y - d) + F_n \cos \xi_n^{(2)}(x - L)$$
$$\cdot \sin \eta_n^{(2)}(y - d)\} \tag{81e}$$

$$\psi_3^{(e)} = \sum_{n=1}^{N} \{G_n \sin \xi_{n+1}^{(2)}(x - L) \sin \eta_{n+1}^{(2)}(y - d) + H_n \sin \xi_{n+1}^{(2)}(x - L)$$
$$\cdot \cos \eta_{n+1}^{(2)}(y - d)\} \tag{81f}$$

where

$$\xi_n^{(1)} = (k_o^2 - \beta^2 - \eta_n^{(1)2})^{1/2} \tag{82a}$$

$$\eta_n^{(1)} = \frac{(n - 1)\pi}{h - d - \Delta} \tag{82b}$$

$$\xi_n^{(2)} = \frac{(n - 1)\pi}{L - t} \tag{82c}$$

$$\eta_n^{(2)} = (k_o^2 - \beta^2 - \xi_n^{(2)2})^{1/2} \tag{82d}$$

k_o is the free-space wavenumber and β is the unknown propagation constant in the guide. The scalar potentials in regions 4 and 5 can

63

be similarly written with coefficients $\overline{Q}_n$, $\tilde{Q}_n$, $\overline{R}_n$, $\tilde{R}_n$, S_n, and T_n. The
wavenumbers in the x- and y-directions are denoted by $\overline{\xi}_n^{(1)}$, $\xi_n^{(2)}$, $\overline{\eta}_n^{(1)}$,
and $\overline{\eta}_n^{(2)}$, and are defined as follows

$$\overline{\xi}_n^{(1)} = (k_o^2 - \beta^2 - \overline{\eta}_n^{(1)2})^{1/2} \tag{83a}$$

$$\overline{\eta}_n^{(1)} = \frac{(n-1)\pi}{d} \tag{83b}$$

$$\overline{\eta}_n^{(2)} = (\varepsilon_r k_o^2 - \beta^2 - \xi_n^{(2)2})^{1/2}. \tag{83c}$$

It should be noted that in Equation (81), N of the TM components
and N + 1 of the TE components have been retained. It should also
be noted that the tangential electric field derived from the scalar
potentials in region 2 satisfies the boundary conditions of the guide
periphery $\overline{BCD}$ as well as at the point I for any coefficients C_n, $\cdots$, $\tilde{D}_n$.

The next step is to match the tangential field components across
the interfaces between the regions and take inner products with a
suitable set of orthogonal basis functions. The appropriate basis
functions are

$$\begin{matrix} \sin \\ \cos \end{matrix} (\eta_n^{(1)} y), \quad d + \Delta \leq y \leq h, \quad x = t \tag{84a}$$

$$\begin{matrix} \sin \\ \cos \end{matrix} (\xi_n^{(2)} x), \quad y = d, \quad d + \Delta, \quad t < x < L \tag{84b}$$

$$\begin{matrix} \sin \\ \cos \end{matrix} (\overline{\eta}_n^{(1)} y), \quad 0 \leq y \leq d, \quad x = t. \tag{84c}$$

The above procedure leads to a homogeneous set of equations for
the unknown coefficients A_n, $\cdots$ T_n. Since the orthogonal functions
are identical to those used in the series expansion of the scalar

potentials, many of the submatrices in the matrix equation become diagonal. Hence, it is possible to eliminate certain sets of coefficients without having to invert the entire matrix. After eliminating all of the coefficients except $\tilde{C}_n$, $\tilde{D}_n$, $\tilde{Q}_n$, and $\tilde{R}_n$, one obtains a $(4N + 2) \times (4N + 2)$ matrix which is the final equation to be solved.

In the actual calculations by Kowalski and Pregla (1971), N = 10 was found to give a reasonable accuracy. The convergence of the solution was checked by increasing the matrix size up to N = 20.

3.2.2 Numerical results

In this section we will present a few representative numerical results obtained by the various techniques described in earlier sections. Refer to Figure 22 which shows the numerical results obtained by Mittra and Itoh (1971), and by Hornsby and Gopinath (1969b). The effect of dispersion is evident at high frequencies where the $k - \beta$ diagram deviates from the linear curve representing the quasi-TEM solution. The variation of the guide wavelength with respect to frequency is plotted in Figure 23 for a number of different dielectric materials. The theoretical results on this curve have been obtained by Zysman and Varon (1969) and Mittra and Itoh (1971). The experimental results are for an open microstrip line and are included here for convenience of comparison. It is seen from Figure 23 that the guide wavelength converges to the quasi-TEM value at low frequencies and approaches the wavelength in the substrate material as the frequencies increased.

An ingenious empirical equation for the normalized wavelength of the lowest-order mode in the microstrip line has been developed by Schneider (1972). His equation reads
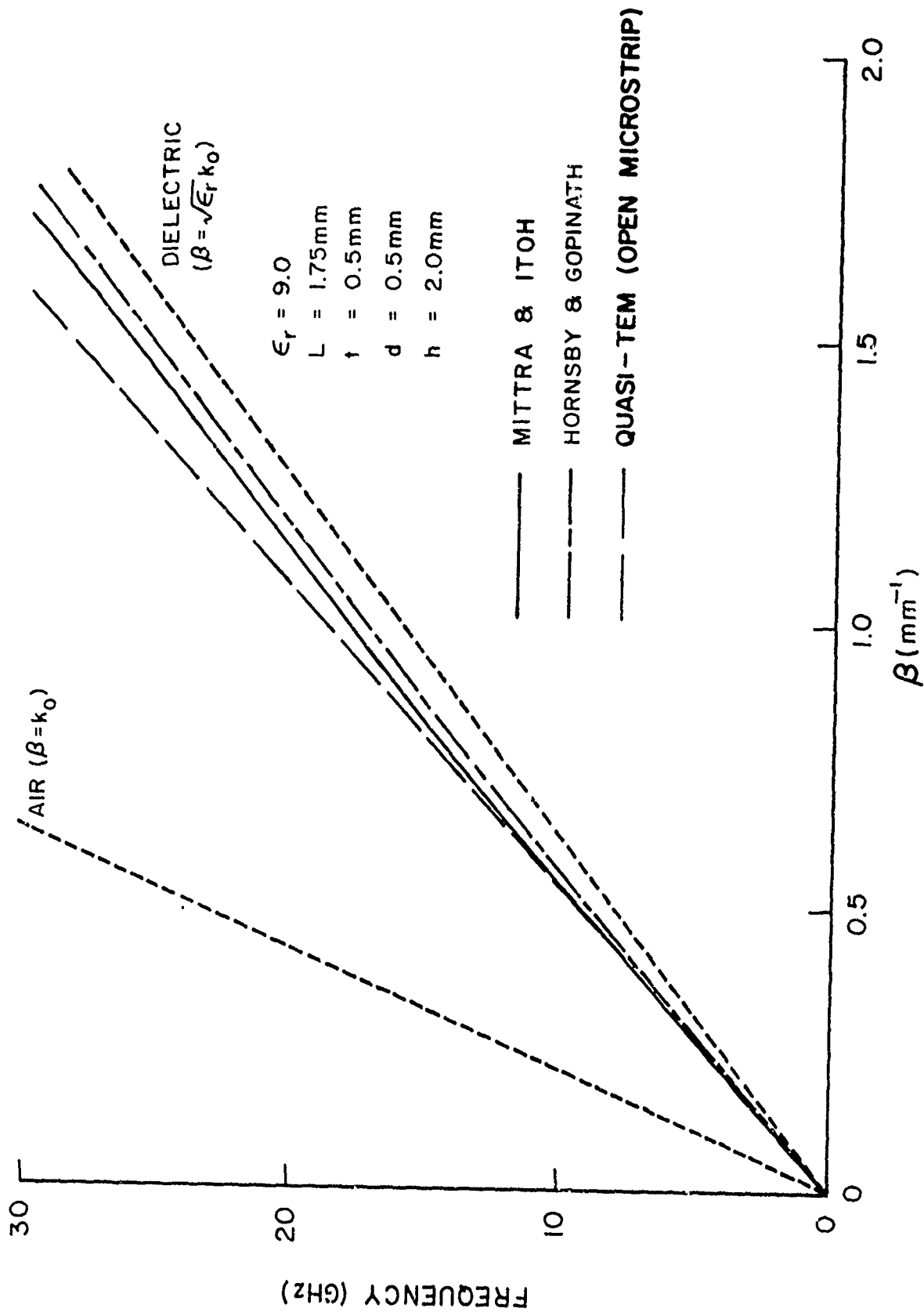
65

Figure 22. Dispersion diagram of the dominant mode in the shielded micro-
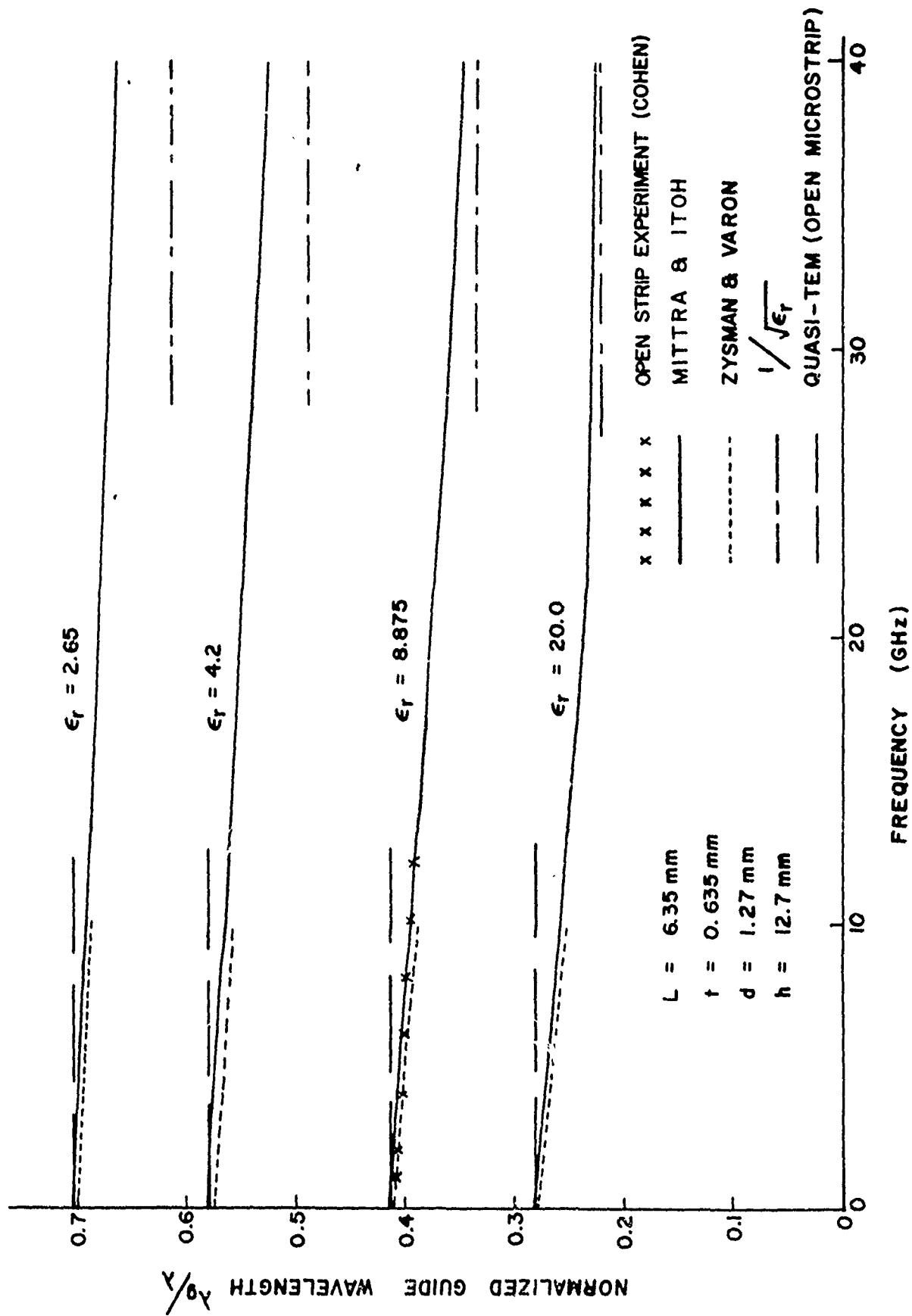strip line shown in Figure 20.

66

Figure 23. Variation of guide wavelength with frequency of the dominant mode in the shielded microstrip line shown in Figure 20.

67

$$\frac{\lambda_g}{\lambda_o} = \frac{1}{\sqrt{\varepsilon_r \varepsilon_{eff}}} \quad \frac{\sqrt{\varepsilon_{eff}} \, f_n^2 + \sqrt{\varepsilon_r}}{f_n^2 + 1} \tag{85}$$

where

$$f_n = \frac{4d\sqrt{\varepsilon_r - 1}}{\lambda_o} \tag{86a}$$

$$\varepsilon_{eff} = \frac{\varepsilon_r + 1}{2} + \frac{\varepsilon_r - 1}{2} \frac{1}{\sqrt{1 + 5 \frac{d}{t}}} \tag{86b}$$

and λ_o is the free-space wavelength.

Before closing this section it will be useful to offer some numerical evidence that the hybrid mode solution approaches the quasi-TEM limit as the frequency is decreased. Refer to Figure 24 which shows the magnitude of the ratio of the longitudinal to the transverse electric field components as a function of frequency (Loadholt, Mittra, and Itoh, 1971). It is evident that this ratio continues to decrease as the frequencies decrease such that in the low frequency limit the solution approaches the quasi-TEM form which has zero longitudinal field components.

3.3 Open Microstrip Line

Having discussed the shielded and boxed versions of the microstrip line, we will now present a number of techniques for analyzing the open microstrip line shown in Figure 25. Even when an open microstrip line is placed in a shielded environment, the effect of the enclosure may be negligible in the event that the walls are far removed from the center strip. In this case the open microstrip line solution corresponds
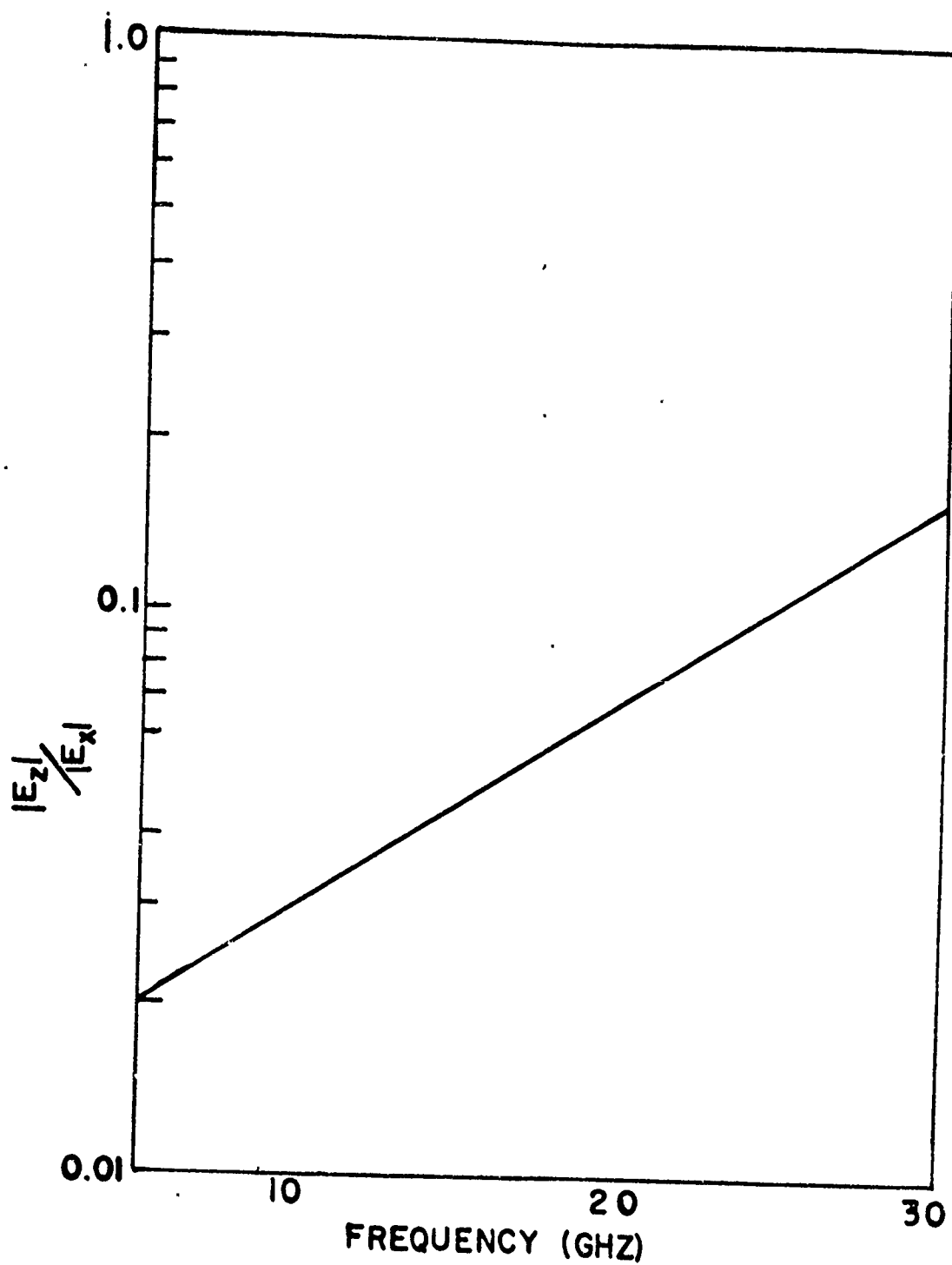
68

Figure 24. Relative magnitudes of the E_x and E_z components as a function of frequency in the structure shown in Figure 20.
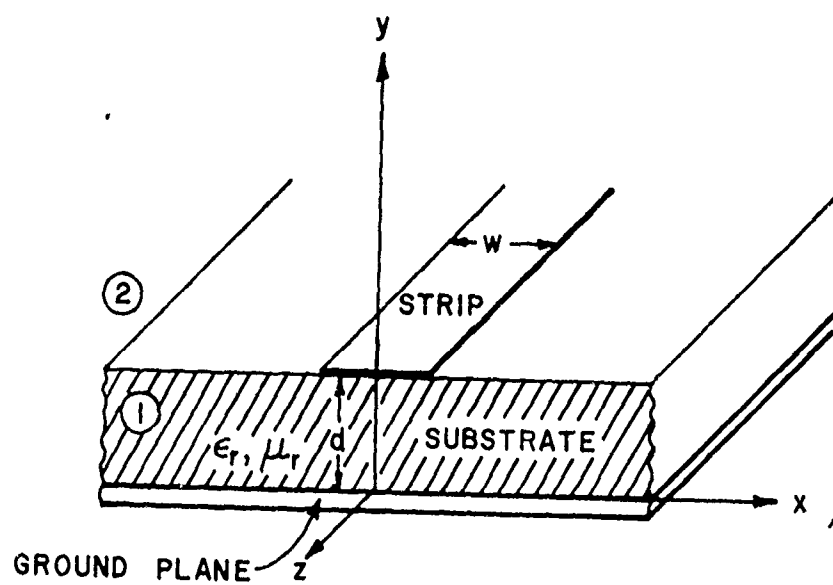
Figure 25. Configuration of an open microstrip line.

to a good approximation of the solution for the enclosed case. Of course, the open microstrip line is an important structure in its own right; it will therefore be useful to discuss the details of the solution for this structure particularly since some of the methods to be described below (the integral equation method, Galerkin's method) are sufficiently different from the ones employed for the other microstrip structures considered earlier.

3.3.1 Integral equation method

An integral equation formulation for this problem has been given by Denlinger (1971) and the development presented below will be based on his work. The starting point in this method is Equation (62) from which it is possible to represent all of the field components in terms of the E- and H-type scalar potentials. However, in contrast to the closed region problems, the scalar potentials $\Psi_i^{(e)}$ and $\Psi_i^{(h)}$ can no longer be expressed in series forms, as the geometry under consideration is infinite in the x direction. (See Figure 25.) It is necessary instead to express the potential in an integral form as follows

$$\Psi_i^{(e)}(x, y) = \frac{1}{2\pi} \int_{-\infty}^{\infty} \tilde{\Psi}_i^{(e)}(\alpha, y) \, e^{-j\alpha x} \, d\alpha \qquad (87a)$$

$$\Psi_i^{(h)}(x, y) = \frac{1}{2\pi} \int_{-\infty}^{\infty} \tilde{\Psi}_i^{(h)}(\alpha, y) \, e^{-j\alpha x} \, d\alpha \qquad (87b)$$

and where $i = 1, 2$ designate the region 1 (substrate) and 2 (air), respectively. It can easily be seen that the transform potentials satisfy the following differential equations

$$\left(\frac{d^2}{dy^2} - \gamma_i^2 \right) \tilde{\Psi}_i^{(e)}(\alpha, y) = 0 \qquad (88a)$$

$$\left(\frac{d^2}{dy^2} - \gamma_i^2 \right) \tilde{\Psi}_i^{(h)}(\alpha, y) = 0 \qquad (88b)$$

71

where

$$\gamma_i^2 = \alpha^2 + \beta^2 - k_i^2 \qquad i = 1, 2 \tag{89}$$

$$k_1^2 = \omega^2 \varepsilon_r \mu_r \varepsilon_o \mu_o \tag{90a}$$

$$k_2^2 = \omega^2 \varepsilon_o \mu_o. \tag{90b}$$

The next step is to write the following solutions for the transformed potential in the various regions involved

$$\tilde{\psi}_1^{(e)}(\alpha, y) = A(\alpha) \sinh \gamma_1 y \tag{91a}$$

$$\tilde{\psi}_2^{(e)}(\alpha, y) = B(\alpha) \exp[-\gamma_2(y - d)] \tag{91b}$$

$$\tilde{\psi}_1^{(h)}(\alpha, y) = C(\alpha) \cosh \gamma_1 y \tag{91c}$$

$$\tilde{\psi}_2^{(h)}(\alpha, y) = D(\alpha) \exp[-\gamma_2(y - d)]. \tag{91d}$$

Note that the above representations satisfy the appropriate boundary conditions at $y = 0$ and the radiation condition at $y \to +\infty$. The unknown coefficients $A(\alpha)$, $B(\alpha)$, $C(\alpha)$, and $D(\alpha)$, will be determined by applying the following continuity conditions at the interface $y = d$ in the Fourier transform domain.

$$\tilde{E}_{z1}(\alpha, d) = \tilde{E}_{z2}(\alpha, d) \tag{92a}$$

$$\tilde{E}_{x1}(\alpha, d) = \tilde{E}_{x2}(\alpha, d) \tag{92b}$$

$$\tilde{H}_{z1}(\alpha, d) - \tilde{H}_{z2}(\alpha, d) = \tilde{J}_x(\alpha) \tag{92c}$$

$$\tilde{H}_{x1}(\alpha, d) - \tilde{H}_{x2}(\alpha, d) = \tilde{J}_z(\alpha) \tag{92d}$$

where $\tilde{J}_x$ and $\tilde{J}_z$ are the Fourier transforms of unknown current components

72

on the strip. Application of the continuity conditions (92) leads

to four simultaneous equations from which the coefficients, $A(\alpha)$,

$B(\alpha)$, $C(\alpha)$, and $D(\alpha)$, can be obtained in terms of the two components

of current on the strip and the unknown propagation constant β. The

expressions for the real field quantities can then be derived by the

use of (87) and (62).

We now return to the space domain (x, y) and apply the final

boundary condition on the strip in the form

$$E_{z2}(x, d) = 0 \tag{93a}$$

$$|x| < w/2.$$

$$\frac{d}{dy} H_{z2}(x, d) = 0 \tag{93b}$$

The use of these equations allows us to represent E_{z2} and H_{z2} in terms

of the coefficients $B(\alpha)$ and $D(\alpha)$ only.

$$E_{z2}(x, y) = j \int_{-\infty}^{\infty} \frac{k_2^2 - \beta^2}{\beta} B(\alpha) \exp[-\gamma_2(y-d)]\exp(-j\alpha x)d\alpha \tag{94a}$$

$$H_{z2}(x, d) = j \int_{-\infty}^{\infty} \frac{k_2^2 - \beta^2}{\beta} D(\alpha) \exp[-\gamma_2(y-d)]\exp(-j\alpha x)d\alpha. \tag{94b}$$

The coefficients $B(\alpha)$ and $D(\alpha)$ are, in turn, expressed in terms of

$\tilde{J}_x(\alpha)$ and $\tilde{J}_z(\alpha)$ as follows

$$B(\alpha) = \frac{1}{\det} [F_1 b_{22} + \frac{\alpha\beta}{k_1^2 - \beta^2} b_{12}] \tilde{J}_x(\alpha) + \frac{1}{\det} b_{12} \tilde{J}_z(\alpha) \tag{95a}$$

$$D(\alpha = \frac{1}{\det} [F_1 b_{21} + \frac{\alpha\beta}{k_1^2 - \beta^2} b_{11}] \tilde{J}_x(\alpha) + \frac{1}{\det} b_{11} \tilde{J}_z(\alpha) \tag{95b}$$

where

73

$$b_{11} = -b_{22} = j\alpha \left(\frac{k_2^2 - \beta^2}{k_1^2 - \beta^2} - 1 \right)$$

$$b_{12} = \frac{\omega\mu_o\gamma_1}{\beta} \left[\frac{\gamma_2}{\gamma_1} + \mu_r \frac{k_2^2 - \beta^2}{k_1^2 - \beta^2} \tanh \gamma_1 d \right]$$

$$b_{21} = \frac{\omega\varepsilon_o\gamma_1}{\beta} \left[\frac{\gamma_2}{\gamma_1} + \varepsilon_r \frac{k_2^2 - \beta^2}{k_1^2 - \beta^2} \coth \gamma_1 d \right]$$

$$\det = b_{11}b_{22} - b_{12}b_{21}$$

$$F_1 = \frac{\omega\mu_o\mu_r\gamma_1}{j(k_1^2 - \beta^2)} \tan \gamma_1 d.$$

Our objective is to derive a set of equations for the unknowns $\tilde{J}_x(\alpha)$ and $\tilde{J}_z(\alpha)$. This is accomplished by substituting (95) into (94) and applying the boundary conditions (93) to (94) resulting in the following coupled integral equations for the two current components.

$$I_{xo} \int_{-\infty}^{\infty} G_{11}(\alpha, \beta) \tilde{I}_x(\alpha) e^{-j\alpha x} d\alpha + I_{zo} \int_{-\infty}^{\infty} G_{12}(\alpha, \beta) \tilde{I}_z(\alpha) e^{-j\alpha x} d\alpha = 0$$

(96a)

$$I_{xo} \int_{-\infty}^{\infty} G_{21}(\alpha, \beta) \tilde{I}_x(\alpha) e^{-j\alpha x} d\alpha + I_{zo} \int_{-\infty}^{\infty} G_{22}(\alpha, \beta) \tilde{I}_z(\alpha) e^{-j\alpha x} d\alpha = 0$$

$$-w/2 < x < w/2$$

(96b)

where

$$G_{11}(\alpha, \beta) = \frac{1}{\det} \left[F_1 b_{22} + \frac{\alpha\beta}{k_1^2 - \beta^2} b_{12} \right] \qquad (97a)$$

$$G_{12}(\alpha, \beta) = \frac{b_{12}}{\det} \qquad (97b)$$

$$G_{21}(\alpha, \beta) = \frac{\gamma_2}{\det} \left[F_1 b_{21} + \frac{\alpha\beta}{k_1^2 - \beta^2} b_{11} \right] \qquad (97c)$$

$$G_{22}(\alpha, \beta) = \frac{\gamma_2 b_{11}}{\det} \qquad (97d)$$

$$\tilde{J}_x(\alpha) = I_{xo} \tilde{I}_x(\alpha) \qquad (98a)$$

$$\tilde{J}_z(\alpha) = I_{zo} \tilde{I}_z(\alpha). \qquad (98b)$$

74

For simplicity, we have used a one-term approximation for the unknown current distributions and have written them in the form of (98a) and (98b). We have also assumed that $\tilde{I}_x$ and $\tilde{I}_z$ have known forms, and the only unknowns in their representation are the amplitude coefficients I_{xo} and I_{zo}.

The unknown propagation constant β can now be solved by equating the determinant of the coefficient matrix for the unknowns I_{xo} and I_{zo} to zero. Obviously, within the one-term approximation being used here the results are critically dependent on the choice of the forms of the current distribution. The distribution chosen by Denlinger (1971) is in the following form.

$$\tilde{I}_z(\alpha) = \frac{2}{\pi\alpha}\left\{ \frac{24}{(\alpha w)^3} + \frac{3[(\alpha w)^2 - 8]}{(\alpha w)^3}\cos\left(\frac{\alpha w}{2}\right) + \frac{[(\alpha w)^2 - 12]}{(\alpha w)^2}\sin\frac{(\alpha w)}{2} \right\}$$

(99a)

$$\tilde{I}_x(\alpha) = \left[\frac{\sin G_1(\alpha)}{G_1(\alpha)} - \frac{\sin G_2(\alpha)}{G_2(\alpha)} + \frac{\cos 0.4\, G_3(\alpha) - \cos 0.5\, G_3(\alpha)}{G_3(\alpha)} \right. $$
$$\left. + \frac{\cos 0.4\, G_4(\alpha) - \cos 0.5\, G_4(\alpha)}{G_4(\alpha)} \right]$$ (99b)

where

$$G_1(\alpha),\ G_2(\alpha) = 0.4\left(\frac{\pi}{0.7} \pm \alpha w\right)$$

$$G_3(\alpha),\ G_4(\alpha) = \alpha w \pm 5\pi.$$

Equations (99) are the Fourier transforms of

$$I_z(x) = \begin{cases} 1 + |\frac{2x}{w}|^3 & |x| \leq w/2 \\ 0 & \text{otherwise} \end{cases}$$

$$I_x(x) = \begin{cases} \sin\frac{\pi x}{0.7w} & |x| \leq 0.8\ w/2 \\ \cos\frac{\pi x}{0.2w} & 0.8\ w/2 < x \leq w/2\ , \\ 0 & \text{otherwise} \end{cases}$$

75

It may be noted that the trial distribution for the current $I_z(x)$ in Denlinger's work is identical to that used by Yamashita (1968) for calculating the quasi-TEM line capacitance.

When the strip width is small as compared to the wavelength, i. e., $w/\lambda < 0.1$, and when we are considering the lowest order hybrid mode, it is a good approximation to neglect the transverse current and to satisfy (93) only at the center of the strip. The above implies that the boundary condition on the strip is imposed only at the midpoint $x = 0$ instead of the entire range $-w/2 < x < w/2$. This artifice allows one to reduce the coupled pair of integral equations (96) into a single integral equation containing the unknown propagation constant β as a parameter. Note that the above approximation also implies the setting of I_{xo} equal to zero and $x = 0$ in (96a). In addition, Equation (96b) now becomes trivial by virtue of the fact that $G_{21}\tilde{I}_z$ is an odd function of α.

This approximation is made because a complete solution of the coupled pair of integral equations (96) requires a rather large amount of computer time. Nevertheless some test calculations have been carried out using the complete equations in (96), and it has been found that the approximate solution obtained by letting I_{xo} equal zero is in excellent agreement with the more exact solution, in the zero frequency limit as well as in the finite but moderate frequency range. This is true as long as the normalized strip with w/λ is less than 0.1.

Figure 26 shows the dispersion diagram computed by the single integral equation approximation. The definition of ε_{eff} is $(\lambda_o/\lambda_g)^2$ where λ_g is the guide wavelength. A study of the curve shows that its
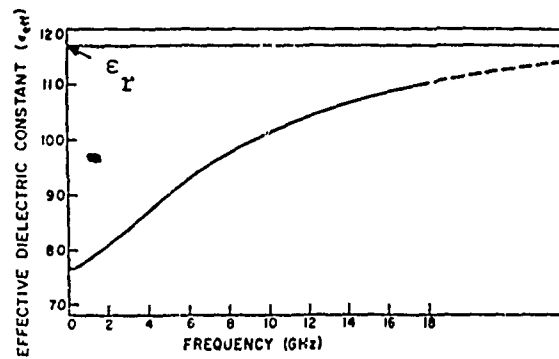
Figure 26. Effective dielectric constant versus frequency. ε_r = 11.7; w/d = 0.96; d = 0.317 cm.

behavior agrees quite well with the experimental results of Hartwig,
Massé and Pucel (1968) even beyond the frequency range over which the
transverse current is negligible. The curves also show that the
effective dielectric constant approaches ε_r in the high frequency
limit, indicating that at high frequencies all of the energy tends to
be confined in the dielectric substrate. Recall that this phenomenon
is similar to the one observed in the case of the shielded microstrip
line discussed in the previous section.

3.3.2 Galerkin's method in the Fourier transform domain

In the previous section we discussed a solution of the coupled
integral equations for the open microstrip line. An inherent step
in the solution was the assumption of a suitable form for the components of the
current on the center strip. Obviously, the result obtained by this
method is critically dependent upon the accuracy of the assumed forms
of the distribution for the currents. A method is now presented for
circumventing this difficulty and systematically solving for the currents
to the desired degree of accuracy. The method is basically a modification
of Galerkin's appraoch adapted for application in the Fourier transform
domain, developed by Itoh and Mittra (1971a). It is quite similar to
the one discussed earlier in Section 2.4 in connection with the derivation
of line capacitance in the quasi-TEM approximation.

We start with Equation (95) which relates the unknown coefficients
$B(\alpha)$ and $D(\alpha)$ in terms of the two current components $\tilde{J}_x(\alpha)$ and $\tilde{J}_z(\alpha)$.
Rather than applying the boundary condition (93) on the strip in the
space domain as was done in the previous section, we impose this condition
in the Fourier transform domain instead. As a first step we rewrite
(93) as

78

$$E_{z2}(x,\ d) = \begin{cases} 0 & -w/2 < x < w/2 \\[2ex] j\ \dfrac{k_2^2 - \beta^2}{\beta}\ u(x), & \text{otherwise} \end{cases} \qquad (100a)$$

$$\frac{d}{dy}\ H_{z2}(x,\ d) = \begin{cases} 0 & -w/2 < x < w/2 \\[2ex] j\ \dfrac{k_2^2 - \beta^2}{\beta}\ v(x), & \text{otherwise} \end{cases} \qquad (100b)$$

The Fourier transforms of the spatial functions in (100) are

$$\tilde{E}_{z2}(\alpha,\ d) = j\ \frac{k_2^2 - \beta^2}{\beta}\ [\tilde{U}_1(\alpha) + \tilde{U}_2(\alpha)] \qquad (101a)$$

$$\frac{d}{dy}\ \tilde{H}_{z2}(\alpha,\ d) = j\ \frac{k_2^2 - \beta^2}{\beta}\ [\tilde{V}_1(\alpha) + \tilde{V}_2(\alpha)] \qquad (101b)$$

where

$$\tilde{U}_1(\alpha) = \int_{-\infty}^{-w/2} u(x)\ e^{j\alpha x}\ dx$$

$$\tilde{U}_2(\alpha) = \int_{w/2}^{\infty} u(x)\ e^{j\alpha x}\ dx$$

$$\tilde{V}_1(\alpha) = \int_{-\infty}^{-w/2} v(x)\ e^{j\alpha x}\ dx$$

$$\tilde{V}_2(\alpha) = \int_{w/2}^{\infty} v(x)\,e^{j\alpha x}\ dx.$$

Using the expressions given by (62) and (95) we obtain the following coupled equations for the two current components

$$G_{11}(\alpha,\ \beta)\tilde{J}_x(\alpha) + G_{12}(\alpha,\ \beta)\tilde{J}_z(\alpha) = \tilde{U}_1(\alpha) + \tilde{U}_2(\alpha) \qquad (102a)$$

$$G_{21}(\alpha,\ \beta)\tilde{J}_x(\alpha) + G_{22}(\alpha,\ \beta)\tilde{J}_z(\alpha) = \tilde{V}_1(\alpha) + \tilde{V}_2(\alpha) \qquad (102b)$$

where G_{11}, G_{12}, G_{21}, and G_{22} are given by (97). Note that the two equations in (102) actually contain six unknowns altogether. However, four of the unknowns, viz., $\tilde{U}_1$, $\tilde{U}_2$, $\tilde{V}_1$, and $\tilde{V}_2$, can be eliminated from these equations by using a technique that was outlined in Section 2.4.

As a first step we expand $\tilde{J}_x$ and $\tilde{J}_z$ in terms of known basis functions $\tilde{J}_{xn}$ and $\tilde{J}_{zn}$ as follows:

$$\tilde{J}_x(\alpha) = \sum_{n=1}^{M} c_n \, \tilde{J}_{xn}(\alpha) \tag{103a}$$

$$\tilde{J}_z(\alpha) = \sum_{n=1}^{N} d_n \, \tilde{J}_{zn}(\alpha). \tag{103b}$$

The basis functions $\tilde{J}_{xn}(\alpha)$ and $\tilde{J}_{zn}(\alpha)$ must be chosen such that their inverse Fourier transforms are nonzero only on the strip $-w/2 < x < w/2$. After substituting (103) into (102) we take the inner products with the basis functions $\tilde{J}_{xn}$ and $\tilde{J}_{zn}$ for different values of n. This yields the matrix equation

$$\sum_{n=1}^{M} K_{mn}^{(1,1)} c_n + \sum_{n=1}^{N} K_{mn}^{(1,2)} d_n = 0 \qquad m = 1, 2, \cdots M \tag{104a}$$

$$\sum_{n=1}^{M} K_{mn}^{(2,1)} c_n + \sum_{n=1}^{N} K_{mn}^{(2,2)} d_n = 0 \qquad m = 1, 2, \cdots N. \tag{104b}$$

where

$$K_{mn}^{(1,1)} = \int_{-\infty}^{\infty} \tilde{J}_{xm}(\alpha) \, G_{11}(\alpha, \beta) \, \tilde{J}_{xn}(\alpha) \, d\alpha \tag{105a}$$

$$K_{mn}^{(1,2)} = \int_{-\infty}^{\infty} \tilde{J}_{xm}(\alpha) \, G_{12}(\alpha, \beta) \, \tilde{J}_{zn}(\alpha) \, d\alpha \tag{105b}$$

$$K_{mn}^{(2,1)} = \int_{-\infty}^{\infty} \tilde{J}_{zm}(\alpha) \, G_{21}(\alpha, \beta) \, \tilde{J}_{xn}(\alpha) \, d\alpha \tag{105c}$$

80

$$K_{mn}^{(2,2)} = \int_{-\infty}^{\infty} \tilde{J}_{zm}(\alpha) \; G_{22}(\alpha, \beta) \; \tilde{J}_{zn}(\alpha) \; d\alpha. \qquad (105d)$$

An application of Parseval's theorem will verify that the right-hand sides of (102) are indeed eliminated by this procedure. Using this theorem we can show that

$$\int_{-\infty}^{\infty} \tilde{J}_{xm}(\alpha) \; [\tilde{U}_1(\alpha) + \tilde{U}_2(\alpha)] \; d\alpha$$

$$= \frac{1}{2\pi} \int_{-\infty}^{\infty} J_{xm}(x) \left[\frac{\beta}{j(k_2^2 - \beta^2)} E_{z2}(x, d) \right] dx \equiv 0$$

The above relation is true since $J_{xm}(x)$, the inverse transform of $\tilde{J}_{xm}(\alpha)$, and $E_{z2}(x, d)$ are nonzero in the complementary regions of x.

The next step is to solve the simultaneous equation (104) for the propagation constant β, by setting the determinant of this set of equations equal to zero and seeking the roots of the resulting equation.

It may be of interest to note that the technique just described is useful for solving the problem of the slot line (Itoh and Mittra, 1971b) which is another useful transmission line structure used in microwave integrated circuits.

81

IV. HIGHER-ORDER MODES

Until now we have restricted ourselves to the discussion of the dominant mode in the microstrip transmission line. In this section we will briefly take up the subject of higher-order modes that can propagate in these lines. Although much has been written on the characteristics of the dominant mode, relatively little has been reported on the subject of higher-order modes.

Let us first consider the open microstrip line. Since the geometry of this structure is an open one, its modal spectrum is comprised of two parts — discrete and continuous. The discrete part of the spectrum corresponds to a finite number of propagating modes which are essentially surface-wave-type in nature. Since the propagation constant β for these modes is real and greater than the free-space wavenumber k_o, they are referred to as slow waves. In contrast, the continuous spectrum is associated with the radiated field or the fast waves. As the frequency of operation is increased, leaky modes or pseudomodes which are alternate representations of portions of the continuous spectrum, can exist simultaneously with the surface-wave-type modes. These leaky modes represent radiation losses, and the use of the microstrip line becomes restricted when these pseudomodes appear.

In addition to the leaky modes, there are higher-order, surface-wave-type modes that also appear as the frequency of operation is increased. The occurrence of these higher-order, surface-wave-type modes may be heuristically explained as follows. If the center strip of the open microstrip lines structure is removed the result is a conventional, dielectric slab, surface-wave line supported by a conducting sheet.

82

Such a surface-wave line supports the even TM and odd TE type of mode (Collin, 1960). The insertion of the center strip perturbs these surface waves, but their modified versions remain similar in character to the dielectric slab modes. The existence of these higher-order modes is undesirable and the use of the microstrip line is typically restricted to frequencies below f_c, the cutoff frequency of the TE_1 surface wave (Denlinger, 1971),which is given by the formula

$$f_c = \frac{c}{4d\sqrt{\varepsilon_r - 1}}, \qquad c = \text{velocity of light in vacuum.}$$

Let us now turn to the problem of higher-order modes in a shielded microstrip line (Figure 20). As expected, this closed waveguide structure only supports an infinite number of discrete modes and the propagation constants for these modes are obtained by solving the characteristic equation derived in Section 3.2.

Figure 27 shows typical plots of the value of the determinant versus the normalized propagation constant $\bar{\beta}$ (Mittra and Itoh, 1971). The curves for increasing frequencies are shown from (a) through (d). It is evident that the number of zeros of the determinant increases with increasing frequency indicating the appearance of higher-order modes. Figure 28 presents the dispersion diagrams for both the dominant and the higher-order modes. It should be mentioned that this mode spectrum is not complete since only the E_z even - H_z odd type of modes are exhibited in the figure. Calculation of the dispersion characteristics of higher-order modes have also been carried out by Daly (1971) and Kowalski and Pregla (1971). A comparative study of these works reveals that some disagreement exists between the results that are reported
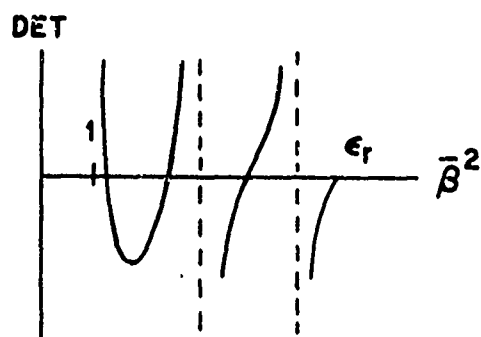
83
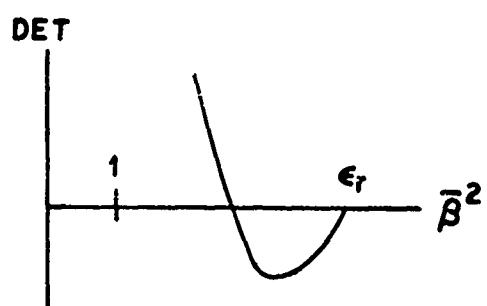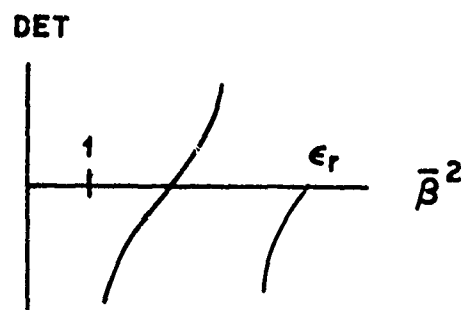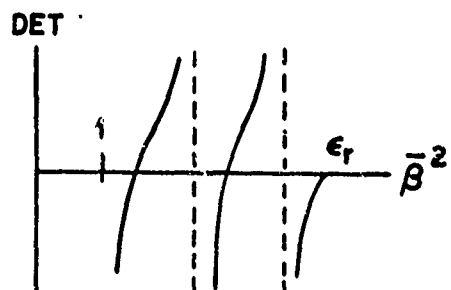
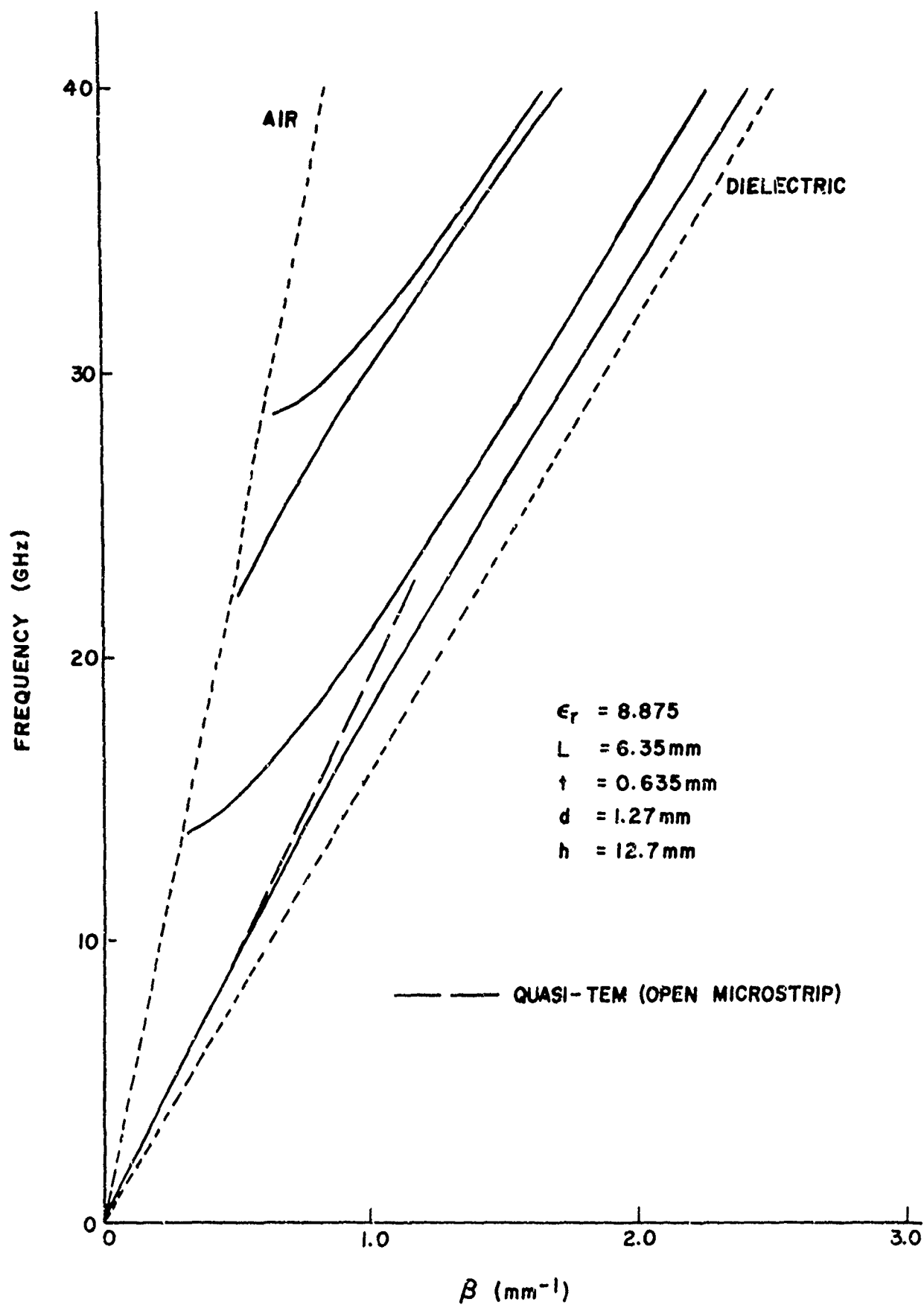Figure 27. Typical plots of $D(\bar{\beta})$ in Equation (74) versus $\bar{\beta}^2$.

Figure 28. Dispersion diagram of the dominant and a number of higher-order modes in the shielded microstrip line shown in Figure 20.

in the works referred to above. It appears that reliable experimental

work is necessary for resolving these discrepancies.

V.   LOSSES IN MICROSTRIP LINES

The discussion of the microstrip line thus far has been based on the assumption that the losses are negligible. However, in practice, losses are always present and it may be quite important to obtain a quantitative estimate of these losses in order to reliably design the microstrip line circuits. It will therefore be pertinent to include here brief descriptions of two methods that have been found useful for evaluating these losses. We restrict our attention to the dielectric and ohmic skin losses only and assume that magnetic losses in the substrate are either absent or negligible.

The analysis will be based on a perturbational approach which is valid when the loss per unit length is small. Except for the case when the substrate material is a semiconductor, the assumption that the losses in the line are small is certainly valid for most practical microstrip structures. The line loss can be quantitatively described in terms of an attenuation constant α defined as

$$P(z) = P_o \exp(-2\alpha z)$$

$$\text{(106)}$$

$$P(0) = P_o$$

where $P(z)$ is the power transmitted along the line at the distance z from the origin. Letting $\alpha = \alpha_d + \alpha_c$, i. e., identifying the total attenuation as the sum of the contribution due to dielectric and ohmic losses, we obtain the following relationships

$$\alpha = -\frac{dP/dz}{2P(z)} \approx \frac{P_c + P_d}{2P(z)} \quad \text{(nepers/m)} \qquad \text{(107a)}$$

and

$$\alpha_d \approx \frac{P_d}{2P(z)} = \frac{\text{Power loss in dielectric material}}{2 \times \text{Power transmitted}} \quad \text{(nepers/m)}$$

$$\text{(107b)}$$

$$a_c \approx \frac{P_c}{2P(z)} = \frac{\text{Power loss in conductors}}{2 \times \text{Power transmitted}} \quad \text{(nepers/m)} . \quad \text{(107c)}$$

The perturbational analysis for loss calculation is based upon the assumption that the field distribution in the structure is not altered due to the presence of losses. Assuming further that the dominant mode is quasi-TEM, the following formula may be written for the two components of α (Yamashita and Atsuki, 1970)

$$\alpha_d = \frac{\iint \sigma_d (\nabla\phi)^2 dxdy}{2 \iint v\varepsilon (\nabla\phi)^2 dxdy} \quad \text{(108a)}$$

$$\alpha_c = \frac{\int R_s i_s^2 d\ell}{2 \iint v\varepsilon (\nabla\phi)^2 dxdy} \quad \text{(108b)}$$

$$i_s = \rho_s v \quad \text{(108c)}$$

where the double integrals are defined over the cross section and the line integral is taken around the center strip and along the ground conductor surface. The various quantities appearing in (108) are

ρ_s = charge distribution on the conductors

ϕ = potential distributions

v = phase velocity (equal to the group velocity)

σ_d = conductivity of dielectric material

$R_s = \sqrt{\omega\mu/2\sigma_c}$ = surface resistance of conductors.

The quantities ϕ, ρ_s, and v in the above expression are calculated by one of the methods presented in Section II with the assumption that there is no loss in the microstrip line.

88

Also, it has been assumed in writing (108) that σ_d and R_s are sufficiently small ($\sigma_d << \omega\varepsilon$; and $R_s << Z$, the characteristic impedance).

An alternative approach has been followed by Pucel, Massé, and Hartwig (1968) who have developed formulas that express α_c and α_d in terms of structural parameters of the guide and the filling factor introduced by Wheeler (1965). The expression for α_d, the contribution due to dielectric losses, is given by

$$\alpha_d \approx 4.34 \frac{q}{\sqrt{\varepsilon_{eff}}} \sqrt{\frac{\mu_o}{\varepsilon_o}} \sigma_d \quad (dB/cm) \tag{109}$$

where q is the filling factor and ε_{eff} is the effective dielectric constant. These quantities were defined earlier in Section 2.2. The factor 4.34 represents the conversion of nepers into decibels. Equation (109) is applicable to an open microstrip line with a single layer dielectric substrate below the center strip and free space above.

To obtain the ohmic attenuation constant α_c, Pucel et al. used a technique based on the so-called "incremental inductance rule" (Wheeler, 1942). This rule expresses the series surface resistance R_s per unit length in terms of that part of the total inductance per unit length which is attributable to the skin effect, i. e., the inductance L_i produced by the magnetic field within the conductors.

It is well known that the surface impedance

$$Z_s = R_s + jX_s \tag{110}$$

has a real part R_s (surface resistance) which is equal to the imaging part X_s, where

89

$$X_s = \omega L_i. \tag{111}$$

According to Wheeler, L_i can be inferred from the external inductance L per unit length as the incremental increase in L caused by an incremental recession of all metallic walls carrying a skin current (see Figure 29). The amount of recession is equal to half the skin depth $\delta = \sqrt{2/\omega\mu\sigma_c}$. An assumption underlying this rule is that the radius of curvature and the thickness of the conductors exposed to the electric field be greater than the skin depth — preferably several skin depths. According to Wheeler, we have

$$L_i = \sum_m \frac{\mu_m}{\mu_o} \frac{\partial L}{\partial n_m} \frac{\delta_m}{2} \tag{112a}$$

$$R_s = \sum \frac{R_{sm}}{\mu_o} \frac{\partial L}{\partial n_m} \tag{112b}$$

where the derivative $\partial L/\partial n_m$ denotes the derivative of L with respect to the incremental recession of wall m, n_m the normal direction to this wall, and $R_{sm} = \omega\mu_m\delta_{cm}/2$ is the surface resistance of wall m. Thus, from the definition (107c)

$$\alpha_c = \frac{|I|^2 R_s}{2|I|^2 Z} = \frac{1}{2\mu_o Z} \sum_m R_{sm} \frac{\partial L}{\partial n_m} \tag{113}$$

where Z is the characteristic impedance of the microstrip line calculated under the quasi-TEM approximation for the lossless case, and I is the total current per conductor.

We assume that the inductance per unit length for the inhomogeneous dielectric case (microstrip line) is approximately the same as that of the unloaded TEM line. This assumption implies that the stored magnetic energy is not affected by the presence of the nonmagnetic
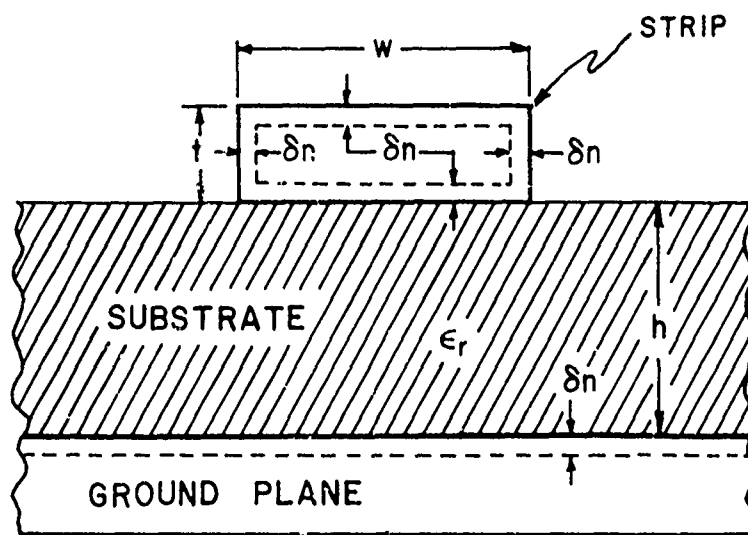
90

Figure 29. Relevant to the derivation of conductor attenuation.

dielectric substrate. This is a reasonable assumption as verified experimentally by Pucel, Massé, and Hartwig (1968).

The remaining task is to derive the expression for the inductance L of the lossless line. From the approximate results by Wheeler (1965) we get

$$L = \frac{\mu_o}{2\pi} \left[\ln\frac{8h}{w'} + \frac{1}{32} \left(\frac{w'}{h} \right)^2 + \cdot \cdot \cdot \right], \quad w/h \leq 2 \qquad (114a)$$

$$L = \frac{\mu_o}{2} \frac{1}{\frac{w'}{2h} + \frac{1}{\pi} \ln[2\pi e(\frac{w'}{2h} + 0.94)]} \quad w/h > 2 \qquad (114b)$$

where

$$w' = w + \frac{t}{\pi} \ln \left(\frac{4\pi w}{t} + 1 \right) \qquad w/h \leq 1/2\pi \quad (115a)$$
$$(2t/h < w/h, \; 1/2\pi)$$

$$= w + \frac{t}{\pi} \ln \left(\frac{2h}{t} + 1 \right) \qquad w/h \geq 1/2\pi. \quad (115b)$$

Assuming that the surface resistance of both the center strip and the ground plane are identical to R_s, we obtain the following result for the ohmic attenuation constant

$$\frac{\alpha_c Zh}{R_s} = \frac{8.64}{2\pi} \left[1 - \left(\frac{w'}{4h} \right)^2 \right] \left\{ 1 + \frac{h}{w'} + \frac{h}{\pi w'} \left[\ln \left(\frac{4\pi w}{t} + 1 \right) - \frac{1 - t/w}{1 + t/4\pi w} \right] \right\}$$
$$(116a)$$
$$w/h \leq 1/2\pi$$

$$\frac{\alpha_c Zh}{R_s} = \frac{8.64}{2\pi} \left[1 - \left(\frac{w'}{4h} \right)^2 \right] \left\{ 1 + \frac{h}{w'} + \frac{h}{\pi w'} \left[\ln \left(\frac{2h}{t} + 1 \right) - \frac{1 + t/h}{1 + t/2h} \right] \right\}$$
$$(116b)$$
$$1/2\pi < w/h \leq 2$$

$$\frac{\alpha_c Zh}{R_s} = \frac{8.68}{\frac{w'}{h} + \frac{2}{\pi} \ln[2\pi e(\frac{w'}{2h} + 0.94)]} \left[\frac{w'}{h} + \frac{w'/\pi h}{\frac{w'}{2h} + 0.94} \right] \left\{ 1 + \frac{h}{w'} + \frac{h}{\pi w'} \right.$$
$$(116c)$$
$$\left. \cdot \left[\ln \left(\frac{2h}{t} + 1 \right) - \frac{1 + t/h}{1 + t/2h} \right] \right\} \qquad w/h > 2$$

92

where α_c is in dB/cm. From the above expression it is evident that for a fixed characteristic impedance which implies fixed t, w, h ratio and ϵ_r, α_c decreases inversely with the substrate thickness h, and increases with the square root of the frequency. The latter results from the fact that R_s is proportional to the square root of the frequency.

Figure 30 shows some numerical results calculated from (116). Figure 31 shows the plots of the results for α_c obtained by Yamashita and Atuki (1970) using Equation (108b). In their paper a comparison was made with the curves in Figure 30. Also, the dielectric attenuation constant α_d was calculated and compared with the experimental results by Hyltin (1965). These are plotted in Figure 32 (Yamashita and Atsuki, 1970). It is evident that the agreement between the theoretical and experimental results is quite good.

The total attenuation constant α was measured by Pucel, Massé, and Hartwig (1968) for a practical microstrip line. The results for the case of a rutile substrate are reproduced in Figure 33. Because of the scatter in measured data points, a curve was drawn through the points by "eye-ball" averaging where possible. The agreement of the experimental data with theory appears to be quite good. The sharp upturn in Figure 33c between 5 and 6 GHz was claimed to be caused by the excitation of the TE_1 surface wave which produces ' a loss through propagation of energy out of the edges of the substrate. This mode has a cutoff frequency $f_c = c/(4h)\sqrt{\epsilon_r - 1} \sim 5.8$ GHz. Indeed, Pucel et al. observed radiation from the sides of the slab in and about this frequency range.
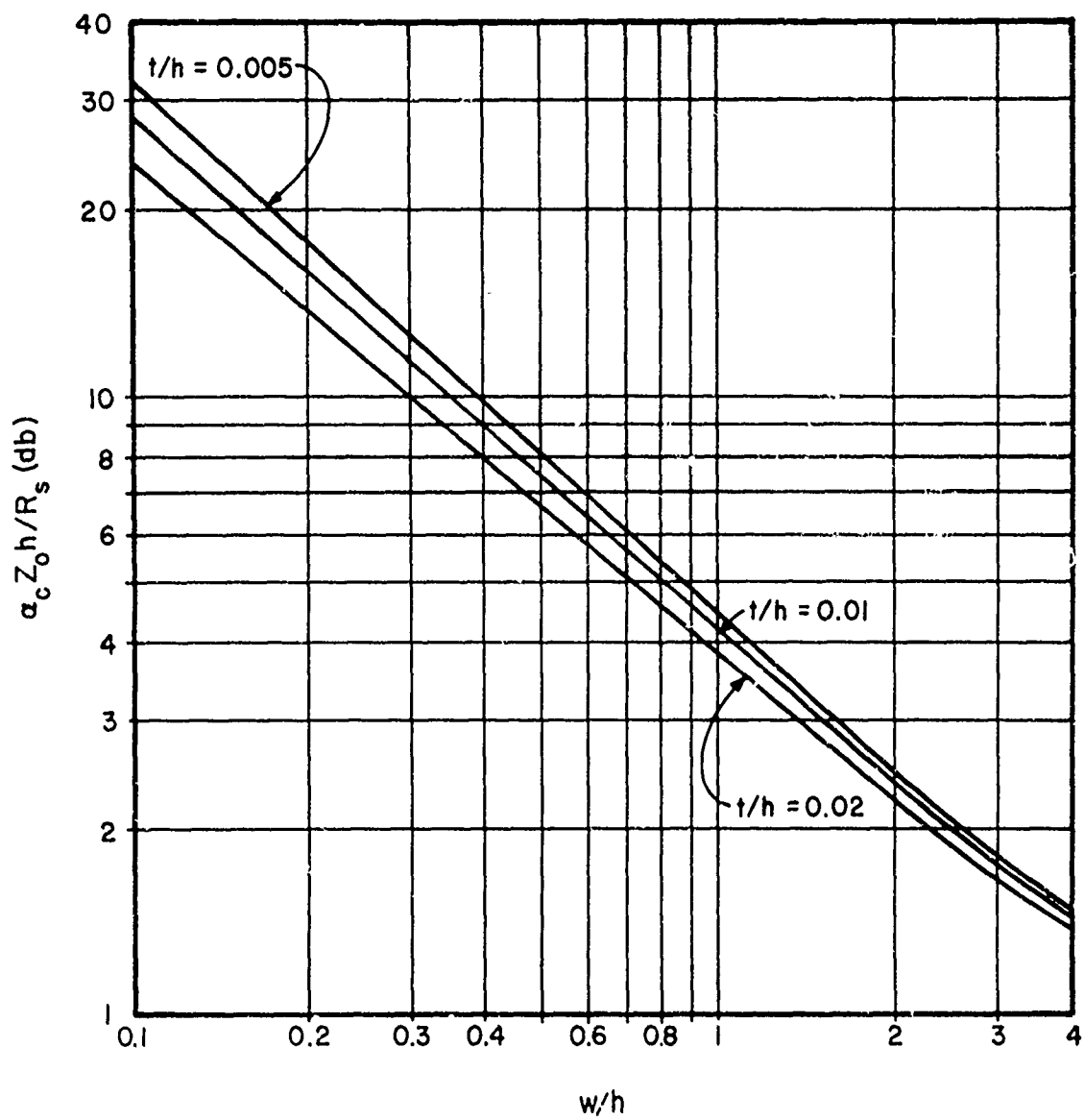
Figure 30. Theoretical conductor attenuation factor of microstrip as a function of w/h, calculated by Pucel et al. (1968).
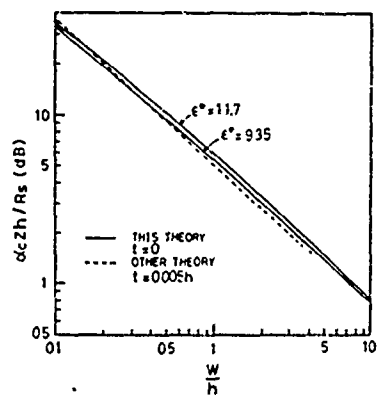
Figure 31. The attenuation constant due to the conductor surface resistance of the microstrip line. [The other theory results are from Pucel et al. (1968).]
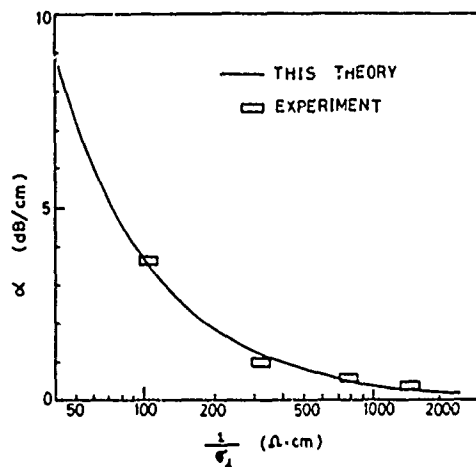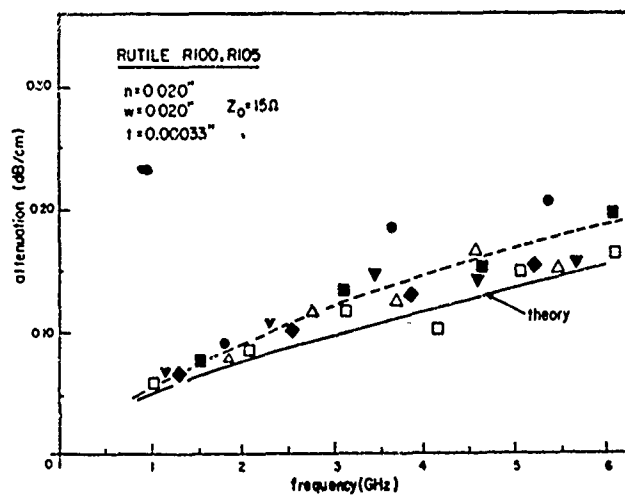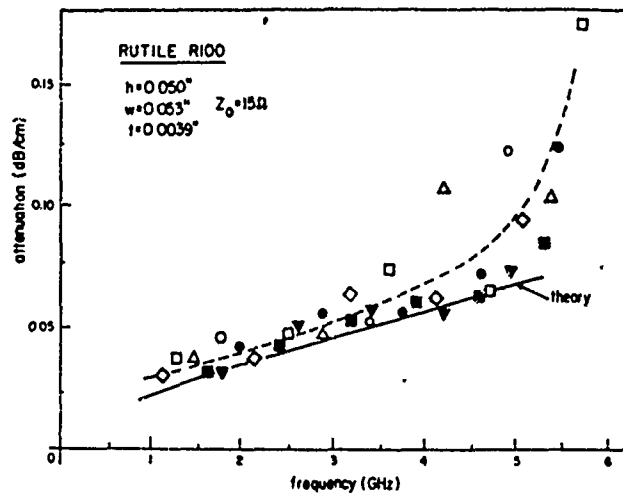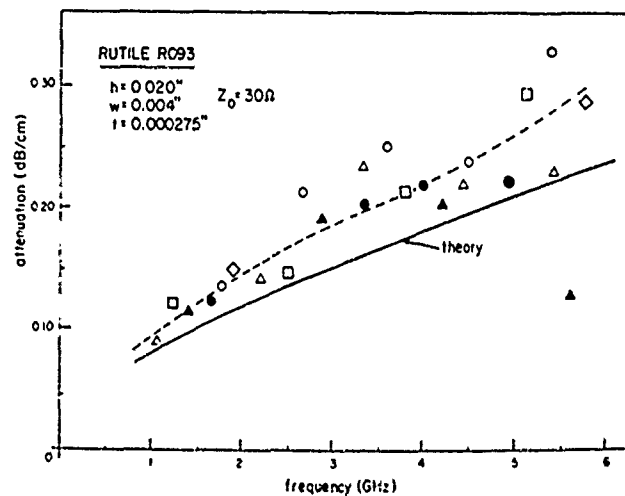

Figure 32. The attenuation constant versus the conductivity of the dielectric substrate of the microstrip line. $\varepsilon^* = 11.7$. [The experimental results are those of Hyltin (1965).]
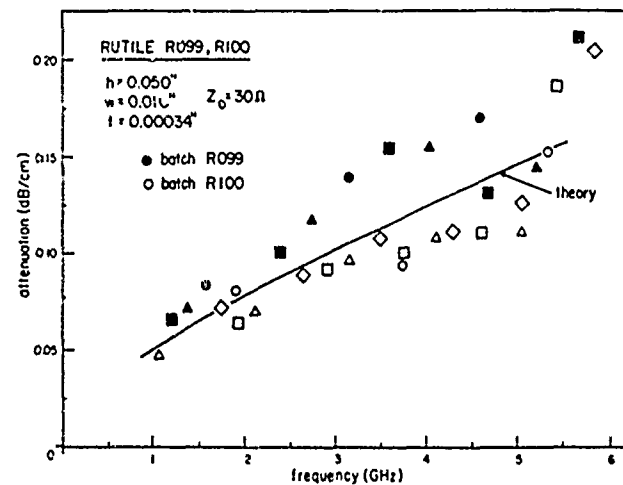
Figure 33. Experimental attenuation data for microstrip on rutile substrates.

VI.   RADIATION AND END LOADING

In the previou sections we have concentrated our attention on

infinitely long microstrip lines. In practice, however, the line

sections are necessarily finite in extent. Thus, it is necessary

in practical designs to evaluate the effects of discontinuities or

junctions introduced in uniform microstrip lines. Typical discontinuities

of interest are T-junctions, gap in the center of the microstrip,

truncated microstrip sections, etc. In this section we discuss the

open-ended microstrip stub as a typical example of such junction

problems.

The open-ended microstrip stub is frequently used as a component

for a filter or a matching network. An ideal lossless stub, with a

true open circuit at the end, appears as a pure susceptance at the

input junction where it is connected to the main line. However,

due to radia·ion and fringing effects that are always present, a true

open cir..iu is never realized at the end of the stub. The effect

of the radiation can be represented by a finite conductance G, whereas

the fringing effects as well as the effect of higher-order modes

generated at the end of the stub may be described by a shunt susceptance

B. The combined effect of these is a finite, complex terminating

impedance at the end of the stub. This and the distributed losses

in the stub (see Section V) cause the input admittance as seen from

the junction of the stub to the main line to be complex. In order to

evaluate this input admittance accurately in the presence of the end

effects just described, it is necessary to calculate the load

admittance at the end of the stub. In the following sections we present

a number of techniques for evaluating this load admittance.

6.1 Radiation Conductance

The problem of radiation at the truncated end of the microstrip
line has been considered by several workers (Lewin, 1960; Denlinger,
1969; Sobol, 1971). Here we follow a method introduced by Sobol (1971)
for calculating the equivalent conductance of an open-ended stub. The
geometry under consideration is shown in Figure 34. In addition to
the quasi-TEM approximation the following assumptions will be made:

1. $h/\lambda \ll 1$;

2. The field distortion at the end of the line is negligible;

3. The center strip is infinitely thin;

4. Only the effect of the dominant mode needs to be considered
   at the discontinuity.

It is also assumed that the x component of the electric field
E_x is a constant, equal to E_o in the region $|z| < w/2$ and $|x| < h/2$
and that it is identically zero outside of this region. The fringing
effect of the field is introduced via the use of the effective
dielectric constant ε_{reff} defined by Wheeler (1965) and discussed
in Section 2.2. The problem of calculating the effect of radiation
from the aperture plane $y = 0$ may be conveniently attacked by first
replacing the aperture electric field by a sheet of conceptual magnetic
current $\overline{M}$. The magnetic current can in turn be used to calculate the
magnetic radiation vector $\overline{L}$. The only nonzero component of the
magnetic current turns out to be M_z, and the corresponding magnetic
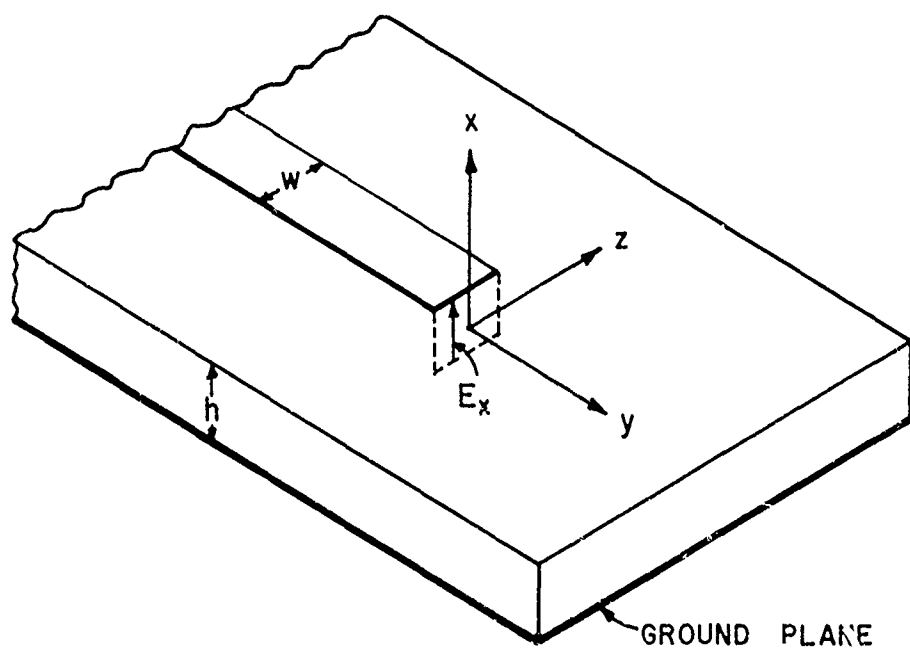radiation vector L_θ is given by

98

Figure 34. Geometry for open-circuited microstrip line.

99

$$L_\theta = - h \sin \theta \int_{-w/2}^{w/2} E_x \exp[j \frac{2\pi}{\lambda} \sqrt{\varepsilon_{reff}} \; z \cos \theta] dz \qquad (117)$$

where λ_o is the free-space wavelength and θ is measured from the z-axis. The total radiated power W, and hence G, is given by

$$W = \frac{1}{2} G(hE_o)^2 = \frac{1}{8\lambda^2 n} \int_0^\pi \int_0^{2\pi} |L_\theta|^2 \sin \theta \; d\phi \; d\theta \qquad (118)$$

where

$$\eta = \frac{120\pi}{\sqrt{\varepsilon_{reff}}} \; .$$

It should be noted that we have made the assumption that $h/\lambda_o \ll 1$ in deriving the above expression for W.

The radiation conductance G is explicitly written as

$$G = \frac{\sqrt{\varepsilon_{reff}}}{240\pi^2} I(\frac{w}{\lambda_o} \sqrt{\varepsilon_{reff}}) \qquad (119)$$

where

$$I = \int_0^\pi \frac{\sin^2 \left(\frac{\pi \sqrt{\varepsilon_{reff}}}{\lambda_o} w \cos \theta \right) \sin^3 \theta}{\cos^2 \theta} \; d\theta \; . (120)$$

It can be shown that I, and hence G, varies as $(w/\lambda_o)^2$ for $w/\lambda_o \ll 1$ as w/λ_o for $w/\lambda_o \gg 1$. For instance, for $\pi \sqrt{\varepsilon_{reff}} \; w/\lambda_o$ much less than unity

$$G \approx \frac{(\varepsilon_{reff})^{3/2}}{180} \left(\frac{w}{\lambda_o} \right)^2 . \qquad (121)$$

This approximation is quite accurate for $(w/\lambda_o) \sqrt{\varepsilon_{reff}}$ less than 0.5.

The asymptotic behaviors of G with respect to w/λ_o are consistent with the ones reported by Lewin (1960) and Marcuvitz (1951).

100

The driving-point admittance of the stub can be calculated in terms of the radiation loading G, susceptance B due to end effect, and distributed line losses expressed in terms of Q_o (unloaded Q). The real part g, of the driving-point admittance, normalized to the stub characteristic admittance, is approximated by

$$g_1 \approx \frac{1}{2Q_o} \cdot \frac{\theta \sec^2\theta - \tan\theta + b \tan\theta + b^2(\theta \sec^2\theta + \tan\theta) + g \sec^2\theta}{(1 - b \tan\theta)^2}$$

$$= g_d + g_r \tag{122}$$

where g and b are the normalized values of G and B, respectively, and θ is the electrical length of the stub. The normalized conductance g_d results from the distributed losses and g_r, the radiation losses.

The ratio of the radiation loss P_{rad}/P_{total} for a 50-Ω line on an aluminum substrate is plotted in Figure 35 as a function of the stub length. It is evident that the radiation losses play an important role for a short stub. The effective length of the stub used in these calculations is obtained by extending it by 0.4h. The justification for this approximation appears in Section 6.2.

For a quarter-wave resonator the ratio of the radiation loss P_{rad} and the distributed loss P_{dist} is given by

$$\frac{P_{rad}}{P_{dist}} \approx \frac{Q_o Z(\epsilon_{reff})^{3/2}(w/\lambda_o)^2}{45\pi\left(1 + 1.6 \frac{h}{\lambda_o}\sqrt{\epsilon_{reff}}\right)} . \tag{123}$$

Figure 36 shows this ratio as a function of frequency and ϵ_r, the dielectric constant of the substrate. The results agree very well with the data presented by Denlinger (1969).
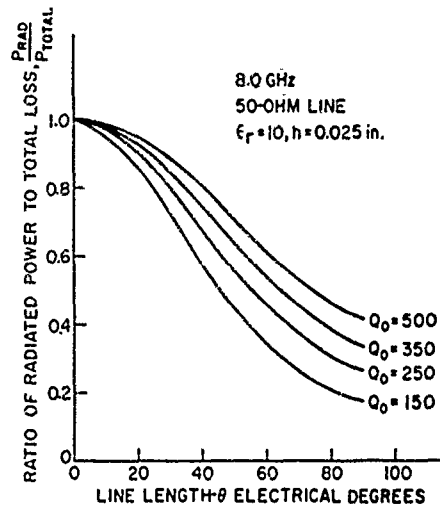
101

Figure 35. Ratio of radiation loss to total loss for 50-Ω line as a function of stub length.
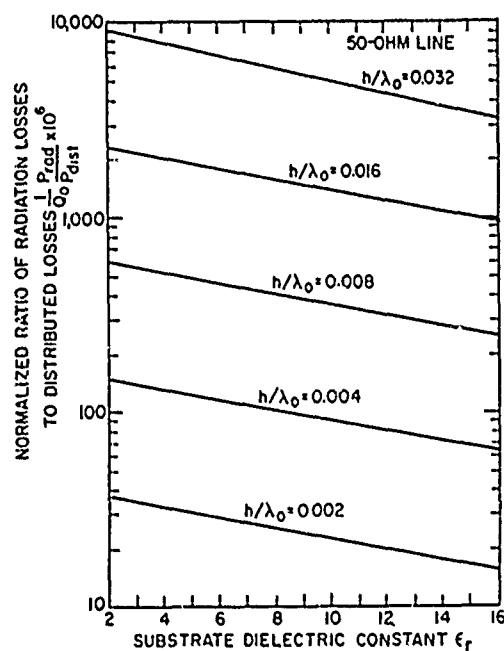

Figure 36. Ratio of radiation loss to distributed loss for 50-Ω line as a function of substrate dielectric constant and frequency.

102

6.2 Edge Susceptance

We next turn to the calculation of the lumped loading susceptance at the truncated edge of the microstrip. The susceptance is often described in terms of an edge capacitance which is represented by a hypothetical extension $\Delta \ell$ of the microstrip. The range of $\Delta \ell$ is approximately 0.2 to 0.5 of the substrate thickness (Napoli and Hughes, 1971; James and Tse, 1972). A simple theory for infinitely wide plates indicates an extension of the length by 0.44h.

Recently a number of attempts have been reported for calculating the edge capacitance by solving the equivalent static problem. Figure 37 shows a finite section of microstrip line of width w and length ℓ. The edge capacitance for a semi-infinite line is calculated by first obtaining the capacitance for a finite section of the line and subtracting from it the contribution of the uniform line. The latter is equal to the line capacitance for unit length multiplied by ℓ, the length of the line section. The excess capacitance is then associated with the fringe effects at the end. In the following, two methods will be presented. The first method is based on the conventional matrix equation approach. On the other hand, in the second method the analysis will be done in the spectral domain.

6.2.1 Matrix method

We begin with the three-dimensional Poisson's equation

$$\nabla^2 \phi(x,\ y,\ z) = - \frac{1}{\varepsilon_o} \rho(x,\ z)\ \delta(y)$$

$$\rho(x,\ z) = 0,\ |x| > w/2,\ |z| > \ell/2.$$

(124)

The Green's function G may be defined as the potential at $(x,\ y,\ z)$ due to the unit charge at (x_o, y_o, z_o). Applying the superposition principle, it is
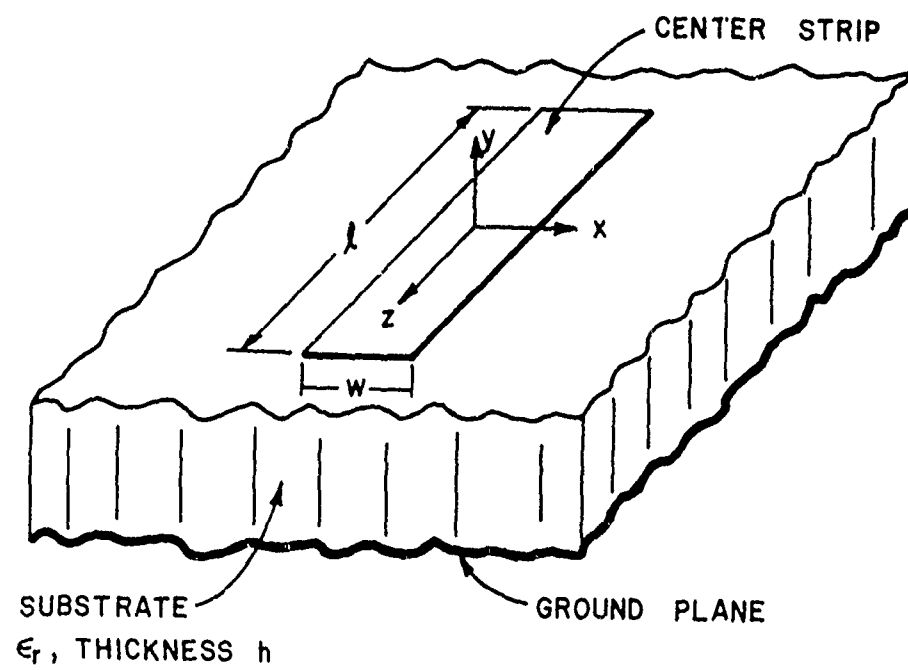
103

Figure 37. Finite section of microstrip line.

104

$$f_n(a, b; c, d) = (c - a) \, \ell n \, \frac{(d - b) + \sqrt{(c - a)^2 + (d - b)^2 + K_n^2}}{(d + \Delta d - b) + \sqrt{(c - a)^2 + (d + \Delta d - b)^2 + K_n^2}}$$

$$g_n(a, b; c, d) = (c + \Delta c - a) \, \ell n \, \frac{(d + \Delta d - b) + \sqrt{(c + \Delta c - a)^2 + (d + \Delta d - b)^2 + K_n^2}}{(d - b) + \sqrt{(c + \Delta c - a)^2 + (d - b)^2 + K_n^2}}$$

$$\xi_n(a, b; c, d) = \frac{(c - a)(d - b)}{K_n \sqrt{(c - a)^2 + (d - b)^2 + K_n^2}}$$

$$K_n = (2n - 2)h$$

$$k = \frac{\varepsilon_r - 1}{\varepsilon_r + 1} \, .$$

Equation (126) is now solved for the unknowns σ_j. After letting $V_i = 1$ for all $i = 1, \cdots N$, the total capacitance of the rectangular microstrip section of length ℓ is given by

$$C(\ell) = \sum_{j=1}^{N} \sigma_j . \tag{129}$$

The value of the fringe capacitance of the open-circuited microstrip is given by

$$C_{ex} = \frac{1}{2} \lim_{\ell \to \infty} [C(\ell) - \ell C_u] \tag{130}$$

where C_u is the line capacitance per unit length of the infinitely long microstrip line, and the factor 1/2 accounts for both ends of the rectangular section. The limit appearing in Equation (130) is numerically computed as follows. The total capacitance for a rectangular section is computed for the sequence of increasing values of ℓ, until convergence is reached for the computed value of the excess capacitance C_{ex}.

easily shown that

$$\phi(x, y, z) = \int_{-\ell/2}^{\ell/2} \int_{-w/2}^{w/2} G(x, y, z; x_o, 0, z_o)\, \rho(x_o, z_o)dx_o\, dz_o. \tag{125}$$

In the method due to Farrar and Adams (1971, 1972) the charge

distribution $\rho(x, z)$ is calculated by numerically solving

Equation (125) in the manner described below. The finite strip is

subdivided into N subsections of elemental area ΔS_j. It is assumed

that the charge distribution σ_j is uniform in a subsection.

Equation (125) is then discretized under this approximation and

yields the matrix equation

$$\sum_{j=1}^{N} D_{ij}\, \sigma_j = V_i, \qquad i = 1, 2, \cdot\cdot\cdot\, N \tag{126}$$

where D_{ij}, the potential at subsection ΔS_i due to a uniform charge

density of magnitude unity on ΔS_j, is given by

$$D_{ij} = G(x_i, 0, z_i; x_j, 0, z_j)\, \Delta x_j\, \Delta z_j. \tag{127}$$

The explicit form of D_{ij} has been derived by using the exact expression

for the potential due to a uniformly charged rectangular plate, and

applying the imaging technique successively across the dielectric

boundary and the ground plate to generate an infinite series of

images. The final expression for D_{ij} is

$$D_{ij} = \sum_{n=1}^{\infty} \frac{k^{n-1}(-1)^{n+1}}{2\pi\varepsilon_o(1 + \varepsilon_r)} \{ f_n(x_i, y_i; x_j, y_j) + g_n(x_i, y_i; x_j, y_j)$$

$$+ f_n(y_i, x_i; y_j, x_j) + g_n(y_i, x_i; y_j, x_j) - K_n[\tan^{-1}\xi_n(x_i,y_i;x_j,y_j)$$

$$+ \tan^{-1}\xi_n(x_i, y_i; x_j + \Delta x_j, y_j + \Delta y_j) - \tan^{-1}\xi_n(x_i, y_i; x_j, y_j+\Delta y_j)$$

$$- \tan^{-1}\xi_n(x_i, y_i; x_j + \Delta x_j, y_j)]\} \tag{128}$$

where

6.2.2 Fourier transform method

An alternative approach to the edge capacitance may be developed by extending the Fourier transform technique presented in Section 2.4 (Itoh, Mittra, and Ward, 1972). The extension is necessary since we are now dealing with a two-dimensional problem as opposed to a one-dimensional case discussed in Section 2.4.

The method proceeds by defining the two-dimensional Fourier transform of the potential function via the equation

$$\tilde{\phi}(\alpha, y, \beta) = \int_{-\infty}^{\infty} \int_{-\infty}^{\infty} \phi(x, y, z) \, e^{j(\alpha x + \beta z)} \, dx \, dz. \qquad (131)$$

Also, taking the Fourier transform of (124) we obtain

$$[\frac{d^2}{dy^2} - (\alpha^2 + \beta^2)] \, \tilde{\phi}(\alpha, y, \beta) = -\frac{1}{\varepsilon_o} \tilde{\rho}(\alpha, \beta)\delta(y) \qquad (132)$$

where $\tilde{\rho}$ is the transform of the charge distribution

$$\tilde{\rho}(\alpha, \beta) = \int_{-\ell/2}^{\ell/2} \int_{-w/2}^{w/2} \rho(x, z) \, e^{j(\alpha x + \beta z)} \, dx \, dz. \qquad (133)$$

In view of the boundary conditions at $y = -h$ and at $y = \infty$, the form of the solution of Equation (132) is taken to be

$$\tilde{\phi}(\alpha, y, \beta) = \begin{cases} A(\alpha, \beta) \, \sinh\sqrt{\alpha^2 + \beta^2} \; y & -h < y < 0 \\ \\ B(\alpha, \beta) \, \exp\{-\sqrt{\alpha^2 + \beta^2} \; y\} & y > 0. \end{cases} \qquad (134)$$

By proceeding in exactly the same manner as in Section 2.4 and applying the boundary conditions on the strip, we obtain after eliminating $A(\alpha, \beta)$ and $B(\alpha, \beta)$ the following equation for the transform of the charge distribution

$$\tilde{G}(\alpha, \beta) \, \tilde{\rho}(\alpha, \beta) = \tilde{\phi}(\alpha, 0, \beta) \qquad (135)$$

107

where

$$\tilde{G}(\alpha, \beta) = \frac{1}{\varepsilon_o \sqrt{\alpha^2 + \beta^2} \; [1 + \varepsilon_r \coth \sqrt{\alpha^2 + \beta^2} \; h]} \; . \quad (136)$$

Note that G is the transform of Green's function and that the algebraic product in the left-hand side of (135) corresponds to the surface convolution integral in (125). This feature is very useful in the actual numerical calculation because the computation of the surface convolution integral is a time consuming operation.

Equation (135) is transformed into a matrix equation via the application of Galerkin's method, which is similar to that discussed in Section 2.4. The matrix equation may be written as

$$b_m = \sum_{n=1}^{N} K_{mn} \, c_n \qquad\qquad m = 1, 2, \cdots N \quad (137)$$

where

$$K_{mn} = \int_{-\infty}^{\infty} \int_{-\infty}^{\infty} \overset{\sim}{\rho}_m(\alpha, \beta) \; \tilde{G}(\alpha, \beta) \; \overset{\sim}{\rho}_n(\alpha, \beta) \; d\alpha \; d\beta$$

$$b_m = \int_{-\infty}^{\infty} \int_{-\infty}^{\infty} \overset{\sim}{\rho}_m(\alpha, \beta) \; \overset{\sim}{\phi}_i(\alpha, 0, \beta) \; d\alpha \; d\beta = \frac{1}{2\pi} \int_{-\ell/2}^{\ell/2} \int_{-w/2}^{w/2} \rho_n(x, z) dx \; dz.$$

The functions $\overset{\sim}{\rho}_n$ are the basis functions of $\overset{\sim}{\rho}(\alpha, \beta)$ and $\overset{\sim}{\phi}_i$ is the transform of the potential on the strip. $\rho_n(x, z)$ is the inverse transform of $\overset{\sim}{\rho}_n(\alpha, \beta)$. The total charge on the strip is given by

$$C(\ell) = \sum_{n=1}^{N} c_n \int_{-\ell/2}^{\ell/2} \int_{-w/2}^{w/2} \rho_n(x, z) \; dx \; dz = 2\pi \sum_{n=1}^{N} c_n \, b_n.$$

$$(138)$$

Figure 38 shows the fringe capacitance of the open-circuited micro-strip line calculated by the two methods presented in this section.
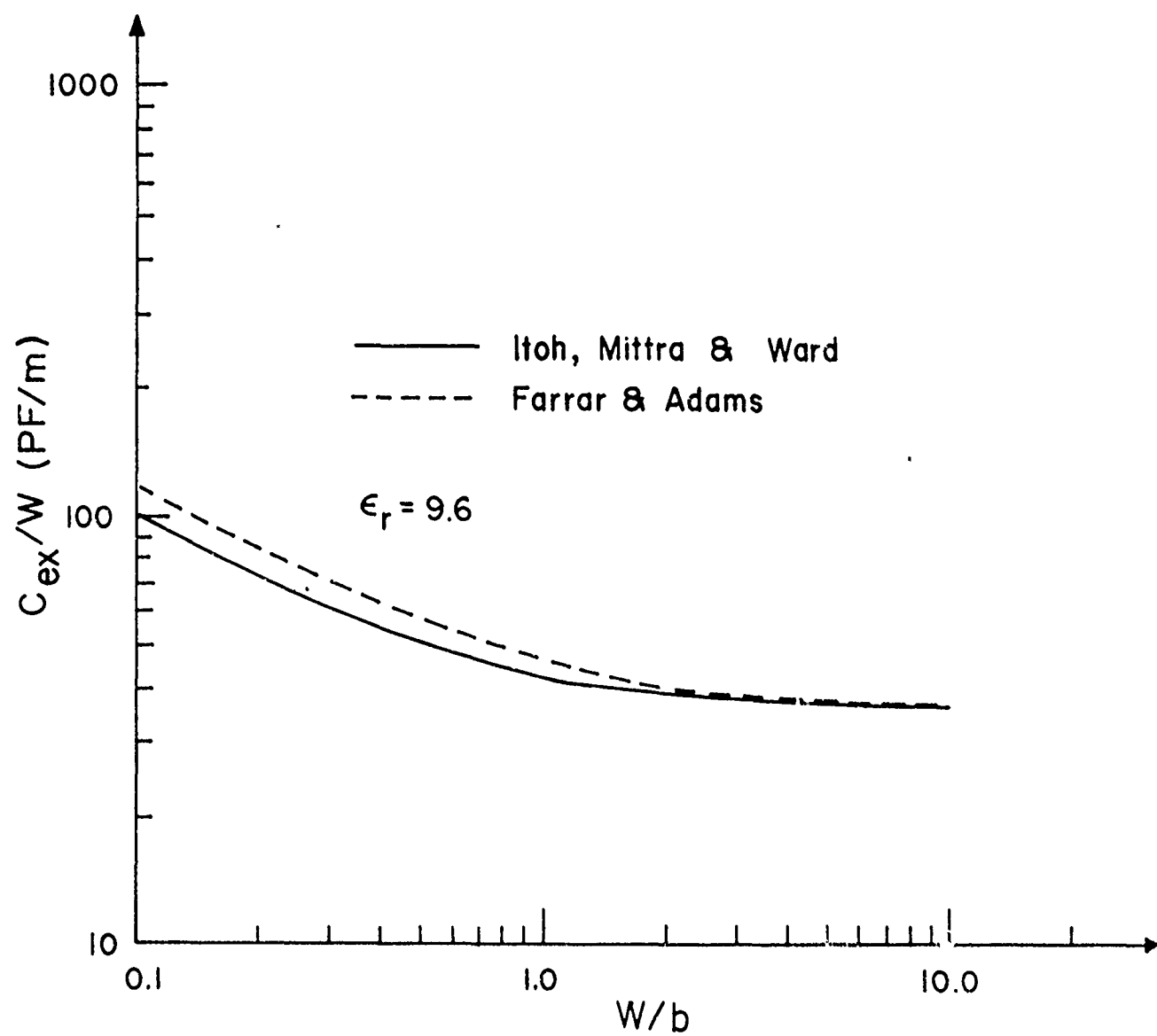
Figure 38. Fringe capacitance of a semi-infinite microstrip.

The values of the fringe capacitance can in turn be used to compute
the loading susceptance due to the end discontinuity.

VII. CONCLUSIONS

In the preceding sections we have discussed a number of features of microstrip-type transmission lines for microwave integrated circuitry. Approximate as well as rigorous analyses for the characteristics of the infinitely long microstrip lines have been presented. Brief discussion of some practical problems encountered in the actual design, such as computation of losses, radiation and junction effects, etc., has been included.

Although much has been written on the subject of microstrip lines, there still remain a number of theoretical as well as practical problems yet to be solved. Some of these problems include: (i) comprehensive analysis of higher-order modes; (ii) complex junction problems; (iii) radiation from a uniform section of open microstrip line; and so on. It is felt that a simultaneous development of both the theoretical and experimental techniques will be needed to successfully resolve these problems.

REFERENCES

Arditi, M. (1955), "Characteristics and applications of microstrip for microwave wiring," IRE Trans. Microwave Theory and Techniques, vol. MTT-3, pp. 31-56.

Collin, R. E. (1960), Field Theory of Guided Waves, McGraw-Hill, New York.

Daly, P. (1971), "Hybrid-mode analysis of microstrip by finite element methods," IEEE Trans. Microwave Theory and Techniques, vol. MTT-19, pp. 19-25.

Denlinger, E. J. (1969), "Radiation from microstrip resonators," IEEE Trans. Microwave Theory and Techniques, vol. MTT-17, pp. 235-236.

Denlinger, E. J. (1971), "A frequency dependent solution for microstrip transmission lines," IEEE Trans. Microwave Theory and Techniques, vol. MTT-19, pp. 30-39.

Deschamps, G. A. (1954), "Theoretical aspects of microstrip waveguides," IRE Trans. Microwave Theory and Techniques, vol. MTT-2, pp. 100-102.

Dukes, J. M. C. (1956), "An investigation into some fundamental properties of strip transmission lines with the aid of an electrolytic tank," Proc. IEE. (London), vol 103B, pp. 319-333.

Farrar, A. and A. T. Adams (1971), "Computation of lumped microstrip capacities by matrix methods -- Rectangular sections and end effect," IEEE Trans. Microwave Theory and Techniques, vol. MTT-19, pp. 495-497.

Farrar, A. and A. T. Adams (1972), "Correction to computation of lumped microstrip capacities by matrix methods — Rectangular sections and end effect," IEEE Trans. Microwave Theory and Techniques, vol. MTT-20, p. 294.

Green, H. E. (1965), "The numerical solution of some important transmission-line problems," IEEE Trans. Microwave Theory and Techniques, vol. MTT-13, pp. 676-692.

Harrington, R. F. (1961), Time-Harmonic Electromagnetic Fields, McGraw-Hill, New York.

Hartwig, C. P., D. J. Massé, and R. A. Pucel (1968), "Frequency dependent behavior of microstrip," IEEE G-MTT International Symposium, Detroit, Michigan, Digest, pp 110-119.

Hornsby, J. S. and A. Gopinath (1969a), "Fourier analysis of a dielectric-loaded waveguide with a microstrip line," Electronics Lett., vol. 5, pp. 265-267.

Hornsby, J. S. and A. Gopinath (1969b), "Numerical analysis of a
dielectric-loaded waveguide with a microstrip line — Finite-
difference methods," IEEE Trans. Microwave Theory and Techniques,
vol. MTT-17,pp. 684-690.

Hyltin, T. M. (1965), "Microstrip transmission on semiconductor
dielectrics," IEEE Trans. Microwave Theory and Techniques, vol.
MTT-13, pp. 777-781.

Itoh, T. and R. Mittra (1971a), "Dispersion characteristics of microstrip
lines," European Microwave Conference, Stockholm, Sweden, Proceedings,
p. c4/3.

Itoh, T. and R. Mittra (1971b), "Dispersion characteristics of slot
lines," Electronics Lett., vol. 7, pp. 364-365.

Itoh, T., R. Mittra and R. D. Ward (1972), "A new method for solving
the discontinuity problems in microstrip lines," IEEE G-MTT
International Symposium, Chicago, Illinois, Digest, pp. 68-70,
(also to be published).

James, D. S. and S. H. Tse (1972), "Microstrip end effects," Electronics Lett.,
vol. 8, pp. 46-47.

Kowalski, G. and R. Pregla (1971), "Dispersion characteristics of shielded
microstrips with finite thickness," Archiv für Elektronik und
Übertragungstechnik, vol. 25, pp. 193-196.

Lewin, L. (1960), "Radiation from discontinuities in strip-line,"
Proc. IEE (London), vol. 107, pp. 163-170.

Lewin, L. (1966), "The use of singular integral equations in the solution
of waveguide problems," in Advances in Microwaves, vol. 1, L. Young,
ed., Academic Press, New York, pp. 212-284.

Loadholt, J. T., R. Mittra, and T. Itoh (1971), "A study of the field
distributions in shielded microstrip lines," Antenna Laboratory
Report No. 71-6, University of Illinois, Urbana, Illinois.

Marcuvitz, N. (1951), Waveguide Handbook, vol. 10 (Radiation Laboratory
Series). McGraw-Hill, New York, p. 179.

Mittra, R. and T. Itoh (1970), "Charge and potential distributions in
shielded striplines," IEEE Trans. Microwave Theory and Techniques,
vol. MTT-18, pp. 149-156.

Mittra, R. and T. Itoh (1971), "A new technique for the analysis of the
dispersion characteristics of microstrip lines," IEEE Trans.
Microwave Theory and Techniques, vol. MTT-19, pp. 47-56.

Mittra, R. and S. W. Lee (1971), Analytical Techniques in the Theory
of Guided Waves, Macmillan, New York.

Mittra, R. and T. Itoh (1972), "Some efficient numerical methods," in
Computer Techniques for Electromagnetics and Antennas, R. Mittra,
ed., Pergamon Press, London.

Napoli, L. S. and J. J. Hughes (1971), "Foreshortening of microstrip open circuits on alumina substrates," IEEE Trans. Microwave Theory and Techniques, vol. MTT-19, pp. 559-561.

Pucel, R. A., D. J. Massé and C. P. Hartwig (1968), "Losses in microstrip," IEEE Trans. Microwave Theory and Techniques, vol. MTT-16, pp. 342-350.

Schneider, M. V. (1972), "Microstrip dispersion," Proc. IEEE, vol. 60, pp. 144-146.

Sobol, H. (1971), "Radiation conductance of open-circuit microstrip," IEEE Trans. Microwave Theory and Techniques, vol. MTT-19, pp. 885-887.

Stinehelfer, H. E., Sr. (1968), "An accurate calculation of uniform microstrip transmission lines," IEEE Trans. Microwave Theory and Techniques, vol. MTT-16, pp. 439-444.

Ward, R. D., R. Mittra and T. Itoh (1971), "Application of Galerkin's method for analyzing microstrip transmission line," Antenna Laboratory Report No. 71-8, University of Illinois, Urbana, Illinois.

Wexler, A.(1969), "Computation of electromagnetic fields," IEEE Trans. Microwave Theory and Techniques, vol. MTT-17, pp. 416-439.

Wheeler, H. A. (1942), "Formulas for the skin effect," Proc. IRE, vol. 30, pp. 412-424.

Wheeler, H. A. (1965), "Transmission-line properties of parallel strips separated by a dielectric sheet," IEEE Trans. Microwave Theory and Techniques, vol. MTT-13, pp. 172-185.

Wu, T. T. (1957), "Theory of microstrip," J. Appl. Phys., vol. 28, pp. 299-302.

Yamashita, E. and R. Mittra (1968), "Variational method for the analysis of microstrip lines," IEEE Trans. Microwave Theory and Techniques, vol. MTT-16, pp. 251-256.

Yamashita, E. (1968), "Variational method for the analysis of microstrip-like transmission lines," IEEE Trans. Microwave Theory and Techniques, vol. MTT-16, pp. 529-535.

Yamashita, E. and K. Atsuki (1970), "Strip line with rectangular outer conductor and three dielectric layers," IEEE Trans. Microwave Theory and Techniques, vol. MTT-18, pp. 238-244.

Yamashita, E. and K. Atsuki (1971), "Analysis of thick-strip transmission lines," IEEE Trans. Microwave Theory and Techniques, vol. MTT-19, pp. 120-122.

Zysman, G. 1. and D. Varon (1969), "Wave propagation in microstrip transmission lines," <u>IEEE G-MTT International Symposium</u>, Dallas, Texas, Digest, pp. 3-9.